DYNAMIC BEHAVIOR OF SPACECRAFT FORMATION FLYING USING COULOMB FORCES

BY

Jer-Hong Chong

B.S.C.M., Michigan Technological University, 2000

A THESIS

Submitted in partial fulfillment of the
requirements for the degree of
MASTER OF SCIENCE IN MECHANICAL ENGINEERING

MICHIGAN TECHNOLOGICAL UNIVERSITY

2002

MICHIGAN TECHNOLOGICAL UNIVERSITY

DEPARTMENT OF MECHANICAL ENGINEERING -
ENGINEERING MECHANICS

WE HEREBY RECOMMEND THAT THE THESIS BY:

Jer-Hong Chong

ENTITLED: Dynamic Behavior of Spacecraft Formation Flying Using Coulomb Forces

BE ACCEPTED IN PARTIAL FULFILLMENT OF THE REQUIREMENTS FOR THE DEGREE OF

MASTER OF SCIENCE IN MECHANICAL ENGINEERING

Gordon G. Parker 5-2-02

Thesis Advisor: Dr. Gordon G. Parker Date

Lyon B King 5-2-02

Thesis Advisor: Dr. Lyon B. King Date

William W. Predebon 5/2/02

Department Chair: Dr. William W. Predebon Date

Abstract

Swarm satellites are being considered for several future space operations. The benefits of using swarm satellites are their small size and simple formations, flexibility in space, reduced launch cost, and a reduced risk of system failure. In addition, the benefit of using formation flying is to apply in the separated spacecraft interferometry for astronomical or Earth imaging. Each spacecraft is required to space 10 meters in such formation. A micro-Newton force that is generate by thruster controller is required for swarm satellites flying in close formation. However, thruster system will emit caustic propellant exhaust that will contaminate neighboring spacecraft. Using Coulomb force to generate a micro-Newton force is proposed in this research. Six satellite formations are formed and their dynamic behaviors are discussed. Hill's equations are used to describe the motion of the collectors (slave satellite) respect to the combiner (center satellite). The equilibrium equations are derived and the equilibrium solutions are solved analytically and numerically. The relationship of charged collectors and the charged combiner for each formation are presented in this research. In addition, the stability and controllability of formations are determined and discussed using Lyapunov's Indirect Method. All the formations are unstable but one is controllable. Deriving a control law is suggested to pay attention for controlling the satellite formations in future work. Also, it is suggested to focus on developing some method to determine the intelligent formation.

Acknowledgements

I would like to thank the following company and people for how they helped me during my graduate study in Michigan Technological University,

- I would like to thank the NASA Institute for Advanced Concepts (NIAC) for funding this research.
- My advisors, Dr. Gordon G. Parker and Dr. Lyon B. King, have supported me throughout my graduate study and given me a lot of advice on the research and life. I would like to thank them for everything I learned and the opportunity to work with them. I appreciate their effort and patience.
- Thank you Dr. Chris E. Passerello and Dr. Mark S. Gockenbach, for kindly being my committee members and for reading and giving suggestions on my thesis.
- I would love to thank Mr. Robert Rowe who always supported me and encouraged me when I was frustrated with my work.
- The Michigan Technological University MEEM Department deserves the acknowledgement for providing me with Teaching Assistant funding and useful facilities for me to finish my graduate study.
- The Michigan Technological University Writing Center Coaches have helped me throughout my study in the United State. Thank you coaches!
- I would like to thank my friends all around the world for encouragement and support.
- One person who has always encouraged me and given me the confidence to face my problems is my boyfriend, Lit-Ming Gho. I would like to show my gratitude to him

for guiding and giving me strength to face all the frustration and confusion I had during my study.

- Last but not least, I want to thank the most important people in my life, my family, especially my parents. Thank you for giving me a great life and always supporting and blessing me wherever you are. In addition, I would love to thank my brothers and relatives for taking care of my parents so that I can concentrate on my study.

Table of Contents

List of Figures

List of Tables

1. Introduction

1.1. Formation Flying Background

Swarms of microsatellites are currently envisioned as an attractive alternative to traditional large spacecraft. Such swarms, acting collectively as virtual satellites, will benefit from the use of cluster orbits where the satellites fly in a close formation.[1] The formation concept, first explored in the 1980's to allow multiple geostationary satellites to share a common orbital slot,[2,3] has recently entered the era of application with many missions slated for flight in the near future. For example, EO-1 will formation fly with LandSat-7 to perform paired earth imagery, ST-3 will use precision formation flight to perform stellar optical interferometry, TechSat 21 will be launched in 2004 to perform sparse-aperture sensing with inter-vehicle spacing as close as 5 m, and the ION-F science mission will perform distributed ionospheric impedance measurements.[4,5] The promised payoff of formation-flying has recently inspired a large amount of research in an attempt to overcome the rich technical problems. A variety of papers can be found in the proceedings of the 1999 AAS/AIAA Space Flight Mechanics Meeting,[6,7,8] the 1998 Joint Air Force/MIT Workshop on Satellite Formation Flying and Micro-Propulsion,[9] a recent textbook on micropropulsion,[10] and numerous other sources.[11,12,13,14,15,16,17]

Relative positional control of multiple spacecraft is an enabling technology for missions seeking to exploit satellite formations. Of the many technologies that must be brought to maturity in order to realize routine formation flying, perhaps the most crucial is the spacecraft propulsion system. In fact, during his keynote address at the 1998 Joint

Air Force/MIT Workshop on Satellite Formation Flying and Micro-Propulsion, Dr. David Miller of the Space Systems Laboratory at MIT delivered a "Top Ten List" of formation-flying technological obstacles. On this list, the two most important technologies were identified as (1) Micropropulsion; and (2) Payload contamination, arising from propellant exhausted from closely spaced satellites.[9]

Constellations of small satellites will require propulsion systems with micro- to milli-Newton thrust levels for deployment, orbit maintenance, disposal, and attitude control.[18,19] Formation-keeping thrusters must be capable of producing finely controlled, highly repeatable impulse bits. Although no suitable thruster has yet been proven in flight, recent research suggests that the best current technologies are micro-pulsed-plasma thrusters (micro PPT),[5] field-emission electric propulsion thrusters (FEEP),[20] and colloid thrusters.[21]

As identified in item (2) from Dr. Miller's technology list, current research-level thruster candidates pose significant contamination problems. In close proximity, the propellant emitted by such devices as micro-PPT's (vaporized Teflon), FEEP (ionized cesium), or colloid thrusters (liquid glycerol droplets doped with NaI) will impinge upon neighboring vehicles and damage payloads. To worsen the problem, orbital mechanics for many clusters of interest mandate continuous thruster firings pointed directly towards other vehicles in the formation. The contamination problem will be amplified as the formation spacing is reduced.

1.2. Coulomb Control Concept

1.2.1. Existing Technology

Of the many technologies that must be brought to maturity in order to validate the satellite formation-flying concept, perhaps the most crucial is the propulsion system. Fine positioning and formation-keeping of low-mass vehicles in a swarm will require development of very low-thrust propulsion systems with finely controllable impulse bits. Even with the high-specific-impulse available from conventional electric propulsion (EP) thrusters, maintaining a formation by forcing individual satellites to occupy non-Keplerian orbit paths will require continuous thrusting over the lifetime of the mission. Over a five- to ten-year mission, such continuous thrust requirements will place heavy demands on thruster reliability and operational lifetime.

For widely spaced formations (inter-spacecraft separation on the order of 100 m or more) the fine-positioning requirements may be met with conventional EP thrusters. However, for very closely spaced swarms, current propulsive systems are not well suited to perform precision formation flying. For space interferometry, configurations are envisioned where the inter-satellite spacing is less than ten meters. In such a tight swarm, precision formation keeping will be extremely difficult. Existing thruster technologies that have been identified as the most promising tools for accomplishing such tight-formation flying include micro pulsed-plasma thrusters (micro PPT's), field-emission electric propulsion (FEEP) thrusters, and colloid thrusters.[22] Although all of these thrusters are technologically immature, each device is capable, in principle, of generating controllable micro-Newton levels of thrust.

Propellant-emitting thrusters will pose a spacecraft integration/contamination problem for tight satellite formations. Each of the thruster technologies currently under development will exhaust damaging propellant. For many spacecraft operating in close proximity, the microthruster propellant (vaporized Teflon for PPT's, liquid cesium for FEEP, and NaI-doped liquid glycerine for colloid) has a high likelihood of contaminating sensitive spacecraft surfaces, optics, and other instruments on neighboring craft. Such contamination would be incompatible with high-resolution imaging systems. In addition to material contamination problems, the potential exists for exhaust plume impingement forces to be transmitted from one spacecraft in the constellation to another, greatly complicating the fine position control.

1.2.2. Overview of Coulomb Concept

The concept proposed in this document uses the principle of Coulomb attraction/repulsion between charged bodies to control the spacing between nodes of a microsatellite cluster. The Coulomb control principle is most easily conveyed by examining the interaction between two neighboring bodies capable of transferring electric charge. Much more detailed analysis of the physical processes will be presented in later chapters.

Consider, for instance, two vehicles separated a distance d in space as shown in Figure 1-1.

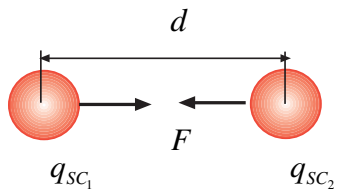

Figure 1-1. Fundamental Coulomb Control Concept using two charge spherical bodies.

Initially, both spacecraft are electrically neutral, i.e., the amount of negative charge (electrons) is equal to the amount of positive charge producing a net vehicle charge of zero and no interaction between the craft. Now, allow one craft to change its charge state through the emission of electrons. This is a trivial process utilizing an electron-gun or similar cathode device. If the electron beam is used to transfer an amount of negative charge, q_{SC}, from spacecraft 1 (SC1) to spacecraft 2 (SC2), the net negative charge of SC2 will equal the net positive charge remaining on SC1, producing an attractive force between the spacecraft given by

Eqn. 1-1
$$F = \frac{1}{4\pi\varepsilon_0}\frac{q_{SC}^2}{d^2}.$$

The charge required to produce a 10 μN attractive force at a spacecraft separation of d = 10 m is $q_{SC} = 3.3\text{x}10^{-7}$ C. Thus, using a 1-mA electron beam current, this charge can be transferred in only 330 μsec.

For discussion purposes, consider 1-m spherical spacecraft (radius of 0.5 m). The potential of the charged-spacecraft surface can be evaluated from Gauss' law as:

Eqn. 1-2
$$V_{SC} = \frac{1}{4\pi\varepsilon_0}\frac{q_{SC}}{r_{SC}},$$

where V_{SC} is the spacecraft potential in volts and r_{SC} is the spacecraft radius. For a charge of $q_{SC} = 3.3\text{x}10^{-7}$ C and radius of r = 0.5 m, the surface of SC1 will assume a

positive potential of 6 kV, while V_{SC2} = -6 kV. Thus, a 12-kV electron beam must be used in order to allow the charge from SC1 to "climb the hill" and reach the surface of SC2. The minimum power required to generate a 10 μN attractive force in 330 μsec between the spacecraft separated a distance d = 10 m is then only 12 Watts. This power can be reduced if longer charging time is acceptable.

It is perhaps more intuitive to discuss inter-spacecraft Coulomb forces in terms of the spacecraft potential in volts, V_{SC}. By combining the above equations, the Coulomb force between two spacecraft can be written as

Eqn. 1-3

$$F_0 = 4\pi\varepsilon_0 \frac{r_{SC1} r_{SC2} V_{SC1} V_{SC2}}{d^2}.$$

Spacecraft charging has historically been associated with negative impacts on satellite payloads. Arcs and other breakdown phenomena arising from such differential charging can wreak havoc on sensitive electronics. Differential charging results when some regions of a spacecraft assume electric potentials drastically different from other regions of the same vehicle. The induced intra-vehicle electric fields can cause spontaneous interruption of payload functions. In this proposal, *absolute* spacecraft charging is proposed as a formation controlling method. If adjusted uniformly over a vehicle, the spacecraft absolute potential with-respect-to space, V_{SC}, can be driven to large values (such as many kilo-volts) with no impact to spacecraft functions and no risk of arc or spontaneous failure.

1.2.3. Supporting Flight Heritage

A wealth of pertinent data and experience is available from the results of the SCATHA flight experiment. The SCATHA satellite was launched in January, 1979 with the goal of measuring the build-up and breakdown of charge on various spacecraft components and to characterize the natural environment at GEO altitudes.[23]

The satellite potential with respect to space plasma potential was monitored on the SCATHA craft. During passive operation of the satellite, the spacecraft potential was seen to vary from near ground to many kilovolts negative. This is a common occurrence. An isolated passive body immersed in plasma will accrue a net negative charge due to the higher mobility of electrons as compared to heavy ions. For hot plasma such as that found at MEO-GEO, this negative charge is substantial. One goal of the SCATHA mission was to test the validity of actively controlling the spacecraft potential by emitting charge through an electron beam. To this end, an electron gun was used to transfer charge from SCATHA to the space plasma at various current and voltage levels up to 13 mA and 3 kV.

Due to the plasma environment, spacecraft routinely charge to negative voltages. However, a very important result, as reported by Gussenhoven, et al., was that, "*the electron beam can achieve large, steady-state changes in the vehicle potential and the returning ambient plasma*."[24] In fact, Gussenhoven found that when a 3 kV electron beam was operated, "*the satellite became positively charged to…a value approaching beam energy for 0.10 mA*" emission current. Similarly, Cohen, et al. report that "*spacecraft frame and surfaces on the spacecraft went positive with respect to points 50 meters from the satellite when the gun was operated. Depending upon ejected electron*

currents and energies, spacecraft frame-to-ambient-plasma potential differences between several volts and 3 kV were generated."[25]

For rough estimation, we can approximate the SCATHA spacecraft as a sphere with a diameter of 1.7 m.[26] If an identical SCATHA spacecraft had been in orbit simultaneously, the satellite potential control demonstrated on this 1979 mission would have been sufficient to actively generate attractive and repulsive forces between the vehicles with magnitudes up to almost 10 μN over 10 meters, at a power expense of only 3 Watts. In addition to the SCATHA data, during a separate flight-experiment the ATS-6 spacecraft demonstrated charging as high as 19 kV.[27,28]. Assuming a spacecraft diameter on the order of 1 meter, findings hint at the possibility to generate and control forces of hundreds of μN.

1.3. Separated Spacecraft Interferometry

1.3.1. Space-based Imaging Problem

It has long been known that increased astronomical imaging capability could be realized if the optics for the imaging system were placed outside of the earth's atmosphere. Missions such as the current Hubble Space Telescope (HST) and planned Next Generation Space Telescope (NGST) exemplify this principle. The increased clarity offered by space-based astronomy is somewhat offset, however, by practical limits placed on angular resolution of the image. The angular resolution (resolving power) of an optic is related to the physical size of the collector by

Eqn. 1-4 $$\theta = \frac{\lambda}{2d},$$

where θ is the minimum resolvable angular feature, λ is the wavelength to be imaged, and d is the physical size of the collecting aperture. Thus, to obtain fine angular resolution (small θ) requires a large aperture. Herein lies the problem for space-based imaging systems: the physical size of the aperture is limited by launch vehicle fairing dimensions. The largest launch fairing currently available is that of the Ariane V, which is approximately 5 meters in diameter. For space-based imaging in the optical wavelengths (400-700 nm) using a monolithic aperture, missions are limited to angular resolution no better than 4×10^{-8} radians (about 8 milli-arcseconds).

The ability to resolve an astronomical object is directly proportional to the size of the object and inversely proportional to the distance from the observer. At the Spaceborne Interferometry Conference, Ridgeway presented a graphical depiction of the apparent size of "interesting" astronomical objects.[29] Ridgeway's schematic is reproduced in Figure 1-2. In this figure, lines of constant apparent angular size (resolution) are shown. It is significant that most of the science topics begin with angular scales of about 1 milli-arcsecond, approximately a factor of 1000 smaller than the typical limit of optical imaging from the ground.

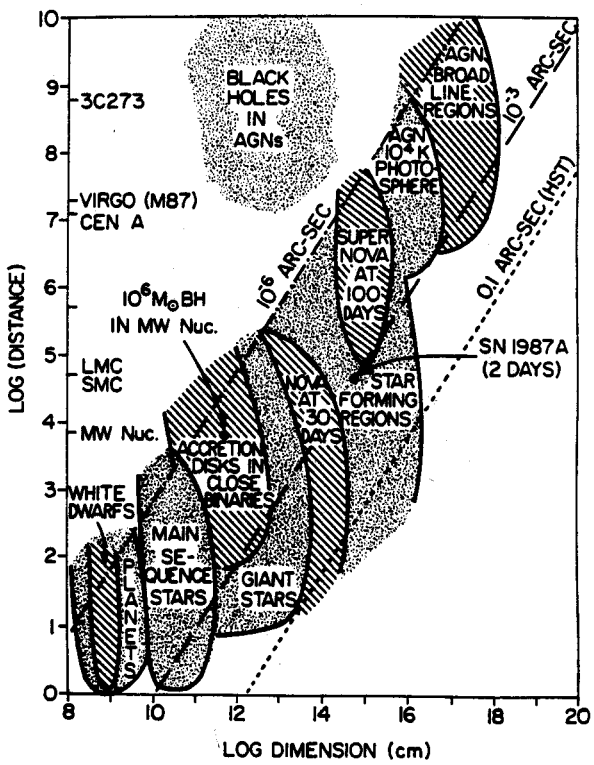

Figure 1-2. Depiction of apparent size of astronomical target objects. The distance to the objects is listed on the vertical axis, with the transverse dimension of the object on the horizontal axis. Diagonal lines denote the angular extent of the target and, thus, the resolution required for imaging. The 0.1 arc-sec line denotes Hubble Space Telescope (HST) capabilities. It is significant that most science topics begin with resolutions better than 1 milli-arcsecond.

1.3.2. Interferometry Fundamentals

There are two options for circumventing the aperture resolution restrictions created by launch vehicles. First, a deployable structure can be designed that can fold to stow into the size-limited fairing. The structure can then be deployed on-orbit to a final size greater than the fairing diameter. Although deployable structures avoid a direct physical size limitation, the stowed structure must still fit within the available launch

volume and is thus constrained at some larger, but finite, dimension related to the launch vehicle size. The second method for overcoming vehicle size restrictions is separated spacecraft interferometry.

Separated spacecraft interferometry is a direct extension of an imaging technique that has been employed with ground-based systems for years. In ground-based interferometry, physically separated apertures collect incident radiation from the target at two or more discrete locations and direct this collected radiation to a common combiner station. Using principles of Fourier optics, the radiation can be interfered to produce image data. The power of interferometry arises from the increased angular resolution: the resolving power of the combined optical system is a function of the separation, or baseline, between individual collectors and not on the collector sizes themselves. Quantitatively, the resolving power is still given by Eqn. 1-4, however d is now the distance *between* the collectors, rather than the *size* of a given optic. In principle, the baseline, d, and thus the resolving power can be increased without limit. Detailed accounts of interferometry theory can be found in many textbooks[30] and descriptions of space-based interferometry can be found in previous research works.[14,15,16] A basic summary will be presented here.

Qualitatively, the information in an image can be represented in two different formats. The first mode, which is most intuitively familiar, is that of a spatial intensity map. For every location (x, y coordinate) in a spatial plane some value of radiant intensity is given. Mapping the intensity values produces an image in the same fashion that the human eye/retina records optical information. The same information contained in the intensity map can be presented in a second format relating to spatial frequencies.

The spatial frequency representation of an image can most easily be understood in the context of a checker-board tile floor. A spatial intensity map summarizes the floor image by assigning an amplitude to every x, y point on the floor corresponding to, say, the brightness of the floor. One can also recognize obvious patterns in the floor that repeat themselves on a regular spatial period. If the tiles in the floor are square, then the repeating pattern in the x direction has the same period, or spatial frequency, as the pattern in the y direction; if they are rectangular the x and y patterns will have different frequencies. Specification of the spatial frequencies then yields some of the image information. For each spatial frequency in the floor, one must also specify an amplitude to fully describe all of the image information. For the square-wave pattern of the checker-board floor, a large amplitude may correspond to black and white tiles, while a smaller amplitude may represent gray and white tiles.

Fourier mathematics extends the simple qualitative tile floor analogy to images of arbitrary complexity. Any function of intensity in the physical plane (x, y space) can be represented by an infinite series of Fourier terms. Each term of the Fourier series has a spatial frequency (u, v point for x and y spatial frequencies respectively) and an amplitude coefficient. Thus, if one knows the amplitude coefficient for every spatial frequency (u, v point), the Fourier representation of the image information can be transformed to produce the more familiar spatial intensity map of the target.

In interferometry, the u-v points in the Fourier plane are obtained by separated collector points in the x-y physical plane. When light of wavelength λ collected by two spacecraft at locations (x_1, y_1) and (x_2, y_2) is combined (interfered), the resulting

interference pattern yields a single value. The single value is the complex amplitude of the Fourier term with spatial frequencies (u, v) denoted by

Eqn. 1-5

$$u = \frac{\pm\left(x_2 - x_1\right)}{\lambda}$$
$$v = \frac{\pm\left(y_2 - y_1\right)}{\lambda}$$

Thus, each unique spacecraft separation vector, or baseline, yields one term of the Fourier representation of the image. To reconstruct the image one must have information from many (theoretically an infinite number) of unique spacecraft baselines. For multiple spacecraft, the u-v coverage is represented by the correlation function of the physical coverage. For N spacecraft, each of the spacecraft has N-1 different position vectors to other vehicles in the array. Thus the total number of u-v points from an array of N spacecraft is N(N-1) plus a zero baseline point.

Judicious use of spacecraft collector assets mandates intelligent placement of the vehicles in physical space. For instance, redundant baselines (separation vectors) between vehicles in a formation produce redundant Fourier information and represent a "waste" of assets. Ideally, each of the N(N-1) u-v points should be unique. Numerous collector formation possibilities exist based upon optimization of various parameters. Golay performed a study of collector placement based upon optimization of the u-v compactness of the overall formation.[31] The resulting Golay formations are shown in Figure 1-3 for N=3, 6, 9, and 12 spacecraft. Similarly, Cornwell derived formations which were designed to optimize the uniformity of coverage in the u-v plane.[32] Representative configurations for N=3-12 spacecraft Cornwell configurations are shown in Figure 1-4.

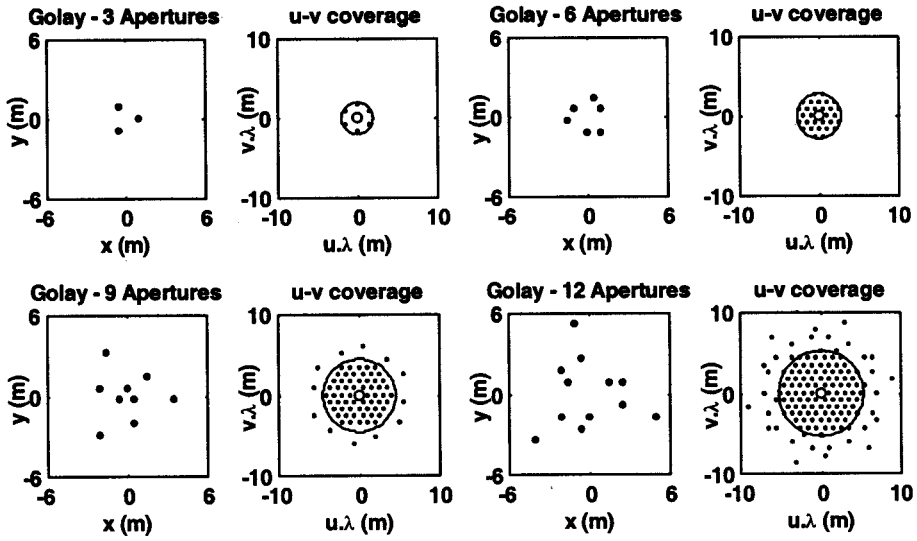

Figure 1-3. Golay interferometric formations based upon optimizing the compactness of the group in u-v space. The aperture locations in x-y space and the corresponding baselines in u-v space are plotted in adjacent diagrams. (Figure reproduced from Ref. 15)

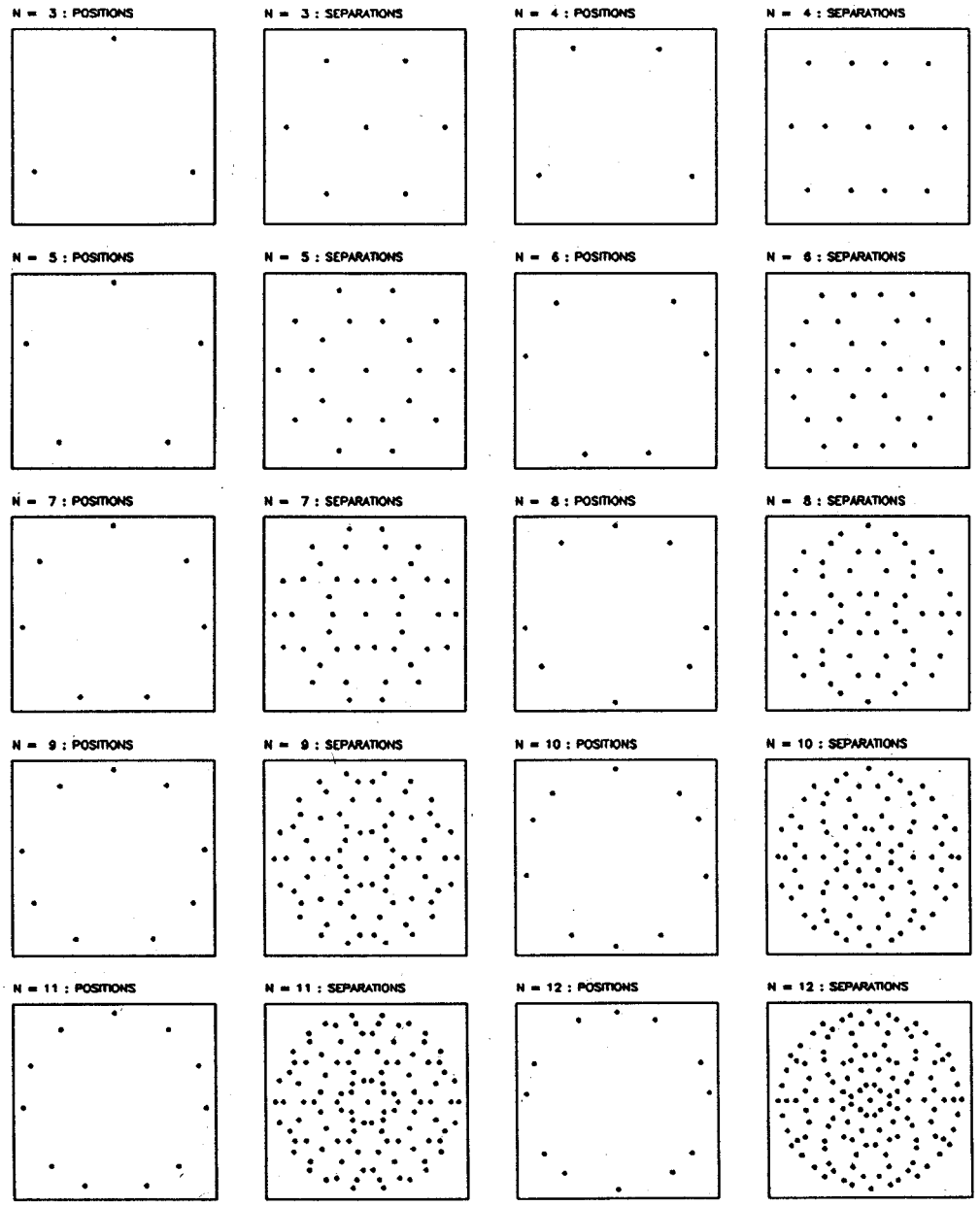

Figure 1-4. Cornwell optimized arrays for uniform u-v coverage for N=3-12. The positions of the apertures (spacecraft) are shown in x-y space, while the unique baselines (separations) show up as points in u-v space. Positions and corresponding separations are plotted in adjacent diagrams.

1.3.3. Practical Aspects of Space Interferometry

The method by which the u-v points are mapped out depends upon the nature of the target object. For static targets whose features are relatively constant (such as astronomical objects), the u-v points can be mapped out sequentially with as few as two collector spacecraft. The vehicles simply move to the specified x-y positions, record a data point, and move on to other locations. The image is then processed after a predefined number of u-v points have been recorded. Such is the method employed by missions such as Deep Space 3 and Terrestrial Planet Finder. For rapidly changing targets, such as those on the surface of the Earth, the image features must be recorded in a "snapshot" mode where all of the u-v points are obtained simultaneously. Such configurations are said to produce full, instantaneous u-v coverage. For such snapshots the number of independent collector spacecraft must be equal to the number of u-v points required to produce the image.

Inteferometric imaging in the optical regime poses a constraint on an imaging array. For lower frequencies, such as those in the radio spectrum for radar imaging, the incoming wavefront from each collector can be recorded and archived, with the actual interferometry between separate collectors performed later through post-processing. Optical signals, however, have frequencies too high to permit recording of the wavefront for post-processing. Instead, the incoming signals from two collectors must be interfered in real time at the combiner. In order to permit interference between the same wavefront from each collector, the light path length from each collector to the combiner must be equal to within a fraction of the radiation wavelength. It is clear from an examination of

Figure 1-3 and Figure 1-4 that Cornwell arrays, with all of the collector apertures lying on the circumference of a circle, are ideally suited to a central combiner for optical path symmetry, while Golay arrays are not amenable to a single combiner vehicle.

For formation-flying spacecraft performing visible imagery, the requirement of equal optical path lengths seems to present an unobtainable formation tolerance between spacecraft of a few nanometers. In practice, however, this constraint is relaxed through the use of on-board delay lines for fine control. In such a delay-line configuration, the individual spacecraft need only keep formation tolerance errors within a few centimeters, while actively controlled movable optics compensate for the coarse position errors down to the interferometry requirement. A schematic is shown in Figure 1-5. By repositioning the optics on-board one or both of the vehicles, the light from one collector can be made to traverse the same distance as that from another collector.

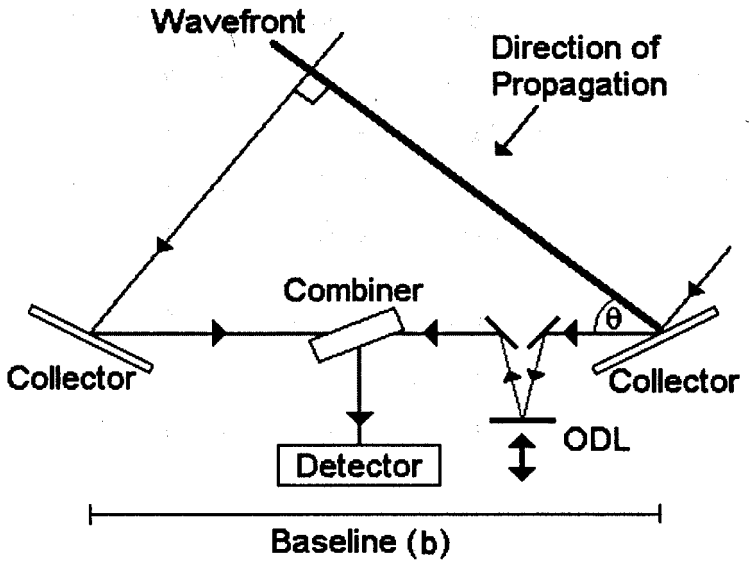

Figure 1-5. Illustration of optical delay line (ODL) for fine adjustment of science light path from collector to combiner in interferometry.

The need for full, instantaneous u-v coverage begs the question of mathematical completeness. To exactly invert the Fourier image information requires an infinite number of amplitude coefficients and, thus, an infinite number of collector locations. This is evidenced in the amount of white space representing missing u-v information in the plots of Figure 1-3 and Figure 1-4. One method for solving the completeness problem lies in post-processing techniques for image reconstruction. Another method relies on intelligent placement of finite-sized collector optics.

To extend the qualitative description of interferometry to finite-sized collectors, one can envision a single collector of diameter *d* as an assembly of sub-collector elements. Image information for u-v points represented by distances between sub-collector elements is then obtained from a single optic as shown in Figure 1-6. In fact, a single optic of diameter *d* yields an infinite number of u-v points for all baselines less than or equal to *d*. All baselines (u-v points) greater than *d* must then come from sub-elements on separated spacecraft. In terms of full, instantaneous u-v coverage, this implies that spacecraft must be separated by a distance comparable to their individual size, *d*, to avoid omission of u-v points. Thus, snapshot-style imaging requires very close formation flying.

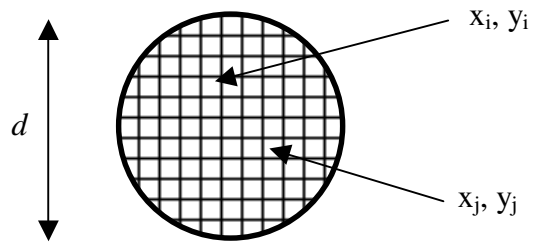

Figure 1-6. Conceptual image of single collector optic as array of sub-collectors. The elements i and j will yield interferometric information for the u-v point representing the baseline between the elements.

1.4. Research Objectives

The ultimate goal of this research is to explore the feasibility of using Coulomb forces between charged spacecraft to maintain non Keplerian formations. This includes examining the spacecraft charge requirements for a variety of formations, and evaluating the ability to implement closed-loop charge control to maintain the formations. Specific objectives of this research are shown as following:

1. Determine the required spacecraft charges within a swarm too maintain an equilibrium orbit formations.
2. Analyze the dynamic behavior of the formations analytically and numerically.
3. Investigate the stability and controllability of the satellite formations.

1.5. Overview

The remainder of the thesis is organized as follows; Chapter 2 provides some background on formation flying from the available literature. Several satellite formations are introduced in Chapter 3 along with the derivation of the dynamic equations. In Chapter 4, analytical and numerical methods are used to find the equilibrium solutions for each satellite formation discussed in Chapter 3. In Chapter 5, stability and controllability are determined for some of the most practical satellite formations. Finally, conclusions and recommendations regarding this research are discussed in Chapter 6.

1.6. Assumptions Used in Analysis

In order to determine and control the dynamic behavior of satellites within the formations, Hill's equations are used in this research. Hill's equations, also known as Clohessy-Willshire equations, are a set of linearized equations for the relative motion of multiple satellites. Hill's equations are used for a preliminary design tool before using the fully nonlinear dynamic equations. Three major assumptions are made in Hill's equations: 1.) The reference satellite is in a circular orbit, 2.) The distance between the satellites is small in comparison to their altitude to support simplification[33], 3.) The distribution force that is acting on the satellites is neglected. In addition, the spacecraft are assumed to be spherical. Furthermore, it is assumed that the ambient plasma Debye length at the formation orbital environment is much larger than the spacecraft separations. While not valid for low-Earth orbit, this assumption is reasonable for high (geostationary) orbits with separations on the order of tens of meters.

2. Literature Review

2.1. Introduction

Using several small satellites to perform the same function as one big satellite has several benefits. It not only saves launch, spacecraft bus, and payload costs, but also reduces the propulsion system mass, and increases the lifetime of the system. Several papers related to formation flying are summarized. Since the Coulomb control idea is new, there is no literature on its application to maintain spacecraft formations.

2.2. Satellite Formation Design

The goal of satellite formation flying is to maintain several satellites in a prescribed geometry appropriate to their task (e.g. imaging). A useful introduction to formation design was given in a paper by Lo[34]. One of the candidate tasks for spacecraft swarms is separated spacecraft interferometry. The reader can find more information regarding interferometry in the literature[35], however this study focuses primarily on the orbital mechanics. In this section, particular attention is given to the formation design and spacecraft dynamics. Kong, Miller and Sedwick[36] developed and compared several "free flying" formations for Earth imaging applications. All the formations were required to satisfy:

- Distances between any collector and the combiner are equal.
- Satellite separation baseline must be equivalent in the two dimensions to provide axi-symmetric angular resolution about the Line-of Sight (LOS) (see Figure 2-1).

- Full coverage of Earth imager to target the image.

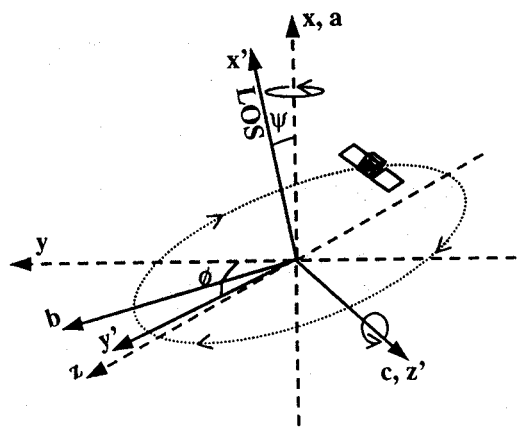

Figure 2-1. Spacecraft trajectory to Hill coordinate frame.

Hill's equations were used to analyze the motion of satellites for a geosynchronous earth orbit (GEO). Three architectures are discussed: planar circular trajectory, free elliptical trajectory, and free elliptical trajectory (with delay lines).

The spacecraft velocity impulse, Δv, can be determined given the spacecraft relative acceleration terms. Comparing the circular to the elliptical trajectories, the optimum imaging configuration is obtained using six collectors. If a large number of satellites are used, then the free elliptical trajectory is recommended to obtain the maximum imaging configuration. Also, the circular architecture required higher spacecraft velocity impulses to maintain the combiner spacecraft at a fixed location on the LOS. In addition, this paper identified that the smallest distance between each collector should be less than two apertures when operating as an Earth imaging system.

Sabol, Burns and McLaughlin investigated the stability of four basic satellite formation flying designs: in-plane, in-track, circular and projected circular formation by applying realistic perturbations on these formations[37]. Again, the formations were

derived from Hill's equations. The minimum amount of velocity impulse, Δv, is calculated to balance the J_2 disturbance force and stabilize the satellite formations. The results show that circular and projected circular formations are very unstable when the perturbation is applied. However, the in-track formation is stable. The in-plane formation will require small, infrequent, along-track maneuvers to offset the effects of atmospheric drag. Therefore, the formation-keeping cost of circular and projected circular formations is 38 times higher than in-track and in-plane formations.

Sparks[38,39] also examined the effects of the J_2 disturbance using Hill's equations. Again, the Gauss' variation of parameters was used to derive the minimum amount of velocity impulse, Δv to balance the J_2 disturbance force. A linear control law was derived and used for producing an approximately theoretical minimum amount of velocity impulse, Δv.

In addition, Sedwick, et al.[40], investigated passive formation flying. This paper first used dimensional analysis then rigorous analysis to determined the effects of perturbation. Dimensional analysis was used to derive the various scaling laws to conduct design trades. The rigorous analysis determined the perturbative effects. The higher altitude, longer period orbits allowed larger maneuvers for a given amount of fuel consumed per orbit. Also, the Δv imparted by atmospheric drag at a given orbit is proportional to cross-sectional area, and decreased with higher altitudes when the atmospheric density decreases. However, the Δv imparted by solar pressure increased with orbital altitude due to the longer period orbits.

Furthermore, Pollard, et al.[41] also described a method to determine the orbital elements of cluster constellations, to predict the cluster disruption based on the natural perturbing forces, and to calculate Δv that balanced perturbing forces in a LEO.

2.3. Satellite Formation Control

Leonard[42] controlled two spacecraft positions using the differential drag between them. In this paper, the atmospheric density was assumed uniformly and the velocities and ballistic coefficients of the satellites were assumed to be initially equal. The differential drag between two satellites is the difference in drag per unit mass acting on each satellite. The equations of motions were derived and a coordinate transformation was made to reduce the formation-keeping problem. A main control law and the eccentricity-minimizing control scheme were derived. The main control law was able to move the average position of the slave vehicles to the origin of the target reference coordinate system (i.e. zero) by reducing as much as eccentricity as possible whereas the eccentricity-minimizing control scheme activated for reducing the eccentricity when the average position of the slaves vehicles was at the target (origin). The formation-keeping problem could be formulated as the simultaneous solutions of both double integrator and harmonic oscillator. Solving both double integrator and harmonic oscillator obtained the position of slave vehicle to target.

Schaub[43] studied and discussed a spacecraft formation flying control strategy in an orbit that was in terms of specific orbit element differences, and an actual relative orbit that was measured in terms of Cartesian coordinates of the rotating chief-satellite-centric reference frame. The coordinate transformation was shown with a numerical study and a hybrid continuous feedback control law was developed.

Other similar papers that related to the control law were studied by Wang, and Hadaegh[44], and de Queiroz, et al.[45]. These papers considered the problem of coordination and control of multiple microspacecraft moving in formation in low Earth orbit (LEO). Wang and Hadaegh assumed that each microspacecraft was modeled by a fixed center of mass of a rigid body. Difference schemes for creating a formation pattern were discussed, and the explicit control laws for formation-keeping were derived. The discussions of deriving a control law, and the integration of the microspacecraft formation coordination and control system with a proposed inter-spacecraft communication or computing network were presented. The result shows that there are no collisions between the microspacecraft due to the small magnitude of the initial deviation from the desired state. De Queiroz, et al. used full nonlinear dynamics to develop a control law. Control performance was illustrated using simulation. A nonlinear adaptive control law for the relative position tracking of multiple spacecraft in formation flying was developed in this paper.

Since NASA has recognized multiple spacecraft formation flying (MSFF) as future missions, a concept of autonomous formation flying (AFF) of spacecraft constellations has been studied by numerous researchers. This concept is related to the control of relative distances and orientations between the spacecraft. Kapila[46] developed a mathematically rigorous control design framework for linear control of spacecraft relative position dynamics with guaranteed closed-loop stability. Lau[47] described AFF concept for extremely precise autonomous relative position and attitude determination for satellite formations. He often used AFF concept in Global positioning system (GPS). On the other hand, Inalhan[48] investigated precise relative sensing and control via differential

GPS for multiple spacecraft formation. He presented autonomous control architecture for formation flying, and a generalized closed-form solution of passive apertures for constellations with mean formation eccentricity.

In addition, Tan, Bainum and Strong developed a strategy that is able to keep the separation distance in between four satellites in a coplanar elliptical orbit configuration constant. This strategy generated a small angular movement in the direction of the axis with respect to the axis of the combiner satellite using the force impulse[49]. The separation distance between collectors was maintained within four percent of nominal separation distance for Keplerian orbits. The perturbation should carefully be evaluated due to the effects of atmospheric drag, Earth's obliqueness, and higher harmonics.

3. Dynamics of Charged Satellite Formations

In this section several formation geometries are introduced which will be used throughout the thesis for a variety of analyses. First, methods for computing individual spacecraft charges to maintain dynamic equilibrium are presented, along with specific numerical examples.

Similar to other work in spacecraft formation dynamics, Hill's equations are used here. Since higher order effects may be of interest in the future, the dynamic equations are first developed without any linearizing assumptions, and then reduced to Hill's equations using the conventional binomial expansion of the gravitational terms and eliminating high order terms. With an application slanted towards separated spacecraft interferometry, the central reference vehicle is referred to as a "combiner" where the surrounding vehicles are called "collectors". It is assumed that the combiner has its own station keeping system, but the collectors do not. Thus the only external forces on the collectors are the Coulomb interactions between them and the combiner.

In the remainder of this section the formation geometries are presented with specific attention given to the nomenclature used in later sections. This is followed by the dynamic equation derivation leading to a compact set of equations for both Earth orbiting and Libration point fixed formations.

3.1. Formation Geometries

Six formations were considered. Five of them were

- 3 satellites in a line (1 combiner, 2 collectors)

- 3 satellites in a plane (1 combiner, 2 collectors)
- 5 satellites in a plane (1 combiner, 4 collectors)
- 6 satellites in a plane (1 combiner, 5 collectors)
- 7 satellites in 3D dimensions (1 combiner, 6 collectors)

were assumed to have a combiner in a circular orbit (shown in Figure 3-1) with collectors positioned relative to it. The sixth case consisted of five satellites (1 combiner and 4 collectors) in a line located at a stable Earth-sun Libration point. In the remainder of this section, the six formations are described in detail with specific attention given to the parameters defining their configuration.

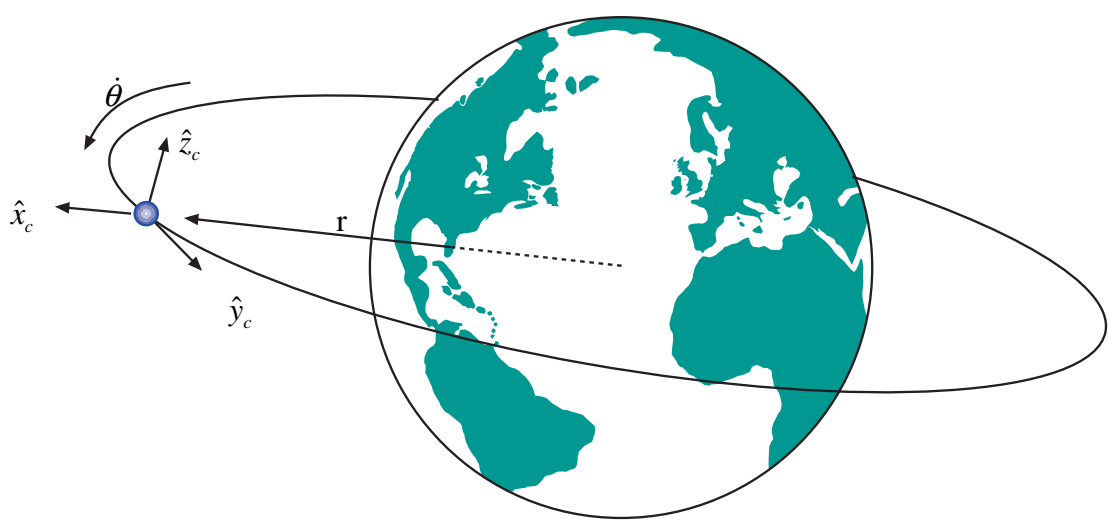

Figure 3-1. Combiner and Its Fixed Frame, {c}, in a Circular Orbit.

3.1.1. *Earth Orbiting Three Satellite - Geometry*

Three different three-satellite formations were considered. In each case the combiner (denoted with a 0 subscript) was assumed to maintain a circular orbit with radius r and true anomaly θ. The combiner-fixed rotating reference frame, denoted *{c}* and shown in Figure 3-1, was used to describe collector motion relative to the combiner.

Spacecraft charges were analytically computed such that the three satellites formed a line shown in Figure 3-2 where m_i are spacecraft masses, q_i are spacecraft charges and L is the separation between the combiner (blue) and either collector (red). The distinguishing feature of the formations was their axis alignment.

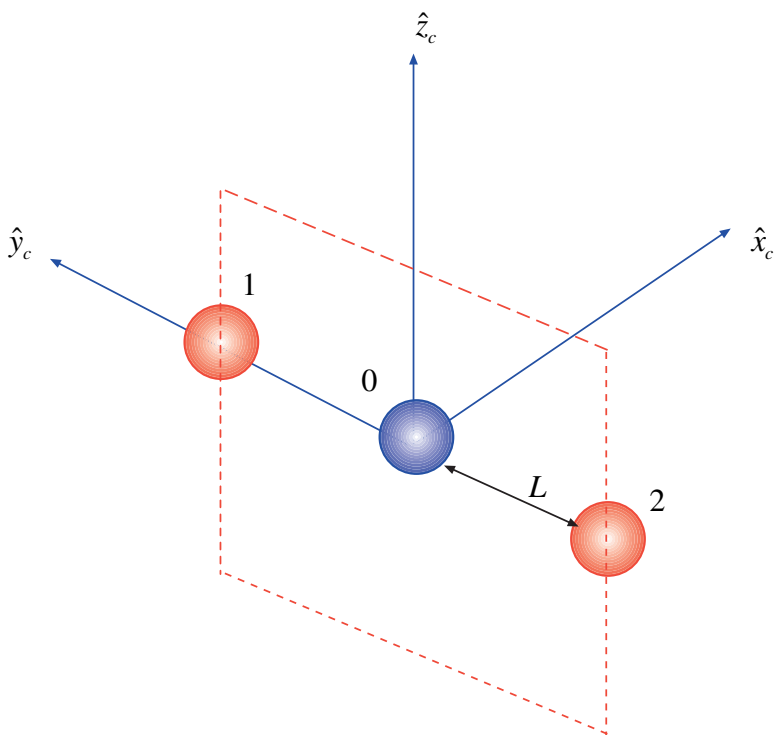

Figure 3-2. Earth Orbiting Three-satellite Formation - Geometry.

Figure 3-3 shows the three cases examined with the spacecraft aligned along the combiner fixed frame, x, y, and z axes. These "virtual tether" formations have little

imaging use, but, provided insight into the solutions of the more complicated formations considered later.

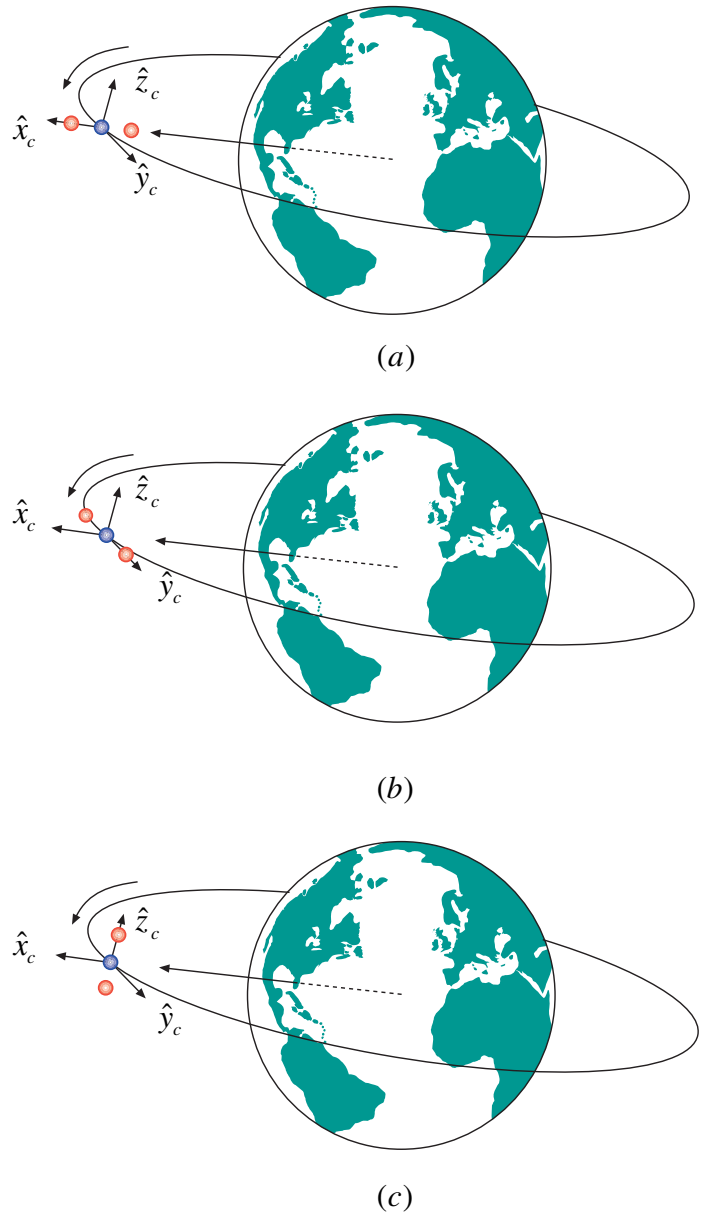

Figure 3-3. The Three Three-satellite Formations Aligned along the x, y, and z {c} Frame Axes.

3.1.2. Earth Orbiting Triangular – Geometry

Again the combiner was assumed to be in a circular orbit with radius r and true anomaly θ. Spacecraft charges were computed analytically such that two collectors

formed a triangle in the combiner fixed $\hat{x}_c - \hat{y}_c$ plane shown in Figure 3-4. Spacecraft masses are denoted as m_i, spacecraft charges as q_i, and L is the distance between the combiner and either collector. The angles between the combiner and the line on which the two collectors lie, ϕ are fixed at 45°. This formation was motivated by the stability and controllability analysis of the Earth orbiting three-satellite formation considered in Section 5.3. It helped to investigate the stability and controllability of more complex formations.

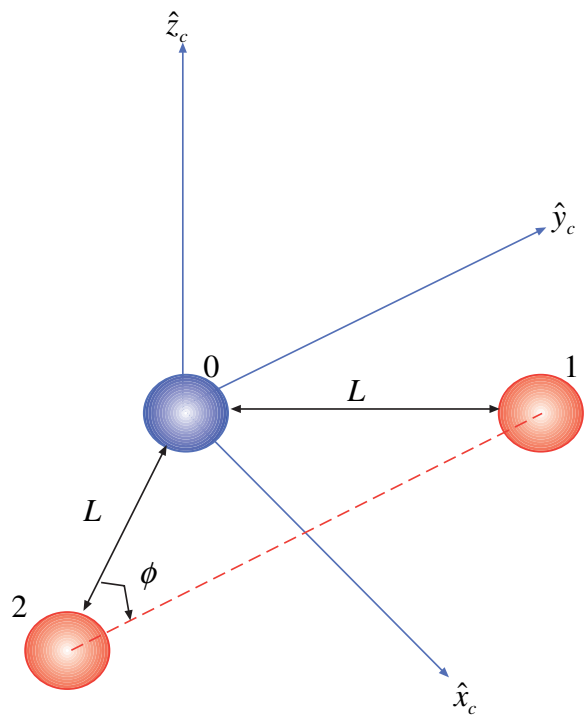

Figure 3-4. Earth Orbiting Triangular– Geometry.

3.1.3. *Earth Orbiting Five Satellite - Geometry*

As in the previous formation, the combiner was assumed to have a circular orbit with radius r and true anomaly θ shown in Figure 3-1. Spacecraft charges were analytically

determined such that the four collectors formed a square in the combiner fixed $\hat{y}_c - \hat{z}_c$ plane with side length $2L$ shown in Figure 3-5. Charges are again denoted q_i and masses as m_i. This geometry was considered as a starting-point for more practical formations that could potentially be used for Earth imaging.

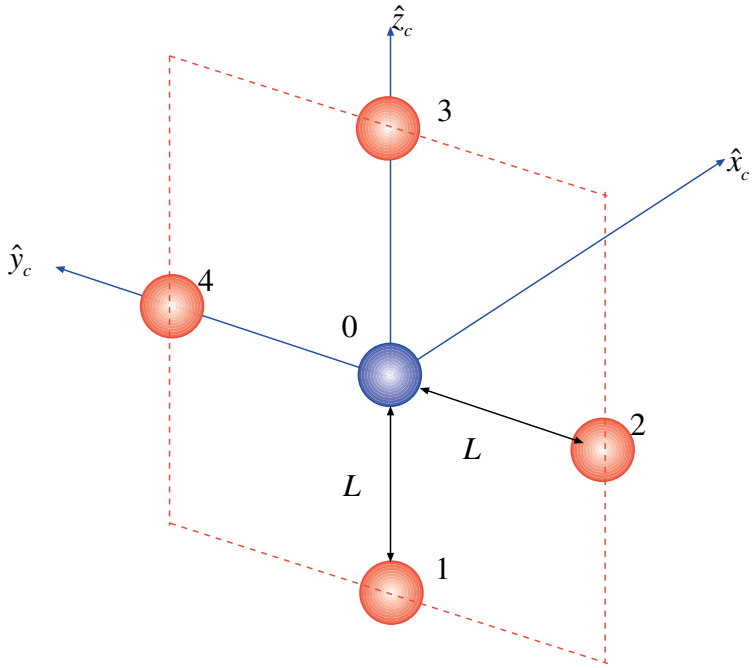

Figure 3-5. The Five-satellite Formation-Geometry.

3.1.4. Earth Orbiting Six Satellite - Geometry

Again the combiner was assumed to be in the circular orbit with radius *r* and true anomaly θ. Spacecraft charges were computed numerically such that the five collectors were in a circle of radius *L* about the combiner, in its $\hat{y}_c - \hat{z}_c$ plane. In addition, the goal was to maintain a pentagon formation, shown in Figure 3-6. This geometry represented an optimal imaging formation for full, simultaneous *u*-*v* coverage as determined by Cornwell[50].

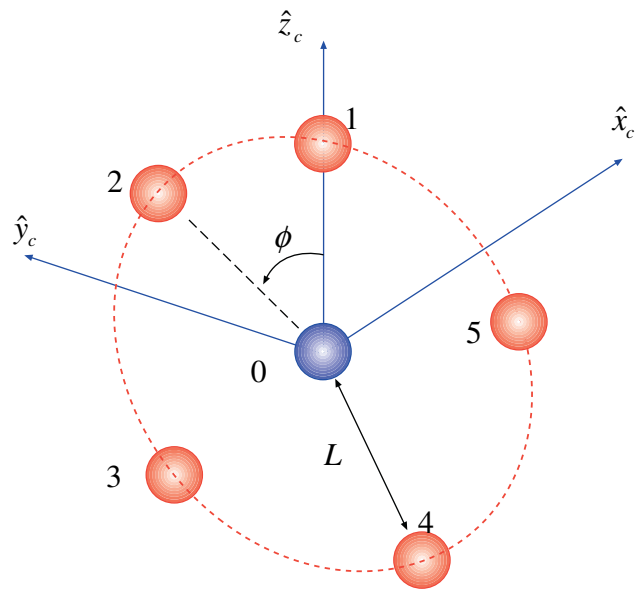

Figure 3-6. In-plane Pentagon Satellite Formation Configuration.

3.1.5. Earth Orbiting Seven Satellite – Geometry

Again, the combiner was assumed to have a circular orbit with radius r and true anomaly θ. Spacecraft charges were determined analytically such that the six collectors formed a tetrahedron shape with a separation distance L shown in Figure 3-7. Charges are again denoted q_i, and the spacecraft masses as m_i.

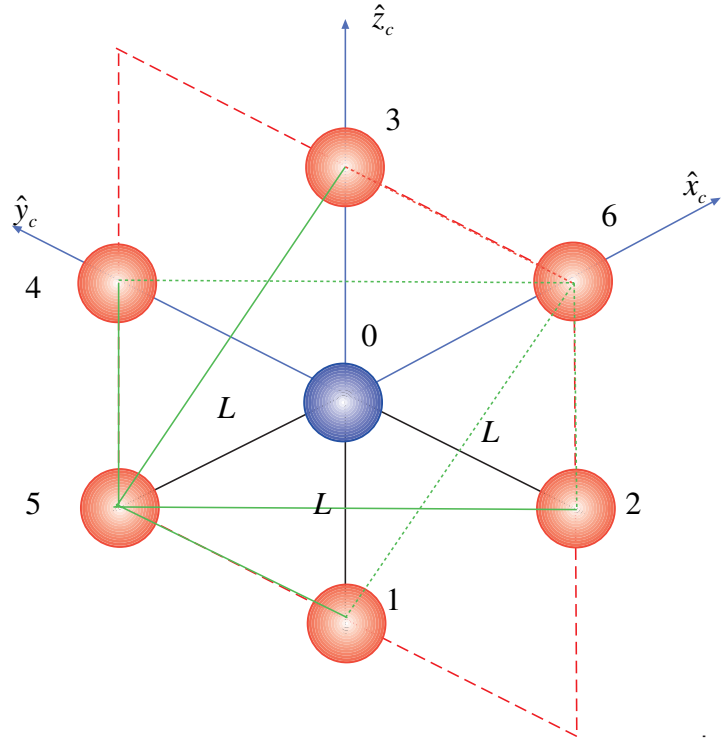

Figure 3-7. Earth Orbiting Seven Satellite – Geometry.

3.1.6. Libration Point Five Satellite – Geometry

The five satellites were assumed to be at a stable Earth-Sun Libration point aligned as shown in Figure 3-8. Charges were numerically computed such that collectors 1 and 3 had a combiner separation of L_1 and collectors 2 and 4 had a separation of $L_1 + L_2$. In addition, the system was assumed to rotate about the combiner fixed z_c-axis with angular rate Ω. This configuration was chosen for its similarity to an imaging concept being considered for NASA's Terrestrial Planet Findes mission

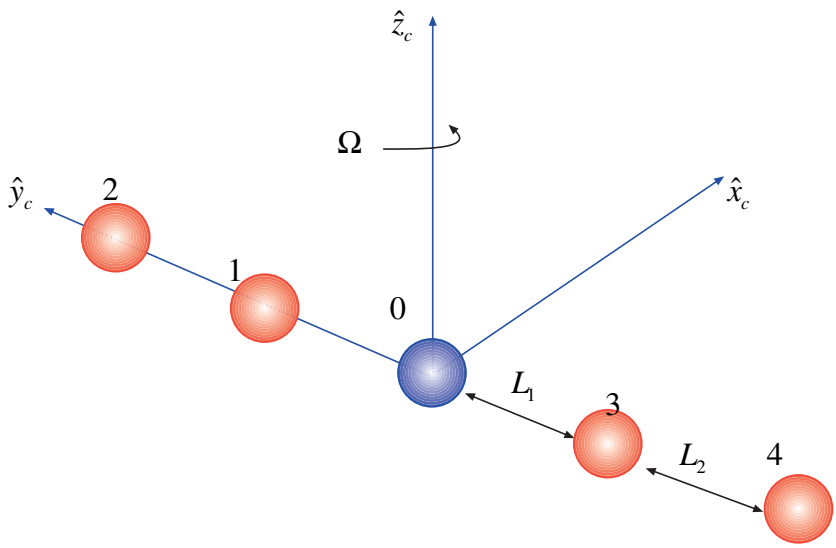

Figure 3-8. Rotating Five-satellites Formation Configuration.

3.2. *Dynamic Equations of the Formations*

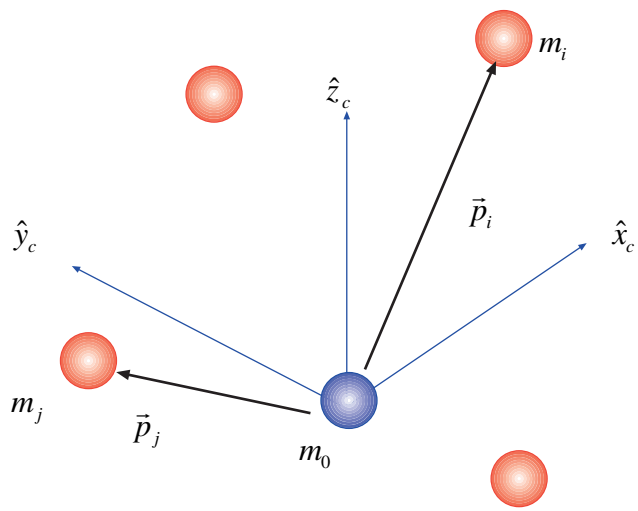

Figure 3-9. Assuming there are n collectors and one combiner, the position vector notation is illustrated for the ith and j^{th} collectors.

Figure 3-9 shows the combiner in a circular orbit along with the ith and jth collector and will aid the development of the generic dynamic equations for n collectors. Lagrange's equations will be used where initially the full nonlinear equations are developed. After imposing linearizing assumptions, the Hill equations remain with Coulomb interaction forces between spacecraft.

The position vector from the origin of the combiner-fixed frame to the ith collector is denoted $\vec{p}_i$ and has components x_i, y_i, and z_i. It should be noted that since the combiner motion is prescribed we have

Eqn. 3-1
$$x_0 = y_0 = z_0 = \dot{x}_0 = \dot{y}_0 = \dot{z}_0 = 0$$

The absolute velocity of the ith spacecraft is

Eqn. 3-2
$$\dot{\vec{p}}_i = \begin{Bmatrix} \dot{x}_i - y_i\dot{\theta} \\ \dot{y}_i + \dot{\theta}(r + x_i) \\ \dot{z}_i \end{Bmatrix}$$

from which the kinetic energy is developed according to

Eqn. 3-3
$$T = \frac{1}{2}\sum_{i=0}^{n} m_i \dot{\vec{p}}_i^T \dot{\vec{p}}_i$$

The total potential energy is expressed as the sum of the gravitational and Coulomb potential energy

Eqn. 3-4
$$V = V_g + V_c$$

The gravitational component, V_g, is

Eqn. 3-5
$$V_g = -\mu \sum_{i=0}^{n} m_i \left[(r + x_i)^2 + y_i^2 + z_i^2 \right]^{-1/2}$$

where μ is the gravitational constant, $\mu = 3.984 \times 10^{14}$. The Coulomb component, V_c, is

Eqn. 3-6

$$V_c = k_c \sum_{i=0}^{n-1} q_i \sum_{j=i+1}^{n} q_j \left[\left(x_j - x_i\right)^2 + \left(y_j - y_i\right)^2 + \left(z_j - z_i\right)^2 \right]^{-1/2}$$
$$= k_c \sum_{i=0}^{n-1} q_i \sum_{j=i+1}^{n} \frac{q_j}{\left|\vec{p}_i - \vec{p}_j\right|}$$

where k_c is Coulomb's constant given by

Eqn. 3-7

$$k_c = \frac{1}{4\pi\varepsilon_o} \approx 8.99 \times 10^9 \frac{Nm^2}{C^2}$$

and ε_0 is the electric permittivity of free space.

Applying Lagrange's equations

$$\frac{d}{dt}\frac{\partial L}{\partial \dot{q}_k} - \frac{\partial L}{\partial q_k} = 0 \qquad k = 1,\ldots,n$$

Eqn. 3-8 where

$$L = T\text{-}V$$

yields the full nonlinear dynamic equations for the ith spacecraft

Eqn. 3-9

$$\ddot{x}_i - 2\Omega\dot{y}_i - (r + x_i)\Omega^2 + \frac{\mu(r + x_i)}{\left[\left(r + x_i\right)^2 + y_i^2 + z_i^2\right]^{3/2}} = \frac{k_c}{m_i}\sum_{j=0}^{n}\frac{(x_i - x_j)}{\left|\vec{p}_i - \vec{p}_j\right|^3} q_i q_j$$
$$\ddot{y}_i - 2\Omega\dot{x}_i - y_i\Omega^2 + \frac{\mu y_i}{\left[\left(r + x_i\right)^2 + y_i^2 + z_i^2\right]^{3/2}} = \frac{k}{m_i}\sum_{j=0}^{n}\frac{(y_j - y_i)}{\left|\vec{p}_i - \vec{p}_j\right|^3} q_i q_j$$
$$\ddot{z}_i + \frac{\mu z_i}{\left[\left(r + x_i\right)^2 + y_i^2 + z_i^2\right]^{3/2}} = \frac{k}{m_i}\sum_{j=0}^{n}\frac{(z_j - z_i)}{\left|\vec{p}_i - \vec{p}_j\right|^3} q_i q_j$$
$$i = 1,\ldots,n \text{ and } i \neq j$$

The gravity terms in Eqn. 3-9 can be linearized by first expressing them as

Eqn. 3-10

$$\frac{\mu m_i (r + x_i)}{\left[(r + x_i)^2 + y_i^2 + z_i^2\right]^{3/2}} = \frac{\mu m_i (r + x_i)}{r^3 \left[1 + \frac{2x_i}{r} + \frac{1}{r^2}(x_i^2 + y_i^2 + z_i^2)\right]^{3/2}}$$

$$\frac{\mu m_i y_i}{\left[(r + x_i)^2 + y_i^2 + z_i^2\right]^{3/2}} = \frac{\mu m_i y_i}{r^3 \left[1 + \frac{2x_i}{r} + \frac{1}{r^2}(x_i^2 + y_i^2 + z_i^2)\right]^{3/2}}$$

$$\frac{\mu m_i z_i}{\left[(r + x_i)^2 + y_i^2 + z_i^2\right]^{3/2}} = \frac{\mu m_i z_i}{r^3 \left[1 + \frac{2x_i}{r} + \frac{1}{r^2}(x_i^2 + y_i^2 + z_i^2)\right]^{3/2}}$$

and then expanding them in a binomial series

Eqn. 3-11

$$(1 + z)^{\alpha} = 1 + z\alpha + \frac{2(\alpha - 1)}{2!} z^2 + \frac{\alpha(\alpha - 1)(\alpha - 2)}{3!} z^3$$

Substituting

Eqn. 3-12

$$\alpha = -3/2$$

$$z = \frac{2x_i}{r} + \frac{x_i^2 + y_i^2 + z_i^2}{r^2}$$

into Eqn. 3-11, noting that the orbital radius of the combiner is much larger than the collector position vectors (A typical value of r is 4.2×10^7 m and $|\vec{p}_i|$ is 10 m).

Eqn. 3-13

$$r >> |\vec{p}_i|$$

and keeping terms up through first order in x_i, y_i, and z_i gives

$$\frac{\mu m_i (r + x_i)}{r^3\left[(r+x_i)^2 + y_i^2 + z_i^2\right]^{3/2}} \approx m_i\Omega^2 (r + x_i)\left[1 - \frac{3x_i}{r}\right] \approx m_i\Omega^2 (r - 2x_i)$$

Eqn. 3-14

$$\frac{\mu m_i y_i}{r^3\left[(r+x_i)^2 + y_i^2 + z_i^2\right]^{3/2}} \approx m_i\Omega^2 y_i\left[1 - \frac{3x_i}{r}\right] \approx m_i\Omega^2 y_i$$

$$\frac{\mu m_i z_i}{r^3\left[(r+x_i)^2 + y_i^2 + z_i^2\right]^{3/2}} \approx m_i\Omega^2 z_i\left[1 - \frac{3x_i}{r}\right] \approx m_i\Omega^2 z_i$$

where it is noted that $\mu = r^3\Omega^2$. Replacing the gravity terms in Eqn. 3-9 with those of Eqn. 3-14 and simplifying yields the final dynamic equations for the ith spacecraft, often called Hills equations

Eqn. 3-15

$$\ddot{x}_i - 2\Omega\dot{y}_i - 3\Omega^2 x_i = \frac{k_c}{m_i}\sum_{j=0}^{n}\frac{(x_i - x_j)}{\left|\vec{p}_i - \vec{p}_j\right|^3} q_i q_j$$

$$\ddot{y}_i + 2\Omega\dot{x}_i = \frac{k_c}{m_i}\sum_{j=0}^{n}\frac{(y_i - y_j)}{\left|\vec{p}_i - \vec{p}_j\right|^3} q_i q_j$$

$$\ddot{z}_i + \Omega^2 z_i = \frac{k_c}{m_i}\sum_{j=0}^{n}\frac{(z_i - z_j)}{\left|\vec{p}_i - \vec{p}_j\right|^3} q_i q_j$$

$$i = 1,\ldots,n \text{ and } i \neq j$$

The dynamic equations of the three Earth orbiting formations of Section 3.1.1 through Section 3.1.5 are obtained directly from Eqn. 3-15 by setting n equal to the number of collectors, or, 2, 4, 5, and 6 respectively. The dynamic equations of the Libration point formation of Section 3.1.6 are readily obtained from Eqn. 3-9. For this case $\mu = 0$ and $r = 0$ from the Libration point assumption. The angular rate Ω is now the angular rate of the system about its center of mass instead of the angular rate of the combiner about the Earth. Finally, the combiner station-keeping assumption is relaxed allowing it to have

three degrees of freedom just like the collectors. Applying these conditions to Eqn. 3-9 yields the dynamic equations

Eqn. 3-16

$$\begin{aligned}
\ddot{x}_i - 2\Omega\dot{y}_i - \Omega^2 x_i &= \frac{k_c}{m_i}\sum_{j=0}^{n}\frac{\left(x_i - x_j\right)}{\left|\vec{p}_i - \vec{p}_j\right|^3} q_i q_j \\
\ddot{y}_i + 2\Omega\dot{x}_i - \Omega^2 y_i &= \frac{k_c}{m_i}\sum_{j=0}^{n}\frac{\left(y_i - y_j\right)}{\left|\vec{p}_i - \vec{p}_j\right|^3} q_i q_j \\
\ddot{z}_i &= \frac{k_c}{m_i}\sum_{j=0}^{n}\frac{\left(z_i - z_j\right)}{\left|\vec{p}_i - \vec{p}_j\right|^3} q_i q_j \\
i = 0,\ldots,4 \; and \; i &\neq j
\end{aligned}$$

3.3. Summary

The main result of this section was the formation descriptions and the dynamic equations of charged spacecraft, Eqn. 3-15 and Eqn. 3-16. These will be used extensively in Chapter 4 where equilibrium solutions for each formation are investigated.

4. Equilibrium Solutions

Analytical and numerical methods were used to find equilibrium solutions for the six constellations introduced in Chapter 3. The three-satellite formations (Section 3.1.1 and 3.1.2), five-satellite formation (Section 3.1.3), and seven-satellite formation (Section 3.1.5) were solved analytically. The six-satellite formation and the Libration point five satellite formation (Section 3.1.4 and Section 3.1.6) were solved numerically due to the complexity of the equilibrium equations. In all cases the equilibrium equations were developed by setting the relative speeds and accelerations to zero in the dynamic equations of Eqn. 3-15 and Eqn. 3-16,

Eqn. 4-1

$$\begin{aligned} \dot{x}_i &= \dot{y}_i = \dot{z}_i = 0 \\ \ddot{x}_i &= \ddot{y}_i = \ddot{z}_i = 0 \\ & i = 1,\ldots,n \end{aligned}$$

For the Earth orbiting formations described by Eqn. 3-15, the equilibrium equations are

Eqn. 4-2

$$\begin{aligned} -3\Omega^2 x_i &= \frac{k_c}{m_i}\sum_{j=0}^{n}\frac{\left(x_i - x_j\right)}{\left|\vec{p}_i - \vec{p}_j\right|^3} q_i q_j \\ 0 &= \frac{k_c}{m_i}\sum_{j=0}^{n}\frac{\left(y_i - y_j\right)}{\left|\vec{p}_i - \vec{p}_j\right|^3} q_i q_j \\ \Omega^2 z_i &= \frac{k_c}{m_i}\sum_{j=0}^{n}\frac{\left(z_i - z_j\right)}{\left|\vec{p}_i - \vec{p}_j\right|^3} q_i q_j \\ & i = 1,\ldots,n \text{ and } i \neq j \end{aligned}$$

while for the Earth-Sun Libration point five-satellite formation described by Eqn. 3-16 the equilibrium equations are

$$-\Omega^2 x_i = \frac{k_c}{m_i}\sum_{j=0}^{n}\frac{(x_i - x_j)}{\left|\vec{p}_i - \vec{p}_j\right|^3} q_i q_j$$

$$-y_i\Omega^2 = \frac{k_c}{m_i}\sum_{j=0}^{n}\frac{(y_i - y_j)}{\left|\vec{p}_i - \vec{p}_j\right|^3} q_i q_j$$

Eqn. 4-3

$$0 = \frac{k_c}{m_i}\sum_{j=0}^{n}\frac{(z_i - z_j)}{\left|\vec{p}_i - \vec{p}_j\right|^3} q_i q_j$$

$$i = 0,\ldots,4 \; and \; i \neq j$$

In the remainder of the section the equilibrium equations are explored for each formation. Specifically, the formation constraints are first imposed often resulting in simpler equilibrium equations. Equilibrium solutions are obtained. In addition spacecraft charges, q_i, will be replaced with the more relevant spacecraft voltage according to Gauss' law, written here in terms of the Coulomb's constant k_c

Eqn. 4-4

$$q_i = \frac{V_i r_i}{k_c}$$

where V_i is the spacecraft voltage and r_i is the spacecraft radius, assuming the spacecraft is spherical.

4.1. Earth Orbiting Three Satellite Formation - Equilibrium

As described in Section 3.1.1, three different three-satellite formations were considered categorized according to their axis alignment. The equilibrium equations for each case were developed by setting $n = 2$ in Eqn. 4-2, along with the appropriate values

of x_i, y_i, and z_i based on axis alignment constraints. For each axis alignment case the specific equilibrium equations are developed and solved below.

4.1.1. X-Axis Aligned Equilibrium Solutions

For three spacecraft aligned along the combiner coordinate frame's x_c-axis as shown in Figure 3-3(a) require the following relative displacement constraints

Eqn. 4-5
$$\begin{aligned} x_1 &= L \\ x_2 &= -L \\ y_1 &= y_2 = z_1 = z_2 = 0 \end{aligned}$$

where L is the distance from the combiner to either collector. Forming all six of the equilibrium equations from Eqn. 4-2 and eliminating duplicate equations leaves only two equations.

Eqn. 4-6
$$\frac{k_c q_1 q_2}{4L^2} + \frac{k_c q_1 q_0}{L^2} + 3m_1 L\Omega^2 = 0$$

Eqn. 4-7
$$\frac{k_c q_1 q_2}{4L^2} + \frac{k_c q_2 q_0}{L^2} + 3m_2 L\Omega^2 = 0$$

If we further assume that the collectors have equal mass, $m = m_1 = m_2$ and introducing the normalized charges defined by

Eqn. 4-8
$$q_{0n} = \frac{q_0}{\sqrt{mL^3}} \qquad q_{1n} = \frac{q_1}{\sqrt{mL^3}} \qquad q_{2n} = \frac{q_2}{\sqrt{mL^3}}$$

allows Eqn. 4-6 and Eqn. 4-7 to be written without explicit mass and length dependencies

Eqn. 4-9
$$\begin{aligned} \frac{k_c q_{1n} q_{2n}}{4} + k_c q_{1n} q_{0n} + 3\Omega^2 &= 0 \\ \frac{k_c q_{1n} q_{2n}}{4} + k_c q_{2n} q_{0n} + 3\Omega^2 &= 0 \end{aligned}$$

where the subscript n denotes a normalized quantity. If we further define the normalized spacecraft voltage

Eqn. 4-10
$$V_{in} = k_c q_{in}$$

then the equilibrium equations of Eqn. 4-9 are

Eqn. 4-11
$$\begin{aligned} V_{1n}V_{2n} + 4V_{1n}V_{0n} + 12k_c\Omega^2 &= 0 \\ V_{1n}V_{2n} + 4V_{2n}V_{0n} + 12k_c\Omega^2 &= 0 \end{aligned}$$

These are readily solved analytically. Given a suitable combiner spacecraft voltage, V_{0n}, the two collectors voltages must be equal and are

Eqn. 4-12
$$V_{1n} = V_{2n} = -2V_{0n} \pm 2\sqrt{V_{0n}^2 - 3k_c\Omega^2}$$

where the collector voltage must satisfy the constraint

Eqn. 4-13
$$V_{0n}^2 - 3k_c\Omega^2 \geq 0$$

Knowing the actual collector mass, m, radius, r, separation, L, and the orbital angular rate Ω, the equilibrium collector voltage can be obtained from Eqn. 4-12 and the normalization relationship

Eqn. 4-14
$$V_{in} = \frac{V_i r_i}{\sqrt{mL^3}}$$

where the quantity $V_i r_i$ is called the *reduced charge* of spacecraft i. The normalized collector voltages, obtained from Eqn. 4-12, are shown in Figure 4-1 as a function of the combiner voltage, V_{0n}. The angular rate Ω is for a geosynchronous orbit, Ω = 7.2915×10^{-5} rad/s.

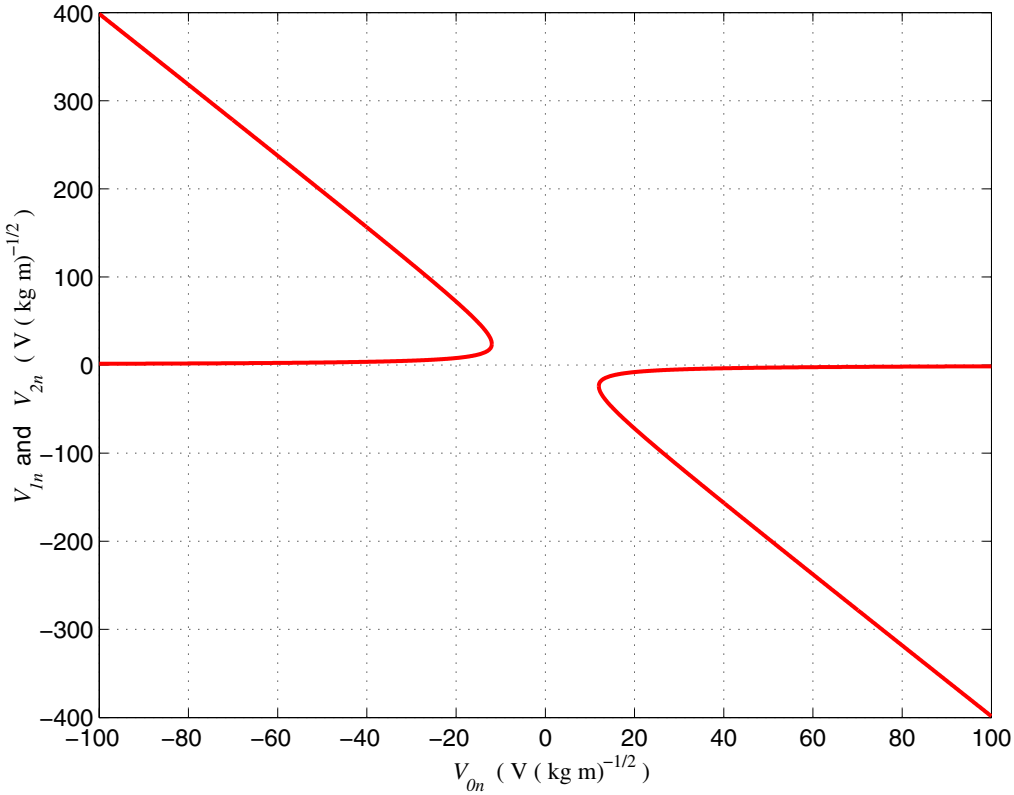

Figure 4-1. Normalized collector charges for a range of combiner charges for the 3-satellite, x-axis aligned formation

Given any valid combiner potential V_{0n} , there exist two collector voltages, one being much smaller in magnitude than the other. It is clear that the sign of the collector voltage must be opposite that of the combiner. Furthermore, the solutions on the negative V_{on} axis are the same as on the positive V_{0n} axis except for a difference in sign.

Better resolution on the solutions is obtained by examining them on a log-log plot as shown in Figure 4-2.

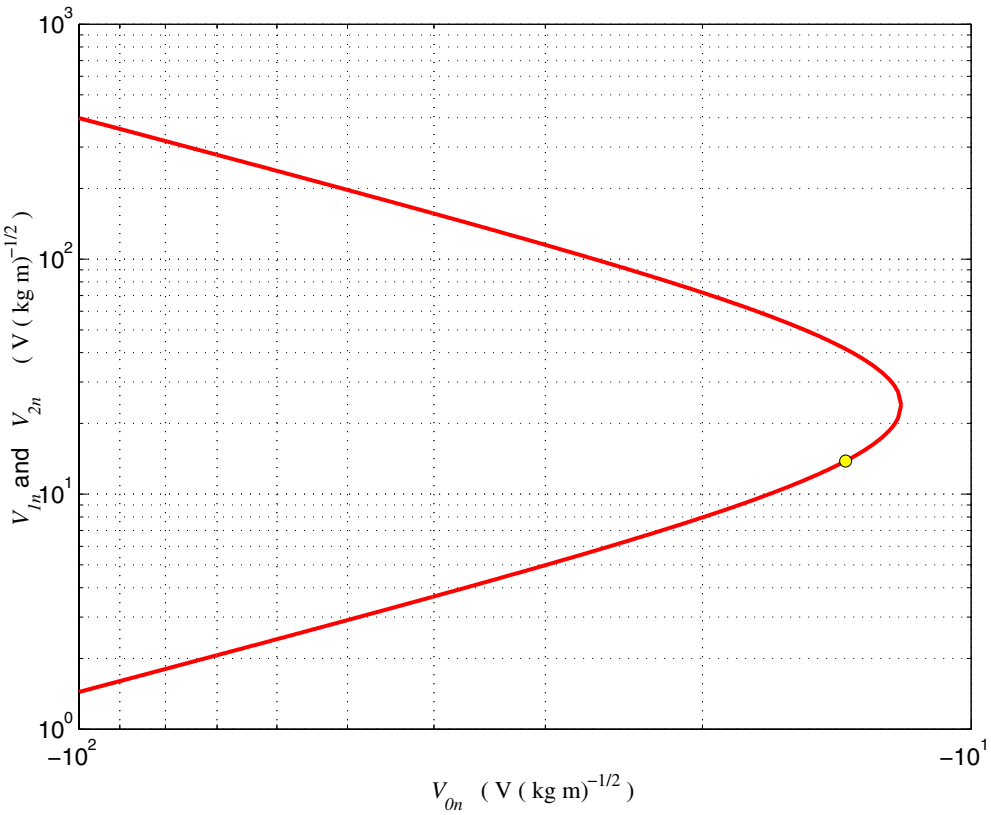

Figure 4-2. Collector equilibrium charges for negative combiner charges using a log-log scale. An "optimal" charge set is shown with the yellow dot.

If the combiner and collector have equal charging capability, then it may be prudent to find the lowest charge solution. This is obtained analytically by solving Eqn. 4-1 with the added constraint that $V_{1n} = -V_{0n}$, that is,

Eqn. 4-15 $$-V_{0n} = -2V_{on} - 2\sqrt{V_{on}^2 - 3k_c\Omega^2}$$

which gives

Eqn. 4-16 $$V_{0n} = 2\Omega\sqrt{k_c}$$

and is shown on Figure 4-2 as a yellow dot, and in 13.8 V (kg m)$^{-1/2}$ for a geosynchronous orbit.

Given that the angular rate, Ω is

Eqn. 4-17
$$\Omega = \sqrt{\frac{\mu}{R^3}}$$

where μ is gravitational constant and R is the orbit radius which is given as 4.2×10^7 m. Substituting Eqn. 4-17 into Eqn. 4-16 gets

Eqn. 4-18
$$V_{0n} = 2\sqrt{\frac{\mu k_c}{R^3}}$$

From the constraint that $V_{1n} = -V_{0n}$, the relationship of V_{1n} for a range of orbit radii is shown in Figure 4-3. The normalized voltage of spacecraft decreases with increasing the orbit radii.

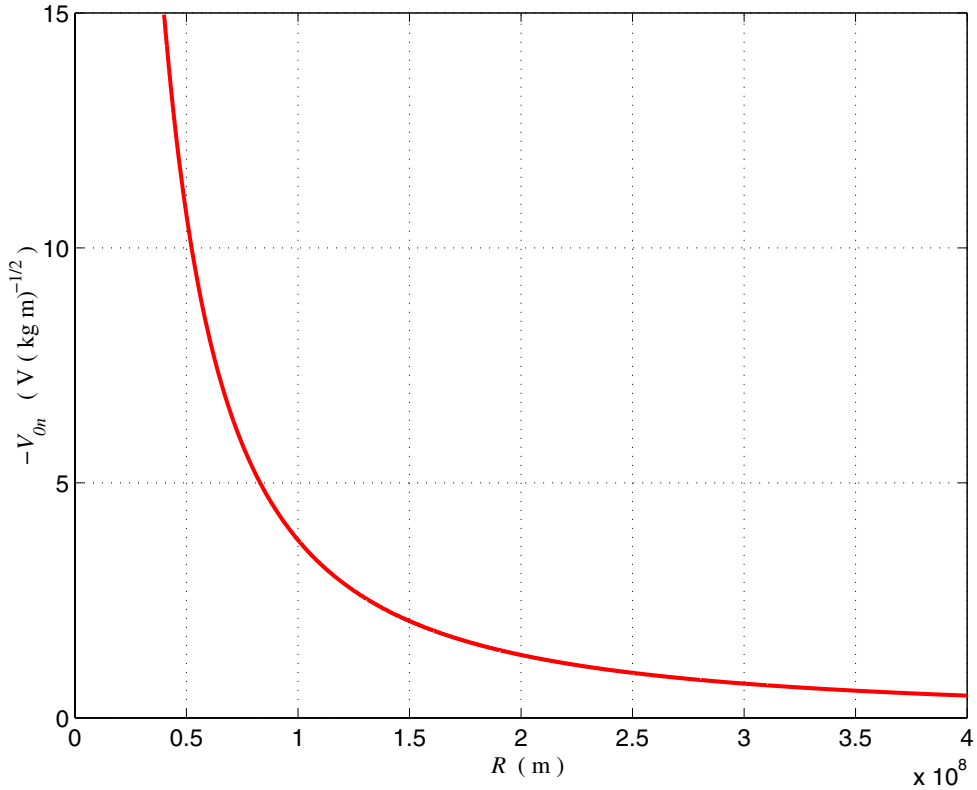

Figure 4-3. Collector equilibrium charges for a range of orbit radii

For a typical set of collector mass and spacing parameters

Eqn. 4-19
$$m = 150kg$$
$$L = 10m$$

the minimum collector charges can be determined from Eqn. 4-14 and Eqn. 4-16

Eqn. 4-20
$$V_1 \cdot r = V_2 \cdot r = 2\Omega\sqrt{k_c} \cdot \sqrt{mL^3} = (13.8)(387.3) = 5.34kV \cdot m$$

assuming a spacecraft radius of r = 1m, the vehicles must maintain a voltage of 5.34 kV to stay in equilibrium.

4.1.2. Y-Axis Aligned Equilibrium Solutions

Here the three satellites are aligned along the combiner's y_c-axis as shown in Figure 3-3(b), the corresponding collector displacements are

Eqn. 4-21
$$\begin{aligned} y_1 &= L \\ y_2 &= -L \\ x_1 &= x_2 = z_1 = z_2 = 0 \end{aligned}$$

where L is again the distance from the combiner to either collector.

Substituting Eqn. 4-21 into Eqn. 4-2 for $n = 2$, the unique equilibrium equations are simply

Eqn. 4-22
$$\begin{aligned} q_2 q_1 + 4 q_0 q_1 &= 0 \\ q_1 q_2 + 4 q_0 q_2 &= 0 \end{aligned}$$

Since in this case there is no mass or separation dependency, charge normalization is not employed. In addition, there is no dependency on the combiner angular rate, Ω. The solution to Eqn. 4-22 is simply

Eqn. 4-23
$$q_1 = q_2 = -4 q_0$$

or in terms of the collector voltages

Eqn. 4-24
$$V_1 = V_2 = -4 V_0$$

where it is assumed that the radii of the collectors and the combiner are equal. This rather simple result is plotted in Figure 4-4 where it is noted that the trivial solution of setting all charges to zero and letting the formation free-fly is permitted.

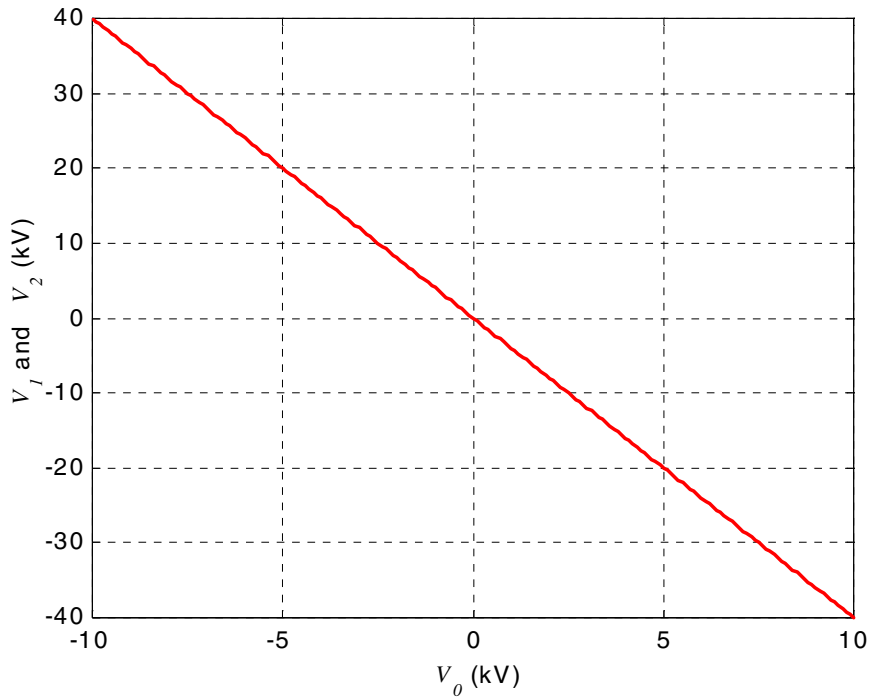

Figure 4-4. Collector voltages as a function of combiner voltage for the three satellite, y-axis aligned formation.

4.1.3. Z-Axis Aligned Equilibrium Solutions

Consider the three satellites aligned along the combiner's z_c-axis shown in Figure 3-3(c). The corresponding combiner displacements are

Eqn. 4-25

$$\begin{aligned} z_1 &= L \\ z_2 &= -L \\ x_1 &= x_2 = y_1 = y_2 = 0 \end{aligned}$$

Substituting Eqn. 4-25 into Eqn. 4-2 and letting $n = 2$ yields 2 unique equilibrium equations

Eqn. 4-26

$$\frac{k_c q_1 q_2}{4L^2} + \frac{k_c q_1 q_0}{L^2} - m_1 L\Omega^2 = 0$$
$$\frac{k_c q_1 q_2}{4L^2} + \frac{k_c q_2 q_0}{L^2} - m_2 L\Omega^2 = 0$$

which when normalized using Eqn. 4-8 and Eqn. 4-10 yield

Eqn. 4-27

$$V_{1n}V_{2n} + 4V_{1n}V_{0n} - 4k_c\Omega^2 = 0$$
$$V_{1n}V_{2n} + 4V_{2n}V_{0n} - 4k_c\Omega^2 = 0$$

assuming that the collector masses are equal as well as all spacecraft radii.

The solution to Eqn. 4-27 again requires that the two collectors have equal charge and is

Eqn. 4-28

$$V_{1n} = V_{2n} = -2V_{0n} \pm 2\sqrt{V_{0n}^2 + k_c\Omega^2}$$

Unlike the x_c-axis aligned case of Section 4.1.1 there is no constraint on the combiner charge. The normalized collector voltages are shown in Figure 4-5 for a range of combiner charges

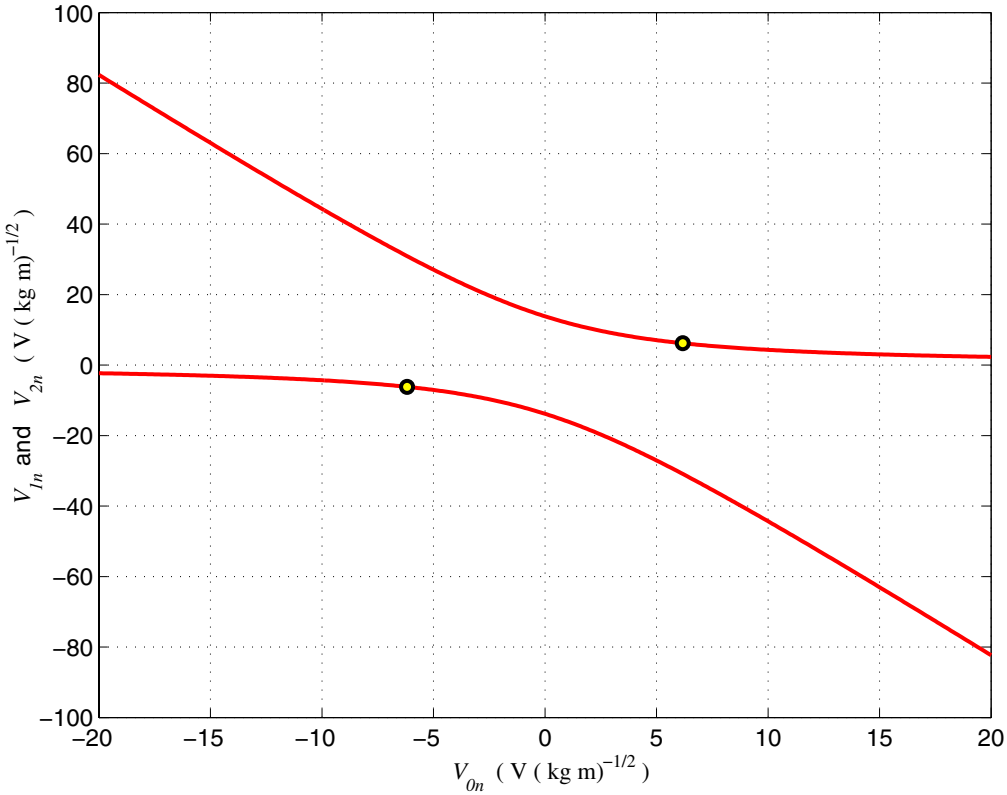

Figure 4-5. Normalized collector voltages for a range of combiner voltages for a geosynchronous orbit. The yellow dots indicate “optimal” voltages.

Similar to the x_c-axis aligned solution, there are two equilibrium voltages for any combiner voltage, one small and one large. However, the small-charge solution is now of the same sign as the combiner, and the large-charge solution of opposite sign. Assuming all the spacecraft have the same radius, an optimal normalized voltage (lowest total charge in formation)can be computed by forcing the collector voltage to be equal to the combiner. This results in all spacecraft having the same voltage given by

Eqn. 4-29 $$V_{0n} = V_{1n} = V_{2n} = \pm\Omega\sqrt{\frac{4}{5}k_c}$$

and is 6.18 V(kg m)$^{-1/2}$ units for geosynchronous orbit. Substituting Eqn. 4-17 into Eqn. 4-29 gets

Eqn. 4-30 $$V_{0n} = V_{1n} = V_{2n} = \pm\sqrt{\frac{4k_c\mu}{5R^3}}$$

The normalized voltages of the combiner and collector contain same charge in both positive and negative sign. The relationship of combiner (or similar collector) equilibrium voltages for a range of orbit radii is shown on Figure 4-6. Again, the normalized voltage of spacecraft decreases with increasing the orbit radii.

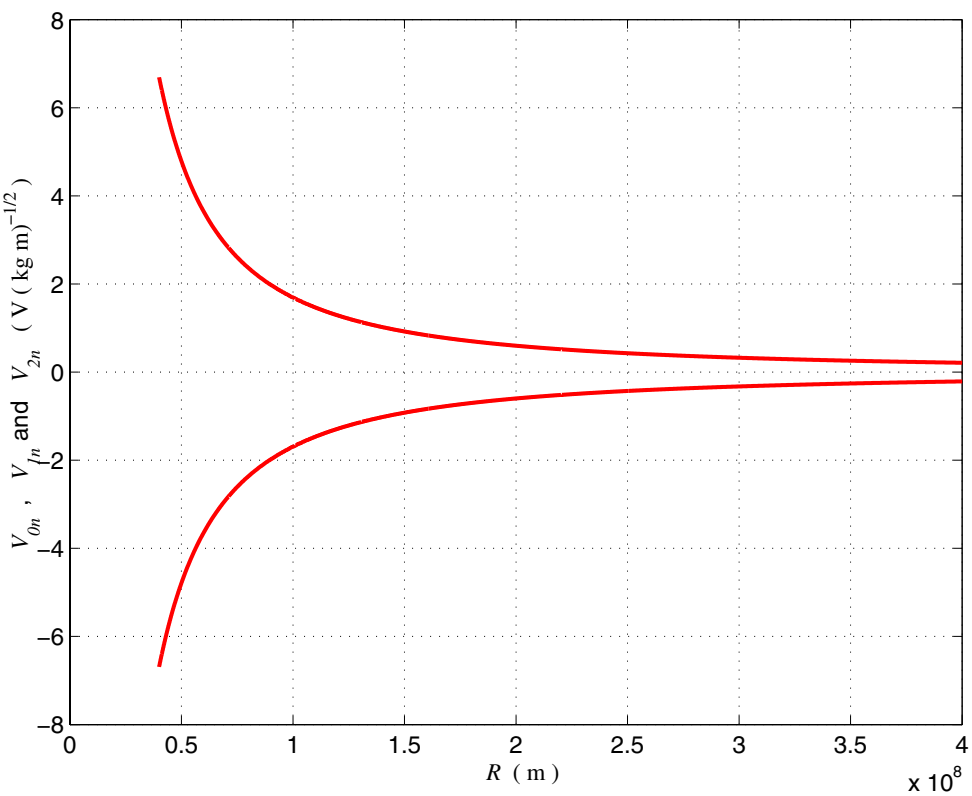

Figure 4-6. Combiner (or collector) equilibrium voltage for a range of orbit radii

Using the same "typical" spacecraft and spacing parameters of Eqn. 4-19, the optimal spacecraft voltages, relative to their equal radii are

Eqn. 4-31 $$V_0 \cdot r = V_1 \cdot r = V_2 \cdot r = \pm\Omega\sqrt{\frac{4}{5}k_c} \cdot \sqrt{mL^3} = (6.18)(387.3) = 2.39kV \cdot m$$

Table 4-1 summarized the results of the spacecraft reduced charges at equilibrium state for three-satellite formation aligned in the x_c and z_c- axis. The equilibrium solutions of the spacecraft reduced charges at y_c-axis are not required for holding the satellite because they were on the reference Keplerian orbit.

Table 4-1. Equilibrium solution spacecraft reduced charges for three-satellite case in geosynchronous orbit for 150 kg spacecraft separated by L = 10 m.

Cases	Optimal Reduced Charges (kV m)		
	V_0 r	V_1 r	V_2 r
x_c	13.8	-13.8	-13.8
z_c	±2.39	±2.39	±2.39

The spacecraft require more voltage to maintain equilibrium in the x_c-axis than z_c-axis. Referring Figure 3-1, the spacecraft are at a higher orbit than geosynchronous when aligned in the x_c-axis. However, when the spacecraft aligned at the z_c-axis, they are at the geosynchronous altitude but constantly changing its nodal crossing.

4.2. Earth Orbiting Triangle Satellite Formation – Equilibrium

As described in the previous chapter, the Earth orbiting triangle satellite formation is shown in Figure 3-4. The equilibrium equations were derived by setting n = 2 in Eqn. 4-2, along with appropriate values of x_i, y_i, and z_i based on the spacing requirements. The relative constraint displacements are given as

Eqn. 4-32

$$
\begin{aligned}
x_1 &= x_2 = L\cos\varphi \\
y_1 &= L\sin\varphi \\
y_2 &= -L\sin\varphi \\
z_1 &= z_1 = 0
\end{aligned}
$$

where L is the distance between the combiner and each collector, and ϕ is the angle between the combiner and the line on which the two collectors lie. Substituting Eqn. 4-32 into Eqn. 4-2 and assuming the masses of the collectors are the same, i.e. $m_1 = m_2 = m$, the equilibrium equations are reduced to the four unique conditions presented in Eqn. 4-33.

Eqn. 4-33

$$
\begin{aligned}
&\frac{\sqrt{2}k_c}{2L^2}q_0q_1 + \frac{3\sqrt{2}}{2}mL\Omega^2 = 0 \\
&\frac{\sqrt{2}k_c}{2L^2}q_0q_1 + \frac{k_c}{2L^2}q_1q_2 = 0 \\
&\frac{\sqrt{2}k_c}{2L^2}q_0q_2 + \frac{3\sqrt{2}}{2}mL\Omega^2 = 0 \\
&\frac{\sqrt{2}k_c}{2L^2}q_0q_2 + \frac{k_c}{2L^2}q_1q_2 = 0
\end{aligned}
$$

Using the normalized charge definition (Eqn. 4-8) applied to Eqn. 4-33 eliminates the explicit mass and length dependencies, yielding

Eqn. 4-34

$$
\begin{aligned}
&\frac{\sqrt{2}k_c}{2}q_{0n}q_{1n} + \frac{3\sqrt{2}}{2}\Omega^2 = 0 \\
&\frac{\sqrt{2}k_c}{2}q_{0n}q_{1n} + \frac{k_c}{2}q_{1n}q_{2n} = 0 \\
&\frac{\sqrt{2}k_c}{2}q_{0n}q_{2n} + \frac{3\sqrt{2}}{2}\Omega^2 = 0 \\
&\frac{\sqrt{2}k_c}{2}q_{0n}q_{2n} + \frac{k_c}{2}q_{1n}q_{2n} = 0
\end{aligned}
$$

where the subscript n denotes a normalized quantity. Employing the definition of the normalized spacecraft voltage (Eqn. 4-10), the equilibrium equations are further simplified to

Eqn. 4-35

$$\begin{aligned}
&\frac{\sqrt{2}}{2}V_{0n}V_{1n} + \frac{3\sqrt{2}}{2}k_c\Omega^2 = 0 \\
&\frac{\sqrt{2}}{2}V_{0n}V_{1n} + \frac{1}{2}V_{1n}V_{2n} = 0 \\
&\frac{\sqrt{2}}{2}V_{0n}V_{2n} + \frac{3\sqrt{2}}{2}k_c\Omega^2 = 0 \\
&\frac{\sqrt{2}}{2}V_{0n}V_{2n} + \frac{1}{2}V_{1n}V_{2n} = 0
\end{aligned}$$

By observation, the two collector spacecraft voltages must be equal, i.e. $V_{1n} = V_{2n}$, leaving only two unique equations while can be solved analytically. Interestingly, the solution for any given orbital radius is simply a point, specifically.

Eqn. 4-36

$$V_{0n} = \mp\frac{3k_c\Omega^2}{V_{1n}}$$

where

Eqn. 4-37

$$V_{1n} = V_{2n} = \pm\sqrt{3\sqrt{2}k_c\Omega^2}$$

Knowing the actual collector mass m, radius r, separation L, and the orbital angular rate Ω, the normalized combiner voltages V_{0n} can be obtained. Figure 4-7 compares the single point solution of this section (blue dots) to the loci of solutions for three satellites aligned along the x_c-axis presented previously (Section 4.1.1).

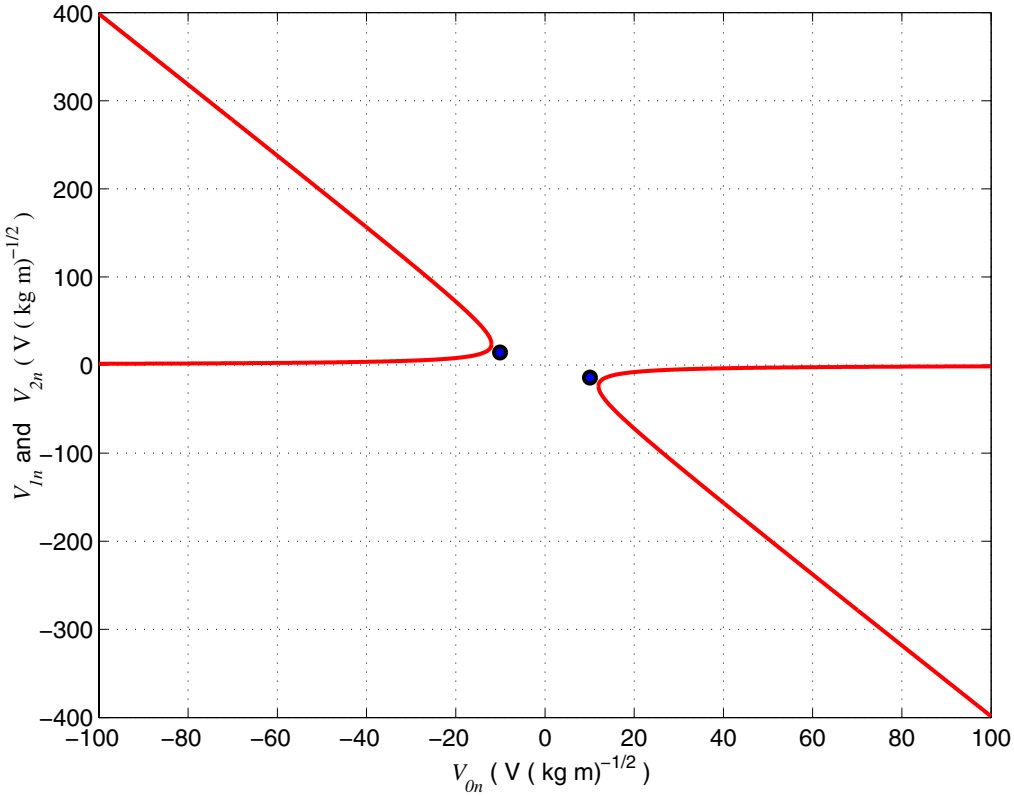

Figure 4-7. Normalized collector charges for the triangle satellite formation and the three-satellite formation aligned at the x-axis

The collector charges for triangular formation are less than the three-satellite aligned along x_c –axis because the separation between collectors 1 and 2 is smaller in triangular formation. Using Eqn. 1-3 to determine the total Coulomb force exert on collector 1 in three-satellite formation aligned at the x_c-axis (see Figure 3-2), the attraction force and repulsion force on collector 1 are

Eqn. 4-38

$$F_{attraction} = F_{10} = \frac{1}{4\pi\varepsilon_0}\frac{q_0 q_1}{L^2}$$

$$F_{repulsion} = F_{12} = \frac{1}{4\pi\varepsilon_0}\frac{q_1 q_2}{(2L)^2}$$

Since the attraction force and repulsion force exert on collector 1 should be equal, and $q_1 = q_2$ from equilibrium solution, so Eqn. 4-38 becomes

Eqn. 4-39
$$q_1 = 4q_0$$

However, in triangular formation (see Figure 3-4), the attraction and repulsion force exert on collector 1 are

Eqn. 4-40
$$F_{attraction} = F_{10} = \frac{1}{4\pi\varepsilon_0}\frac{q_0 q_1}{L^2}$$
$$F_{repulsion} = F_{12} = \frac{1}{4\pi\varepsilon_0}\frac{q_1 q_2}{\left(\sqrt{2}L\right)^2}$$

When the attraction force is equal to repulsion force at collector 1 and $q_1 = q_2$ from equilibrium solution gets

Eqn. 4-41
$$q_1 = 2q_0$$

Comparing the charge of collector 1 in the two different formations by assuming q_0 as constant, the charge of collector 1 in the triangular formation is less than three-satellite formation aligned at the x_c-axis due to the smaller separation between collectors 1 and 2.

In order to better view the solutions, a log-log scale is plotted and shown in Figure 4-8. The blue dot is the only solution in the triangular formation and the yellow dot is the optimum charge solution if $V_{1n} = -V_{0n}$ in the three-satellite formation.

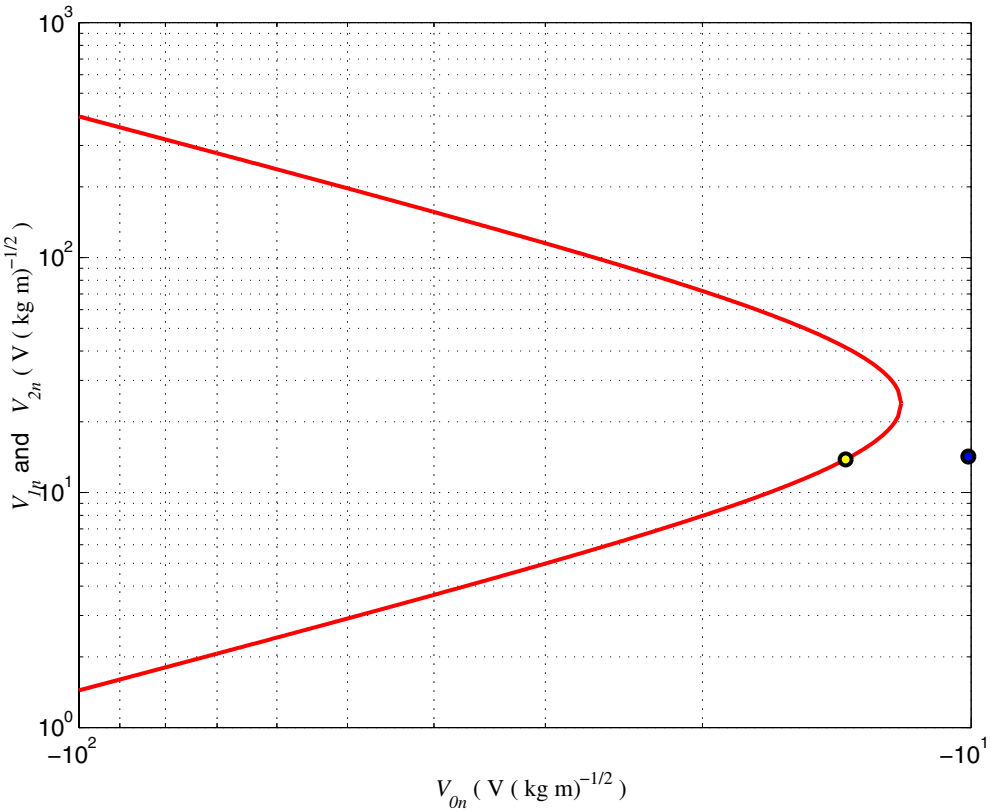

Figure 4-8. Collector equilibrium charges for negative combiner charges using a log-log scale at triangle satellite formation and the three-satellite formation aligned at the x-axis.

The normalized collector and combiner voltages for the triangle satellite formation are 14.2 V(kgm)$^{-1/2}$ and -10.1 V(kgm)$^{-1/2}$ for a geosynchronous orbit respectively. Typical charges for V_{0n} and V_{1n} are determined using Eqn. 4-14 for the collector mass and spacing parameters given in Eqn. 4-19, and are

Eqn. 4-42

$$V_1 \cdot r = V_2 \cdot r = \pm\sqrt{3\sqrt{2}k_c\Omega^2} \cdot \sqrt{mL^3} = \pm(14.2)(387.3) = \pm 5.52kV \cdot m$$
$$V_0 \cdot r = \mp\frac{3k_c\Omega^2}{V_{1n}} \cdot \sqrt{mL^3} = \mp(10.1)(387.3) = \mp 3.90kV \cdot m$$

where r is the spacecraft radius.

4.3. Earth Orbiting Five Satellite Formation - Equilibrium

Consider the square, in-plane, 5-satellite formation shown in Figure 3-5. The relative position constraints are

Eqn. 4-43

$$\begin{aligned} &x_1 = x_2 = x_3 = x_4 = 0 \\ &y_1 = y_3 = z_2 = z_4 = 0 \\ &y_2 = z_1 = -L \\ &y_4 = z_3 = L \end{aligned}$$

When substituted into the equilibrium equations (Eqn. 4-2) yield the following subset of unique necessary conditions for equilibrium.

Eqn. 4-44

$$\begin{aligned} &q_1 q_4 - q_1 q_2 = 0 \\ &\frac{k_c}{L^2}\left(q_0 q_1 + \frac{1}{4} q_1 q_3 + \frac{\sqrt{2}}{4} q_1 q_2 + \frac{\sqrt{2}}{4} q_1 q_4 \right) - mL\Omega^2 = 0 \\ &\frac{k_c}{L^2}\left(q_0 q_2 + \frac{1}{4} q_2 q_4 + \frac{\sqrt{2}}{4} q_1 q_2 + \frac{\sqrt{2}}{4} q_2 q_3 \right) = 0 \\ &-q_1 q_2 + q_2 q_3 = 0 \\ &q_3 q_4 - q_2 q_3 = 0 \\ &\frac{k_c}{L^2}\left(-q_0 q_3 - \frac{1}{4} q_1 q_3 - \frac{\sqrt{2}}{4} q_3 q_4 - \frac{\sqrt{2}}{4} q_2 q_3 \right) + mL\Omega^2 = 0 \\ &\frac{k_c}{L^2}\left(-q_0 q_4 - \frac{1}{4} q_2 q_4 - \frac{\sqrt{2}}{4} q_1 q_4 - \frac{\sqrt{2}}{4} q_3 q_4 \right) = 0 \\ &-q_1 q_4 + q_3 q_4 = 0 \end{aligned}$$

Two different analytical solutions were obtained. The first is trivial and consists of setting $q_2 = q_4 = 0$, resulting in the same z_c-axis aligned three-satellite formation considered in Section 4.1.3. Applying this to Eqn. 4-44 results in

Eqn. 4-45

$$\frac{k_c}{L^2}\left(q_0 q_1 + \frac{1}{4} q_1 q_3\right) - mL\Omega^2 = 0$$
$$\frac{k_c}{L^2}\left(-q_0 q_3 - \frac{1}{4} q_1 q_3\right) + mL\Omega^2 = 0$$

These are the same results of Eqn. 4-26 except, due to a collector numbering change between the 3 and 5 satellite formations, the subscripts of the three-satellite system are

$$1 \rightarrow 3$$
$$2 \rightarrow 1$$

Thus, the solutions obtained for the z_c-axis aligned three-satellite formation apply to this special case.

The second set of solutions assumes the following charge symmetry

Eqn. 4-46

$$q_1 = q_3$$
$$q_2 = q_4$$

resulting in only two unique equilibrium equations compared to eight in the original set of Eqn. 4-44

Eqn. 4-47

$$\frac{k_c}{L^2}\left(q_0 q_3 + \frac{1}{4} q_3^2 + \frac{\sqrt{2}}{2} q_3 q_4\right) - mL\Omega^2 = 0$$
$$\frac{k_c}{L^2}\left(q_0 q_4 + \frac{1}{4} q_4^2 + \frac{\sqrt{2}}{2} q_3 q_4\right) = 0$$

Assuming a value of q_4, Eqn. 4-47 can be solved conditionally such that the q_1 and q_3 spacecraft charges have the form

Eqn. 4-48

$$q_1 = q_1(q_4)$$

Using these values of q_1, the combiner charge, q_0 can be expressed as

Eqn. 4-49

$$q_0 = q_0(q_1, q_4)$$

This procedure works equally well when the equilibrium equations are represented using the normalized voltages from Eqn. 4-8 and Eqn. 4-10,

Eqn. 4-50
$$4V_{0n}V_{3n} + V_{3n}^2 + 2\sqrt{2}V_{3n}V_{4n} - k_c\Omega^2 = 0$$
$$4V_{0n}V_{4n} + V_{4n}^2 + 2\sqrt{2}V_{3n}V_{4n} = 0$$

assuming all spacecraft are of equal radius.

The solutions for collector 1 and 3 normalized voltage are

Eqn. 4-51
$$V_{1n} = V_{3n} = \frac{1}{2}V_{4n} \pm \frac{1}{2}\sqrt{V_{4n}^2 - \frac{16}{2\sqrt{2}-1}k_c\Omega^2}$$

where V_{4n} (and similarly V_{2n}) must satisfy the constraint

Eqn. 4-52
$$V_{4n}^2 - \frac{16}{2\sqrt{2}-1}k_c\Omega^2 \geq 0$$

Since V_{1n} and V_{3n} are known at this point, the combiner normalized voltage is readily computed from

Eqn. 4-53
$$V_{0n} = -\frac{1}{4}V_{4n} - \frac{\sqrt{2}}{2}V_{3n}$$

Figure 4-9 shows the two sets of V_{1n}, V_{3n} solutions to Eqn. 4-51, and the corresponding V_{0n} from Eqn. 4-53 for a range of V_{2n}, V_{4n} values satisfying the constraint of Eqn. 4-52 in a geosynchronous orbit. The red lines are the locus of solutions when V_{4n} is positive whereas the magenta lines are the solution loci for negative V_{4n}. The dashed or solid portions of the curves represent formation solution sets. For instance, if V_{2n} is chosen to be 50 V(kgm)$^{-1/2}$, then the solution requires either $V_{1n} = V_{3n}$ = -46 V(kgm)$^{-1/2}$

with V_{0n} = 47.6 V(kgm)$^{-1/2}$, or $V_{1n} = V_{3n}$ = 2.6 V(kgm)$^{-1/2}$ with V_{0n} = -14.3 V(kgm)$^{-1/2}$.

Using the sum of the squared voltages as a cost function,

Eqn. 4-54
$$J = \sum_{i=0}^{4} V_{in}^2$$

An optimal charge set can be computed analytically as

Eqn. 4-55
$$V_{2n} = V_{4n} = \pm 4\Omega\sqrt{\frac{k_c}{2\sqrt{2}-1}}$$
$$V_{1n} = V_{3n} = \pm 2\Omega\sqrt{\frac{k_c}{2\sqrt{2}-1}}$$
$$V_{0n} = \mp\Omega\sqrt{\frac{k_c(3+2\sqrt{2})}{2\sqrt{2}-1}}$$

and are shown as yellow dots in Figure 4-9.

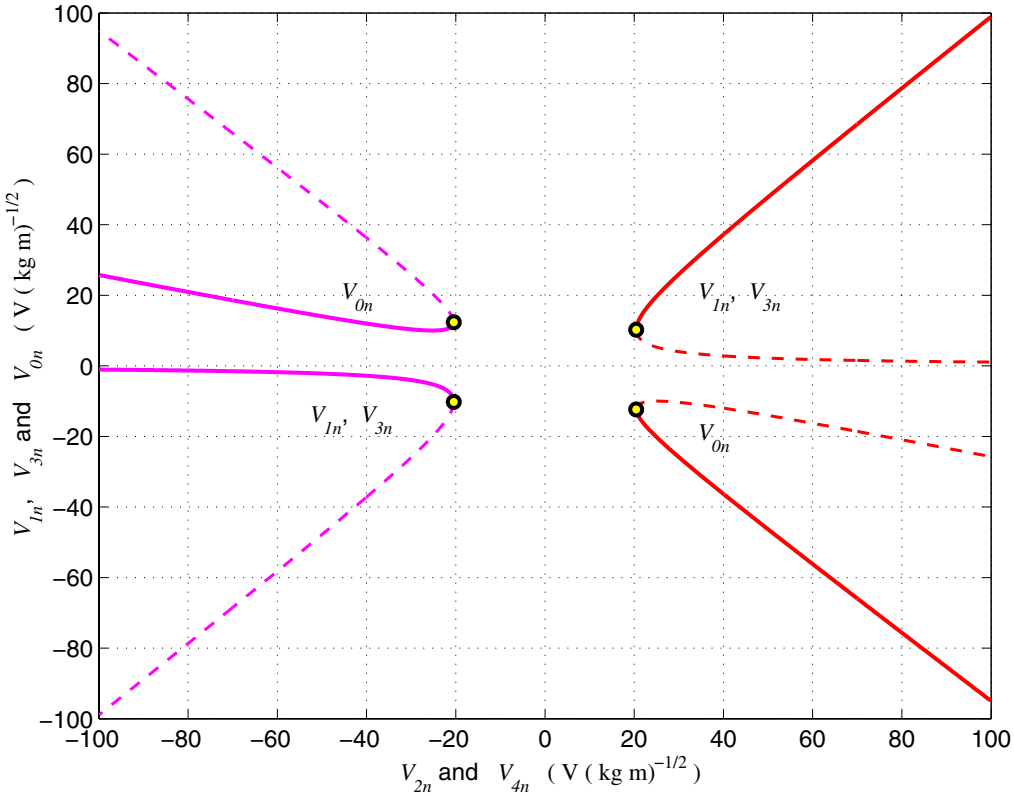

Figure 4-9. Normalized voltages of collectors 1 and 3, and the combiner for a range of acceptable collector 2 and 4 normalized voltages

Using the "typical" spacecraft parameters of Eqn. 4-19, the actual spacecraft voltages, relative to their assumed equal radii, are

$$r \cdot V_2 = r \cdot V_4 = \pm 4\Omega \sqrt{\frac{k_c}{2\sqrt{2}-1}} \cdot \sqrt{mL^3} = \pm(20.45)(387.3) = \pm 7.92kV$$

Eqn. 4-56 $$r \cdot V_{1n} = r \cdot V_{3n} = \pm 2\Omega \sqrt{\frac{k_c}{2\sqrt{2}-1}} \cdot \sqrt{mL^3} = \pm(10.23)(387.3) = \pm 3.96kV$$

$$r \cdot V_{0n} = \mp \Omega \sqrt{\frac{k_c(3+2\sqrt{2})}{2\sqrt{2}-1}} \cdot \sqrt{mL^3} = \mp(12.34)(387.3) = \mp 4.78kV$$

4.4. Earth Orbiting Six Satellite Formation - Equilibrium

The equilibrium equations for the pentagon shaped formation, shown in Figure 3-6, were obtained by imposing the formation constraints

Eqn. 4-57
$$\begin{array}{lll} x_1 = 0 & y_1 = 0 & z_1 = L \\ x_2 = 0 & y_2 = L\sin(\varphi) & z_2 = L\cos(\varphi) \\ x_3 = 0 & y_3 = L\sin(2\varphi) & z_3 = L\cos(2\varphi) \\ x_4 = 0 & y_4 = L\sin(3\varphi) & z_4 = L\cos(3\varphi) \\ x_5 = 0 & y_5 = L\sin(4\varphi) & z_5 = L\cos(5\varphi) \end{array}$$

on Eqn. 4-2 where the central angle ϕ is nominally 72°. Due to the lack of symmetry, the resulting ten equilibrium conditions were too complicated to yield an analytical solution. Instead, a numerical optimization approach was employed. The cost function J was defined as the sum of the squared residuals of Eqn. 4-2, that is

Eqn. 4-58
$$J = \sum_{i=1}^{5} (R_{yi}^2 + R_{zi}^2)$$

where

Eqn. 4-59
$$\begin{aligned} R_{yi} &= \frac{k_c}{m_i} \sum_{j=0}^{5} \frac{(y_i - y_j)}{\left|\vec{p}_i - \vec{p}_j\right|^3} q_i q_j \\ R_{zi} &= \frac{k_c}{m_i} \sum_{j=0}^{5} \frac{(z_i - z_j)}{\left|\vec{p}_i - \vec{p}_j\right|^3} q_i q_j - z_i \Omega^2 \\ & i = 1,\ldots,5 \; and \; i \neq j \end{aligned}$$

where all the spacecraft masses were assumed to be equal.

The first approach was to fix the central angle at 72° and allow all six spacecraft charges to vary. MATLAB's sequential quadratic programming, constrained optimization code was then used to determine the "best" set of charges to minimize J.

Unfortunately, there was inadequate degrees-of-freedom to permit a solution. The best value of J was only about 10% of the Ω^2 term in the residual equations. So, while a near-equilibrium solution could be found, there were not enough optimizable parameters to permit a solution.

The next approach was to increase the number of degrees-of-freedom by permitting near-pentagon formations. Specifically, the spacecraft were constrained to lie in a circle about the combiner, but were allowed to stray from the 72° central angle by 10%. In addition one combiner was constrained to lie on the y_c-axis. The circle constraint maintained the integrity of the formation's imaging attributes while allowing the minimum cost function to be 3 orders of magnitude lower than the Ω^2 terms in the residuals. Although no proof is given showing that these are true equilibrium solutions, they do represent operating points that should require only small amounts of corrective thrust.

Equilibrium *position* solutions for four different formation radii are shown in Figure 4-10 with the numerical values of the central angles given in Table 4-2. Again, the spacecraft radii were assumed equal, the orbit was geosynchronous, and the "typical" spacecraft parameters of Eqn. 4-19 were used. Normalization was not employed due to the spacecraft specific nature of the solution approach.

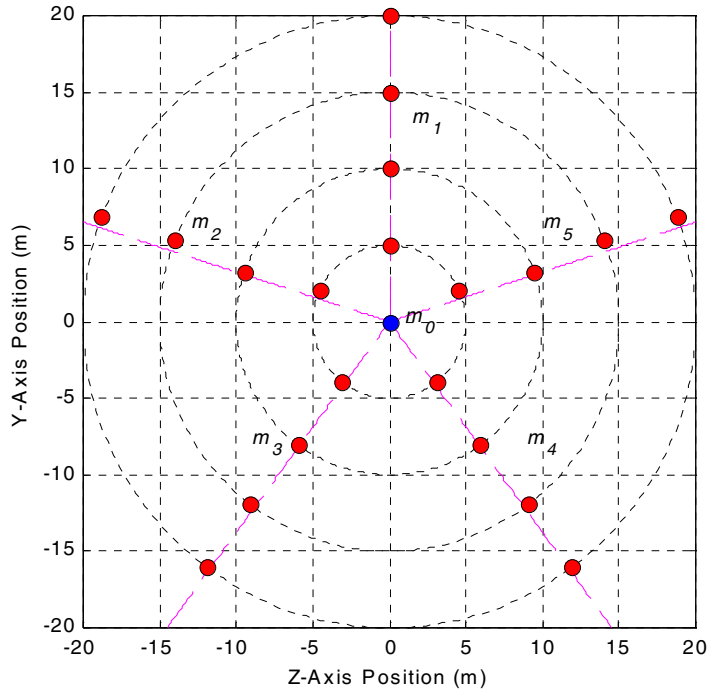

Figure 4-10. Equilibrium collector positions for 4 different radii from the combiner.

Table 4-2. Central angle results for 4 different radii.

Distance L (m)	Central Angle			
	ϕ_1 (72°)	ϕ_2 (144°)	ϕ_3 (216°)	ϕ_4 (288°)
5	65.36	141.14	218.89	294.65
10	70.89	143.62	216.36	289.09
15	69.17	142.88	217.11	290.83
20	84.18	156.15	203.84	275.82

The corresponding spacecraft specific voltages are plotted in Figure 4-11 with the numerical values given in Table 4-3. Examining the results indicates that collectors 2 and 5, and collectors 3 and 4 may require identical charge. However, this could not be shown analytically. Furthermore, when imposed as a constraint during optimization, this resulted in larger cost function solutions.

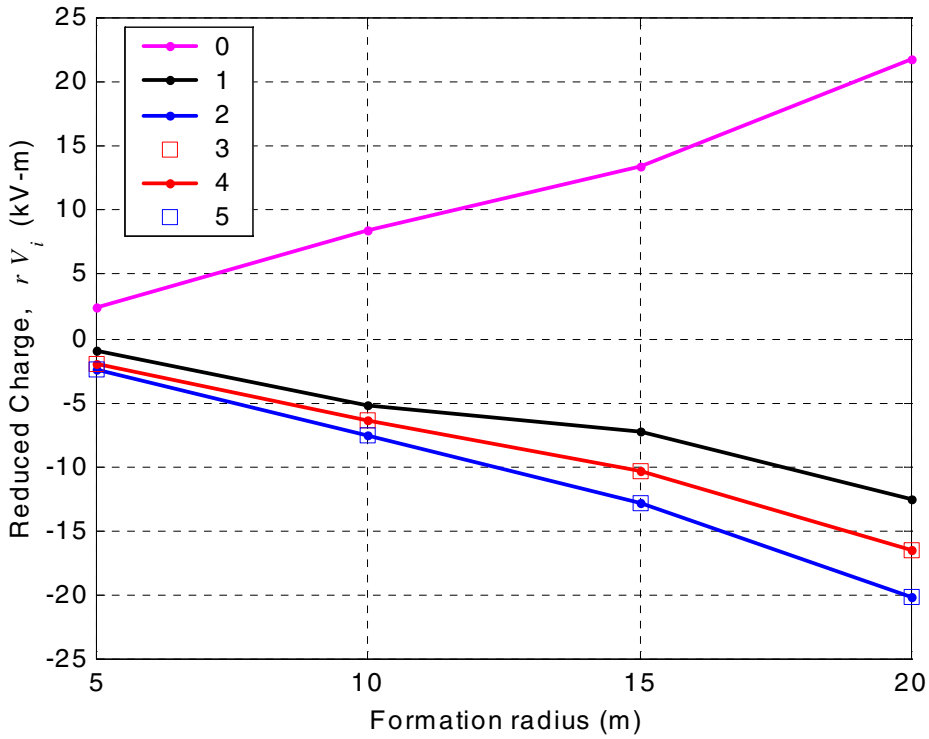

Figure 4-11. Spacecraft equilibrium reduced charges for 4 different formation radii.

Table 4-3. Equilibrium solution spacecraft reduced charges for four different collector radii.

Radius L (m)	Optimal Reduced Charges (kV m)					
	V_0 r	V_1 r	V_2 r	V_3 r	V_4 r	V_5 r
5	2.38	-1.00	-2.4	-1.99	-1.99	-2.40
10	8.47	-5.21	-7.56	-6.33	-6.33	-7.56
15	13.34	-7.19	-12.78	-10.35	-10.35	-12.78
20	1.18	-6.04	-25.55	-4.47	-4.47	-25.55

4.5. Earth Orbiting Seven-Satellite formation – Equilibrium

The Earth orbiting seven-satellite formation is described in Chapter 3 and shown in Figure 3-7. The dynamic equilibrium equations were derived by setting $n = 7$ in Eqn. 4-2, along with the specific relative distance constraints that are given as

Eqn. 4-60

$$
\begin{aligned}
&x_1 = x_2 = x_3 = x_4 = 0 \\
&y_1 = y_3 = y_5 = y_6 = 0 \\
&z_2 = z_4 = z_5 = z_6 = 0 \\
&x_5 = -L \qquad x_6 = L \\
&y_2 = -L \qquad y_4 = L \\
&z_1 = -L \qquad z_3 = L
\end{aligned}
$$

where L is the distance from the combiner to either collector in meters. Assuming the collectors' masses are the same, the eighteen equilibrium equations are

Eqn. 4-61

$$
\begin{aligned}
&-k_c q_1 q_5 + k_c q_1 q_6 = 0 \\
&-k_c q_1 q_2 + k_c q_1 q_4 = 0 \\
&\frac{k_c}{L^2} q_0 q_1 + \frac{\sqrt{2}}{4L^2} k_c q_1 q_2 + \frac{\sqrt{2}}{4L^2} k_c q_1 q_4 + \frac{1}{4L^2} k_c q_1 q_3 + \frac{\sqrt{2}}{4L^2} k_c q_1 q_5 + \frac{\sqrt{2}}{4L^2} k_c q_1 q_6 - mL\Omega^2 = 0 \\
&-k_c q_2 q_5 + k_c q_2 q_6 = 0 \\
&\frac{1}{L^2} k_c q_0 q_2 + \frac{\sqrt{2}}{4L^2} k_c q_1 q_2 + \frac{\sqrt{2}}{4L^2} k_c q_3 q_2 + \frac{1}{4L^2} k_c q_2 q_4 + \frac{\sqrt{2}}{4L^2} k_c q_2 q_5 + \frac{\sqrt{2}}{4L^2} k_c q_2 q_6 = 0 \\
&-k_c q_1 q_2 + k_c q_2 q_3 = 0 \\
&-k_c q_3 q_5 + k_c q_3 q_6 = 0 \\
&-k_c q_2 q_3 + k_c q_3 q_4 = 0 \\
&\frac{1}{L^2} k_c q_0 q_3 + \frac{\sqrt{2}}{4L^2} k_c q_3 q_2 + \frac{\sqrt{2}}{4L^2} k_c q_3 q_4 + \frac{1}{4L^2} k_c q_1 q_3 + \frac{\sqrt{2}}{4L^2} k_c q_3 q_5 + \frac{\sqrt{2}}{4L^2} k_c q_3 q_6 - mL\Omega^2 = 0 \\
&-k_c q_4 q_5 + k_c q_4 q_6 = 0 \\
&\frac{1}{L^2} k_c q_0 q_4 + \frac{\sqrt{2}}{4L^2} k_c q_1 q_4 + \frac{\sqrt{2}}{4L^2} k_c q_3 q_4 + \frac{1}{4L^2} k_c q_2 q_4 + \frac{\sqrt{2}}{4L^2} k_c q_4 q_5 + \frac{\sqrt{2}}{4L^2} k_c q_4 q_6 = 0 \\
&-k_c q_1 q_4 + k_c q_3 q_4 = 0 \\
&\frac{1}{L^2} k_c q_0 q_5 + \frac{\sqrt{2}}{4L^2} k_c q_2 q_5 + \frac{\sqrt{2}}{4L^2} k_c q_4 q_5 + \frac{\sqrt{2}}{4L^2} k_c q_1 q_5 + \frac{\sqrt{2}}{4L^2} k_c q_3 q_5 + \frac{1}{4L^2} k_c q_5 q_6 + 3mL\Omega^2 = 0 \\
&-k_c q_3 q_5 + k_c q_1 q_5 = 0 \\
&-k_c q_3 q_5 + k_c q_1 q_5 = 0 \\
&\frac{1}{L^2} k_c q_0 q_6 + \frac{\sqrt{2}}{4L^2} k_c q_2 q_6 + \frac{\sqrt{2}}{4L^2} k_c q_4 q_6 + \frac{\sqrt{2}}{4L^2} k_c q_1 q_6 + \frac{\sqrt{2}}{4L^2} k_c q_3 q_6 + \frac{1}{4L^2} k_c q_5 q_6 + 3mL\Omega^2 = 0 \\
&-k_c q_2 q_6 + k_c q_4 q_6 = 0 \\
&-k_c q_1 q_6 + k_c q_3 q_6 = 0
\end{aligned}
$$

Assuming the following charge symmetry

Eqn. 4-62
$$q_1 = q_3$$
$$q_2 = q_4$$
$$q_5 = q_6$$

and eliminating duplicated equations leaves only three unique equilibrium equations,

Eqn.4-63
$$\frac{k_c}{L^2} q_0 q_1 + \frac{\sqrt{2}}{2L^2} k_c q_1 q_2 + \frac{1}{4L^2} k_c q_1^2 + \frac{\sqrt{2}}{2L^2} k_c q_1 q_5 - mL\Omega^2 = 0$$
$$\frac{1}{L^2} k_c q_0 q_2 + \frac{\sqrt{2}}{2L^2} k_c q_1 q_2 + \frac{1}{4L^2} k_c q_2^2 + \frac{\sqrt{2}}{2L^2} k_c q_2 q_5 = 0$$
$$\frac{1}{L^2} k_c q_0 q_5 + \frac{\sqrt{2}}{2L^2} k_c q_2 q_5 + \frac{\sqrt{2}}{2L^2} k_c q_1 q_5 + \frac{1}{4L^2} k_c q_5^2 + 3mL\Omega^2 = 0$$

Assuming a value of q_2 (or similarly q_4), Eqn.4-63 can be solved analytically such that the collectors' charges are functions of q_2

Eqn. 4-64
$$q_1 = q_3 = q_1(q_2)$$
$$q_5 = q_6 = q_5(q_2)$$

The combiner charge, q_0 can then be expressed as

Eqn. 4-65
$$q_0 = q_0(q_1, q_2, q_5)$$

Employing the normalized spacecraft voltage definition of Eqn. 4-8 and Eqn. 4-10, and assuming all the spacecraft have the same radius, the equilibrium equations can be represented in terms of normalized spacecraft potentials as

Eqn. 4-66

$$V_{0n}V_{1n} + \frac{\sqrt{2}}{2}V_{1n}V_{2n} + \frac{1}{4}V_{1n}^2 + \frac{\sqrt{2}}{2}V_{1n}V_{5n} - k_c\Omega^2 = 0$$
$$V_{0n}V_{2n} + \frac{\sqrt{2}}{2}V_{1n}V_{2n} + \frac{1}{4}V_{2n}^2 + \frac{\sqrt{2}}{2}V_{2n}V_{5n} = 0$$
$$V_{0n}V_{5n} + \frac{\sqrt{2}}{2}V_{2n}V_{5n} + \frac{\sqrt{2}}{2}V_{1n}V_{5n} + \frac{1}{4}V_{5n}^2 + 3k_c\Omega^2 = 0$$

The normalized voltages for collectors 1 and 3, and collectors 5 and 6 are

Eqn. 4-67

$$V_{1n} = V_{3n} = \frac{1}{2}V_{2n} \pm \frac{-2\left(1+2\sqrt{2}\right)}{7}\sqrt{\frac{9-4\sqrt{2}}{16}V_{2n}^2 + \left(1-2\sqrt{2}\right)k_c\Omega^2}$$
$$V_{5n} = V_{6n} = \frac{1}{2}V_{2n} \pm \frac{-2\left(1+2\sqrt{2}\right)}{7}\sqrt{\frac{9-4\sqrt{2}}{16}V_{2n}^2 - 3\left(1-2\sqrt{2}\right)k_c\Omega^2}$$

where V_{2n} or V_{4n} must satisfy the constraint

Eqn. 4-68

$$V_{2n}^2 - \frac{16\left(2\sqrt{2}+1\right)}{7}k_c\Omega^2 \geq 0$$

Therefore, the normalized voltages for the combiner can be determined as

Eqn. 4-69

$$V_{0n} = -\left(\frac{\sqrt{2}}{2}V_{5n} + \frac{1}{4}V_{2n} + \frac{\sqrt{2}}{2}V_{1n}\right)$$

Figure 4-12 shows the two sets of collector voltages solutions (V_{1n}, V_{3n}, V_{5n}, and V_{6n}) from Eqn. 4-67, and the corresponding combiner voltages V_{0n}, from Eqn. 4-69 for a range of V_{2n} and V_{4n} values that satisfy the constraint in Eqn. 4-68 in a geosynchronous orbit. The solutions on the right side are determined when V_{2n} is positive whereas the solutions on the left are determined when V_{2n} is negative. Again, the dashed or solid portions of the curve represent formation solution sets. For instance, if V_{2n} is chosen to be 50 V(kgm)$^{-1/2}$, then the solution requires *either* $V_{1n} = V_{3n} = 49.7$ V(kgm)$^{-1/2}$, and $V_{5n} =$

V_{6n} = 55.5 V(kgm)$^{-1/2}$ with V_{0n} = -87.1 V(kgm)$^{-1/2}$ *or* $V_{1n} = V_{3n}$ = 1.75 V(kgm)$^{-1/2}$, and $V_{5n} = V_{6n}$ = -5.26 V(kgm)$^{-1/2}$ with V_{0n} = -9.94 V(kgm)$^{-1/2}$.

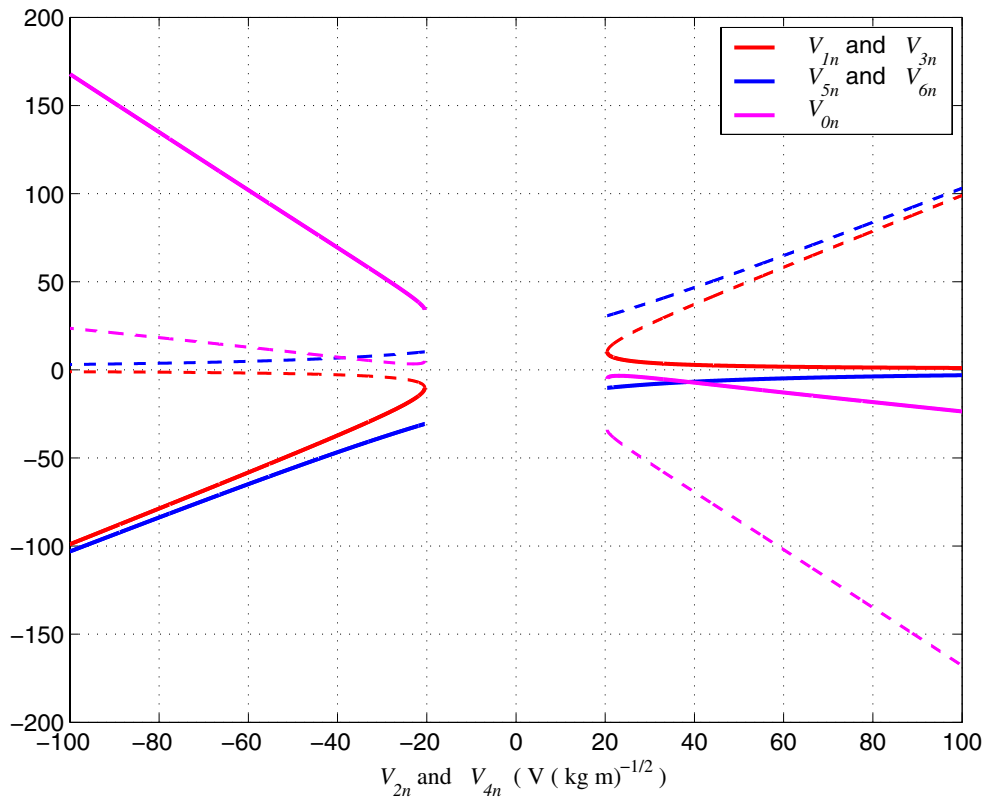

Figure 4-12. Normalized voltages of collectors 1 and 3, 5 and 6, and the combiner for a range of normalized voltages of collectors 2 and 4 which satisfy the constraint.

Using the sum of the squared voltages as a cost function, an optimal charge set can be calculated analytically as

Eqn. 4-70

$$V_{2n} = V_{4n} = \pm 4\Omega\sqrt{\frac{\left(2\sqrt{2}+1\right)}{7}k_c}$$

$$V_{1n} = V_{3n} = \pm 2\Omega\sqrt{\frac{\left(2\sqrt{2}+1\right)}{7}k_c}$$

$$V_{5n} = V_{6n} = \pm 2\Omega\left(\sqrt{\frac{\left(2\sqrt{2}+1\right)}{7}k_c} + \sqrt{\left(2\sqrt{2}-1\right)k_c}\right)$$

$$V_{0n} = \mp\Omega\left(\sqrt{2\left(2\sqrt{2}-1\right)k_c} + \sqrt{\frac{22\sqrt{2}+25}{7}k_c}\right)$$

For a better view, the normalized charges of the collectors 1 and 3 are examined on a log-log plot that is shown in Figure 4-13. .

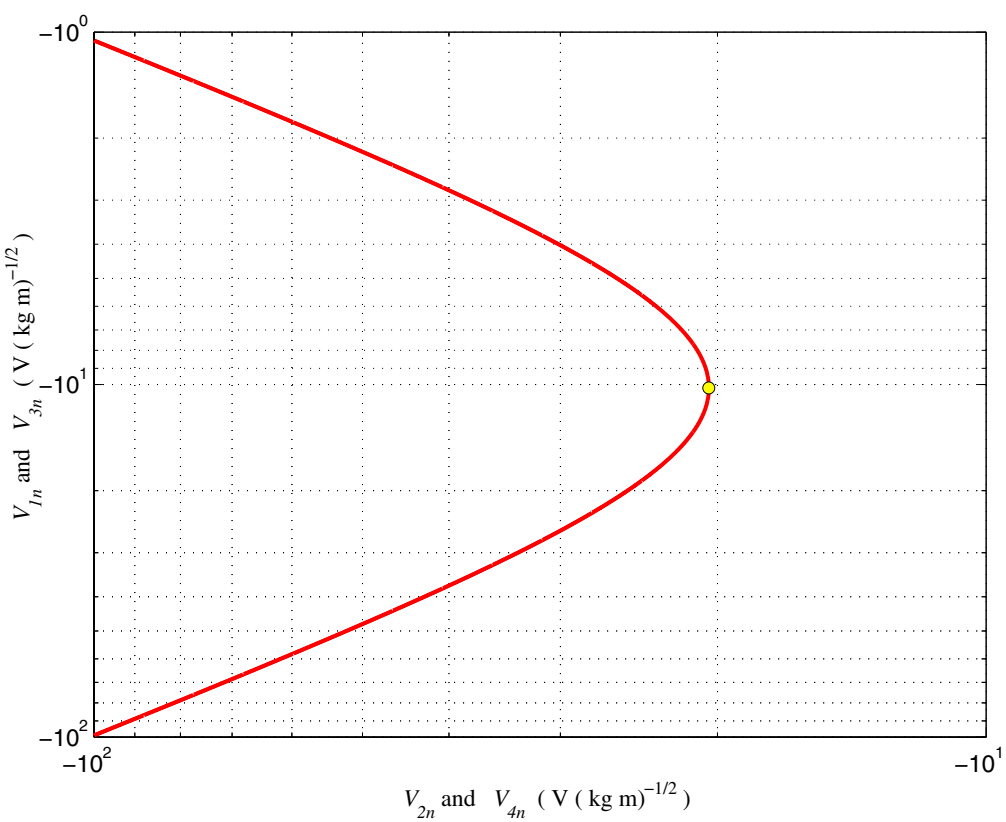

Figure 4-13. Collector equilibrium charges for negative collector 2 charges using a log-log scale. An “optimal” charge set is shown with yellow dot

The optimal charge for collectors 2 and 4 is 20.45 V(kgm)$^{-1/2}$ in a geosynchronous orbit. The yellow dot represents the optimal charges of collectors 1 and 2, which is about 10.2 V(kgm)$^{-1/2}$ in a geosynchronous orbit. Using the typical collector mass and the length parameters from Eqn. 4-19, the minimum charges of collectors 2 and 4, and collectors 1 and 3 are calculated as

$$V_2 \cdot r = V_4 \cdot r = \pm 4\Omega \sqrt{\frac{\left(2\sqrt{2}+1\right)}{7} k_c} \cdot \sqrt{mL^3} = \pm(20.45)(387.3) = \pm 7.92 kV \cdot m$$

Eqn. 4-71

$$V_1 \cdot r = V_3 \cdot r = \pm 2\Omega \sqrt{\frac{\left(2\sqrt{2}+1\right)}{7} k_c} \cdot \sqrt{mL^3} = \pm(10.2)(387.3) = \pm 3.95 kV \cdot m$$

where r is the collector radius.

The optimal charges of the normalized voltages of collectors 5 and 6 are shown in Figure 4-14.

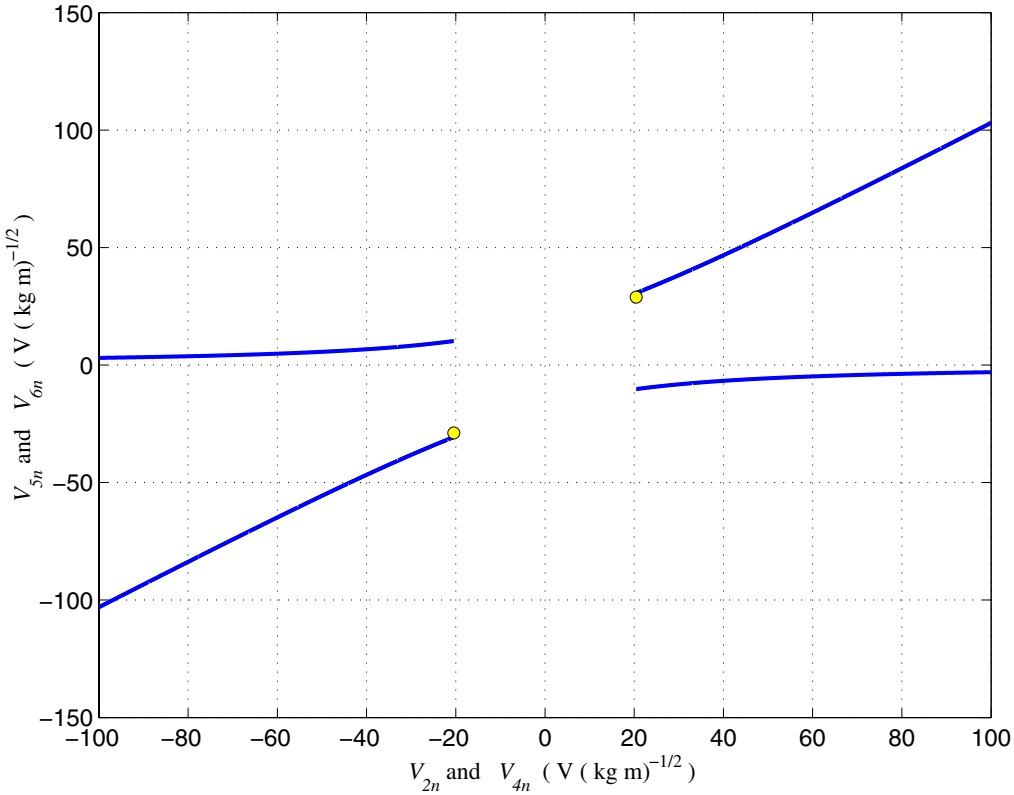

Figure 4-14. Normalized collector voltages for a range of collectors 2 and 4 for a geosynchronous orbit. The "optimal" voltages are indicated as yellow dots

The optimal charges (yellow dots) are 28.9 V(kgm)$^{-1/2}$ in geosynchronous orbit. Using the same mass and length parameters of Eqn. 4-19, the optimal spacecraft voltages, relative to their equal radii are given as

Eqn. 4-72
$$V_5 \cdot r = V_6 \cdot r = \pm 2\Omega\left(\sqrt{\frac{\left(2\sqrt{2}+1\right)}{7}k_c} + \sqrt{\left(2\sqrt{2}-1\right)k_c}\right)\cdot\sqrt{mL^3}$$
$$= \pm(28.9)(387.3) = \pm 11.19 kV \cdot m$$

Again, the optimal charge of normalized voltage of the combiner is shown in Figure 4-15.

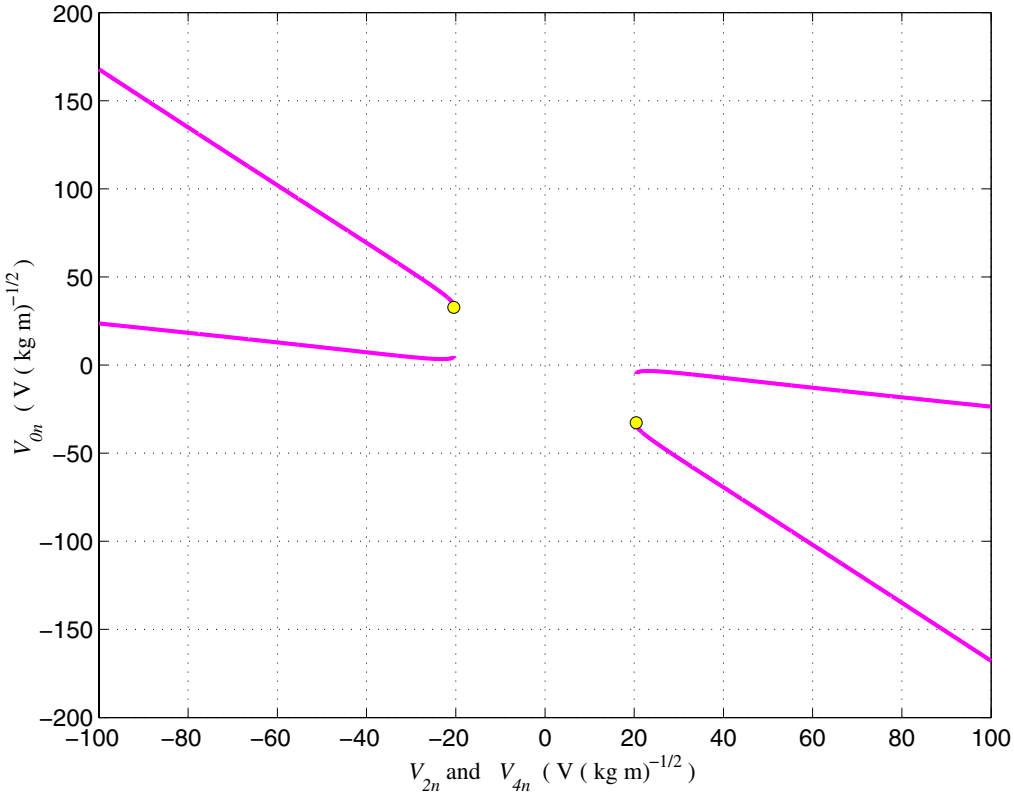

Figure 4-15. Normalized collector voltages for a range of combiner voltages for a geosynchronous orbit. The yellow dots indicate "optimal" voltages

The optimum voltages are 32.79 V(kgm)$^{-1/2}$ for geosynchronous orbit. Again using typical spacecraft mass and distance parameters and assuming the spacecraft radii are equal, the minimum spacecraft voltages are given as following

Eqn. 4-73

$$V_0 \cdot r = \mp\Omega\left(\sqrt{2\left(2\sqrt{2}-1\right)k_c} + \sqrt{\frac{22\sqrt{2}+25}{7}k_c}\right)\cdot\sqrt{mL^3}$$
$$= \mp(32.79)(387.3) = \mp 12.70 kV \cdot m$$

Table 4-4. Optimal reduced charges for all spacecraft in seven-satellite formation.

Optimal Reduced Charges (kV m)						
V_0 r	V_1 r	V_2 r	V_3 r	V_4 r	V_5 r	V_6 r
∓ 12.70	±3.95	±7.92	±3.95	±7.92	±11.19	±11.19

4.6. Libration Point Five Satellite Formation - Equilibrium

As discussed in Chapter 3, this case is different from those considered previously as the formation is not orbiting the Earth, but rather is at an Earth-Sun Libration point. The system of 5 spacecraft is shown in Figure 3-8 where it is assumed to rotate about the z_c-axis with angular rate Ω. The fifteen equilibrium equations of Eqn. 4-3 are greatly simplified by enforcing the geometry constraints

Eqn. 4-74
$$\begin{aligned} &x_1 = L_1 \qquad x_2 = L_1 + L_2 \\ &x_3 = -L_1 \qquad x_4 = -L_1 - L_2 \\ &y_1 = y_2 = y_3 = y_4 = 0 \\ &z_1 = z_2 = z_3 = z_4 = 0 \end{aligned}$$

and imposing the symmetry requirements

Eqn. 4-75
$$\begin{aligned} m_1 &= m_3 \\ m_2 &= m_4 \\ q_1 &= q_3 \\ q_2 &= q_4 \end{aligned}$$

Only two unique equilibrium equations remain

Eqn. 4-76
$$\begin{aligned} &-m_1 L_1 \Omega^2 + \frac{k_c q_1 q_2}{L_2^2} - \frac{k_c q_0 q_1}{L_1^2} - \frac{k_c q_1^2}{4L_1^2} - \frac{2k_c q_1 q_2 L_1}{(2L_1 + L_2)^3} - \frac{k_c q_1 q_2 L_2}{(2L_1 + L_2)^3} \\ &-m_2 (L_1 + L_2)\Omega^2 - \frac{k_c q_1 q_2}{L_2^2} - \frac{k_c q_1 q_2}{(2L_1 + L_2)^2} - \frac{k_c q_2^2}{4(L_1 + L_2)^2} - \frac{k_c q_0 q_2}{(L_1 + L_2)^2} \end{aligned}$$

where L_1 is the distance between the combiner and collectors 1 and 3, and L_2 is the distance between collectors 1 and 2 (and also collectors 3 and 4). Both of these equations can be solved for $k_c q_0$, and then equated yielding the single quadratic

Eqn. 4-77
$$a_2 q_2^2 + a_1 q_2 + a_0 = 0$$

where

Eqn. 4-78
$$a_2 = k_c q_1 \left(\frac{L_1^2}{L_2^2} - \frac{L_1^2}{(2L_1 + L_2)^2} + \frac{1}{4} \right)$$
$$a_1 = -m_1 L_1^3 \Omega^2 - k_c q_1^2 \left[\frac{(L_1 + L_2)^2}{L_2^2} + \frac{(L_1 + L_2)^2}{(2L_1 + L_2)^2} - \frac{1}{4} \right]$$
$$a_0 = m_2 (L_1 + L_2)^3 q_1 \Omega^2$$

Eqn. 4-77 can be solved for q_2 assuming a range of q_1 is known that satisfies the constraint

Eqn. 4-79
$$a_1^2 - 4 a_2 a_0 \geq 0$$

For each q_1, q_2 pair, a unique $k_c q_0$ can be obtained from either of the equilibrium conditions in Eqn. 4-76, such as

Eqn. 4-80
$$k_c q_0 = L_1^2 \left[\frac{-M_1 L_1 \Omega^2}{q_1} + \frac{k q_2}{L_2^2} - \frac{k q_1}{4 L_1^2} - \frac{k q_2}{(2L_1 + L_2)^2} \right]$$
$$k_c q_0 = (L_1 + L_2)^2 \left[\frac{-M_2 (L_1 + L_2) \Omega^2}{q_2} - \frac{k q_1}{L_2^2} - \frac{k q_1}{(2L_1 + L_2)^2} - \frac{k q_2}{4(L_1 + L_2)^2} \right]$$

where k_c is Coulomb's constant.

One approach to finding an optimum equilibrium point is to minimize the cost function

Eqn. 4-81
$$J = q_o^{\ 2} + 2q_1^2 + 2q_2^2$$

A specific example was considered with the following spacecraft and separation parameters

Eqn. 4-82
$$\begin{aligned} m_0 &= m_1 = m_3 = 150kg \\ m_2 &= m_4 = 150kg \\ L_1 &= 12.5m \\ L_2 &= 25m \end{aligned}$$

with all spacecraft radii being equal. Three different formation-spin rates, Ω, were investigated

Eqn. 4-83
$$\begin{aligned} \Omega_1 &= 0.5\frac{rev}{hr} = \frac{\pi}{3600}\frac{rad}{\sec} \\ \Omega_2 &= 0.05\frac{rev}{hr} = \frac{.1\pi}{3600}\frac{rad}{\sec} \\ \Omega_3 &= 0.005\frac{rev}{hr} = \frac{.01\pi}{3600}\frac{rad}{\sec} \end{aligned}$$

Specific spacecraft voltages are shown in Figure 4-16 (collectors 2 and 4) and Figure 4-17 (combiner) for a range of collector 1 and 3 voltages using the spin rate of Ω_1. Using the cost function given in Eqn. 4-81, an optimal solution was obtained resulting in the smallest charge across all spacecraft and is shown with yellow dots on the plots. The optimal spacecraft voltages for all spin rate cases are provided in Table 4-5.

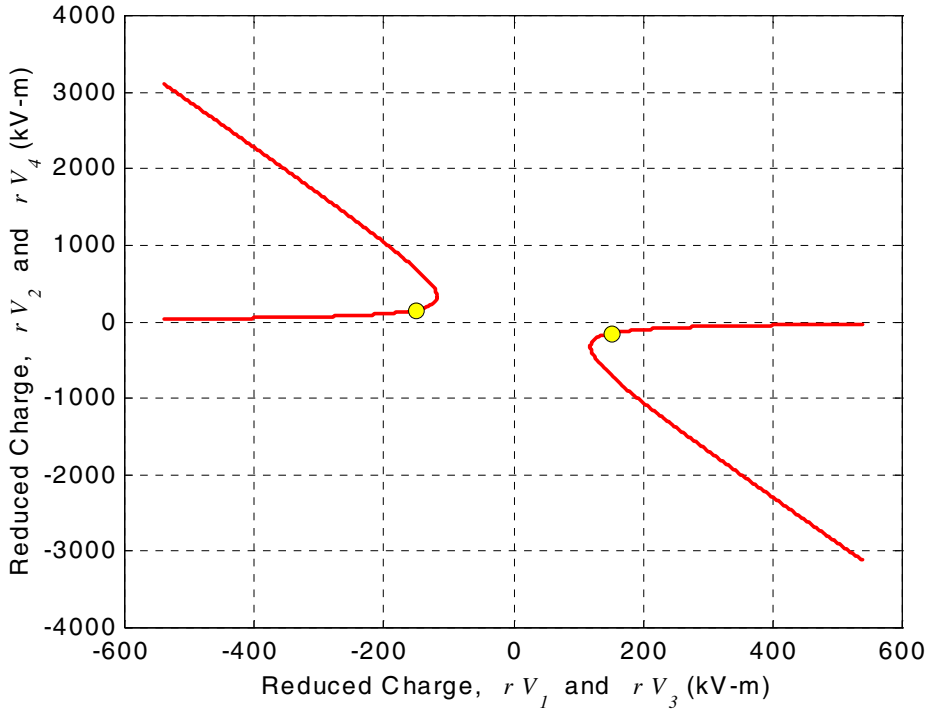

Figure 4-16. All sets of collector 2 and 4 reduced charges for a range of collector 1 and 3 charges for a spin rate of 0.5 rev/hr. The yellow dots indicate the "optimal" solution resulting in the smallest charge across all spacecraft.

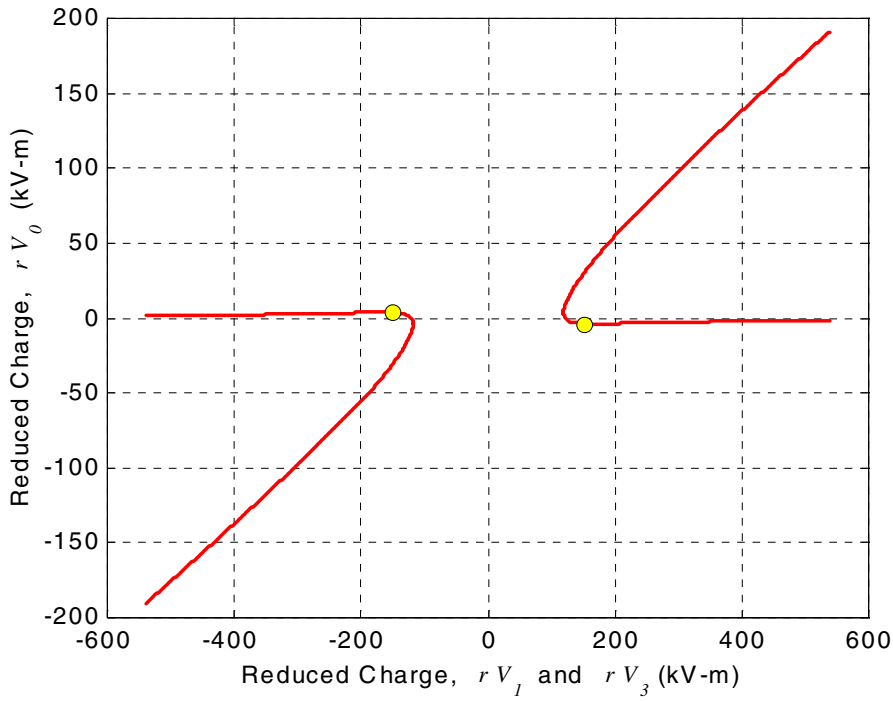

Figure 4-17. All sets of combiner reduced charges for a range of collector 1 and 3 charges for a spin rate of 0.5 rev/hr. The yellow dots indicate the "optimal" solution resulting in the smallest charge across all spacecraft.

Table 4-5. Optimal reduced charges for all spacecraft using three different spin rates.

Spin Rate (rad /s)	Optimal Reduced Charges (kV m)				
	V_0 r	V_1 r	V_2 r	V_3 r	V_4 r
8.73E-06	3.73E-02	-1.52E+00	1.52E+00	-1.52E+00	1.52E+00
8.73E-05	3.73E-01	-1.52E+01	1.52E+01	-1.52E+01	1.52E+01
8.73E-04	3.73E+00	-1.52E+02	1.52E+02	-1.52E+02	1.52E+02

It is noted that for the "optimal" solutions assumed the condition

Eqn. 4-84 $$V_2 = -V_1$$

is required, resulting in a linear relationship between the spacecraft charges and the spin rate as observed in Table 4-5. This will not be the case for other solutions.

4.7. Summary

Equilibrium spacecraft charges were computed for several formation examples. In theory, once the formation is placed in an equilibrium configuration, it should remain there. If the equilibrium state is stable, then the formation will return to it given small external perturbations.

For small numbers of spacecraft (up to 7) analytical solutions were readily obtained. A numerical optimization approach was developed for determining equilibrium solutions for formations with n spacecraft illustrated by the six-satellite, pentagon-like formation of Section 4.4 and the libration point five satellite in Section 4.6. Future work should address the equilibrium point stability question including active charge control. One approach would be to modify the optimality criteria used for selecting a particular solution from the solution loci to include a relative stability metric.

5. Stability and Controllability

5.1. Introduction

In chapters 3 and 4, the dynamic equations and equilibrium solutions were determined. Although formations based on equilibrium solutions may be attractive from a propellant cost perspective, they may not be stable, or controllable. The stability and controllability of satellite formations are investigated in this chapter.

First, some fundamental concepts of dynamic system stability and controllability are reviewed. The Coulomb force formation equations are then linearized in both the states and their inputs. Stability and controllability are then evaluated for three formations:

- Earth orbiting three-satellite formation (Section 4.1.1)
- Earth orbiting triangular formation (Section 4.2)
- Earth orbiting seven-satellite formation (Section 4.5)

5.2. Stability Review

5.2.1. Linear System Stability

Given the linear dynamic system

Eqn. 5-1

$$\underline{\dot{x}} = \underline{\underline{A}}\,\underline{x} + \underline{\underline{B}}\,\underline{u}$$

where $\underline{x}$ is an $n \times 1$ state vector, $\underline{\underline{A}}$ is the $n \times n$ state matrix, $\underline{\underline{B}}$ is the $n \times m$ input weighting matrix and $\underline{u}$ is a $m \times 1$ vector of inputs, the system is stable if all the eigenvalues of $\underline{\underline{A}}$ have negative real parts. Physically, given any initial condition x_0 the state will progress to the origin, bounded above by an exponentially decaying function of time.

5.2.2. *Nonlinear System Stability – Lyapunov Stability*

There are several methods for determining the stability of a nonlinear system most of which are based on two by Lyapunov. Lyapunov's Direct Method has its foundation in the observation that if the total energy of a system decreases with time, the system motion decays to $\underline{0}$ [51,52]. Lyapunov generalized this approach to energy-like functions (positive definite, Lyapunov candidate function denoted V). If the directional derivative of V in the direction $\underline{f}$ is always negative then the equilibrium point is stable. One difficulty in applying this method is the determination of a Lyapunov function.

For nonlinear system of the form

Eqn. 5-2
$$\dot{\underline{x}} = \underline{f}(\underline{x})$$

stability must be described in terms of the system equilibrium points that satisfy

Eqn. 5-3
$$\underline{f}(\underline{x}) = 0$$

Physically, if the system is placed at an equilibrium point then released it will stay there. Stability in sense of Lyapunov answers the question "if the system is perturbed from an equilibrium point, will its motion remain bounded?"

Formally, we say that an equilibrium point at $\underline{x} = \underline{0}$ is stable (in the sense of Lyapunov) if $\forall R > 0 \; \exists \, r > 0$ such that if $\|\underline{x}(0)\| < r$ then $\|x(t)\| < R \;\; \forall t \geq 0$. It should be noted that $\| \; \|$ represents any vector norm (e.g. Euclidean) and any equilibrium point could be shifted to $\underline{x} = \underline{0}$ using a transformation of variables.

Lyapunov's Indirect Method[52] is based on the linearized form of the dynamic equations. That is, expanding the nonlinear for $\underline{f}(\underline{x})$ about the equilibrium point at the origin

Eqn. 5-4 $$\underline{f}(\underline{x}) = \underline{\underline{A}}\underline{x} + \underline{r}(\underline{x})$$

as long as $\underline{f}(\underline{x})$ is not an explicit function of time, and $\underline{\underline{A}}$ is $n \times n$ matrix Jacobian of $\underline{f}$

Eqn. 5-5 $$\underline{\underline{A}} = \nabla \underline{f}\Big|_{\underline{x}=0}$$

Lyapunov showed that if $\underline{\underline{A}}$ is stable (all its eigenvalues having negative real parts), then this behavior will dominate any effects of $\underline{r}(\underline{x})$ and the equilibrium point is stable. If $\underline{\underline{A}}$ has any eigenvalues with positive real parts, then the equilibrium point is unstable. Finally if $\underline{\underline{A}}$ has no positive real eigenvalues, but one or more eigenvalues that lie on the imaginary axis, then the system's stability is unknown. That is, the ignored remainder terms $\underline{r}(\underline{x})$, decide the stability. This approach will be used in Sections 5.5.3, 5.6.3 and 5.7.3 to assess the stability of the three formations mentioned in the introduction.

It should be noted that even if a Lyapunov's Indirect Method shows an equilibrium point to be unstable a closed-loop controller could be applied to stabilize. Unfortunately, its usefulness will be limited to some unknown region about the equilibrium point.

5.3. *Controllability Review*

A linear system

Eqn. 5-6 $$\dot{\underline{x}} = \underline{\underline{A}}\,\underline{x} + \underline{\underline{B}}\,\underline{u}$$

is controllable if $\forall \underline{x}$ ($n \times 1$ state vector) $\exists$ an input $\underline{u}$ (control signal with $m \times 1$ matrix). Physically, this says that it is theoretically possible to move a system from any initial state to any final state using the available inputs. Linear system controllability is easily checked by examining the rank of the controllability matrix

Eqn. 5-7 $$W = \left\lfloor \underline{\underline{B}} \vdots \underline{\underline{A}}\,\underline{\underline{B}} \vdots \underline{\underline{A}}^2 \underline{\underline{B}} \vdots \cdots \vdots \underline{\underline{A}}^{n-1} \underline{\underline{B}} \right\rfloor$$

If the controllability matrix has rank n, then the system is controllable.

This idea can be extended to nonlinear system, which is affine in the input[52]

Eqn. 5-8 $$\dot{\underline{x}} = \underline{f}(\underline{x}) + \underline{g}(\underline{x})\underline{u}$$

Unfortunately, our Coulomb controlled spacecraft Eqn. 3-15 are non affine in the input. Therefore, we will assess controllability by examining the controllability of a completely linearized system.

5.4. *Linearized Dynamic Equations*

In Section 5.4 through Section 5.7, stability (using Lyapunov's Indirect Method) and controllability are investigated for three formations. Both features will be

investigated numerically by computing eigenvalues of the linearized state matrix and the controllability matrix of the state equations. To reduce the effect of round-off errors, normalized and linearized dynamic equations will be created based on nondimensional time as described below.

The Coulomb forced Hill's equations from Eqn. 3-15 are first expressed using nondimensional time with the substitution

Eqn. 5-9
$$T = \Omega t$$

The relative speeds and accelerations can be expressed as

Eqn. 5-10
$$\frac{dx}{dt} = \frac{dx}{dT}\frac{dT}{dt} \qquad \frac{dy}{dt} = \frac{dy}{dT}\frac{dT}{dt} \qquad \frac{dz}{dt} = \frac{dz}{dT}\frac{dT}{dt}$$
$$\dot{x} = \Omega\, x' \qquad \dot{y} = \Omega\, y' \qquad \dot{z} = \Omega\, z'$$
$$\ddot{x} = \Omega^2\, x'' \qquad \ddot{y} = \Omega^2\, y'' \qquad \ddot{z} = \Omega^2\, z''$$

Substituting Eqn. 5-10 into Hill's equations (see Eqn. 3-15) gives

Eqn. 5-11
$$x_i'' - 2y_i' - 3x_i = \frac{k_c}{m_i\Omega^2}\sum_{j=0}^{n}\frac{(x_i - x_j)}{\left|\vec{p}_i - \vec{p}_j\right|^3} q_i q_j$$
$$y_i'' + 2x_i' - y_i = \frac{k_c}{m_i\Omega^2}\sum_{j=0}^{n}\frac{(y_i - y_j)}{\left|\vec{p}_i - \vec{p}_j\right|^3} q_i q_j$$
$$z_i'' + z_i = \frac{k_c}{m_i\Omega^2}\sum_{j=0}^{n}\frac{(z_i - z_j)}{\left|\vec{p}_i - \vec{p}_j\right|^3} q_i q_j$$
$$i = 1,\ldots,n \text{ and } i \neq j$$

Coulomb's constant k_c, collector mass $m_i = m$ (assuming all collector masses are equal), and the orbital angular rate Ω, will be combined to normalize the charges according to

$$\hat{q}_j = \sqrt{\frac{k_c}{m\Omega^2}} q_j$$

Eqn. 5-12

$$j = 0,\ldots,n$$

The normalized, and nondimensional time representations of the dynamic equations are

$$x_i'' - 2y_i' - 3x_i = \sum_{j=0}^{n} \frac{(x_i - x_j)}{\left|\vec{p}_i - \vec{p}_j\right|^3} \hat{q}_i \hat{q}_j$$

$$y_i'' + 2x_i' - y_i = \sum_{j=0}^{n} \frac{(y_i - y_j)}{\left|\vec{p}_i - \vec{p}_j\right|^3} \hat{q}_i \hat{q}_j$$

Eqn. 5-13

$$z_i'' + z_i = \sum_{j=0}^{n} \frac{(z_i - z_j)}{\left|\vec{p}_i - \vec{p}_j\right|^3} \hat{q}_i \hat{q}_j$$

$$i = 1,\ldots,n \text{ and } i \neq j$$

Linearization is performed by expanding all the displacements and charges as being the sum of a nominal value (denoted with an over bar) and a perturbation, that is

Eqn. 5-14

$$\begin{aligned} x_i &= \bar{x}_i + \delta x_i \\ y_i &= \bar{y}_i + \delta y_i \\ z_i &= \bar{z}_i + \delta z_i \\ \hat{q}_j &= \bar{\hat{q}}_j + \delta \hat{q}_j \\ i &= 1,\ldots,n \\ j &= 0,\ldots,n \end{aligned}$$

Next, the denominator of Eqn. 5-13, $\left|\vec{p}_i - \vec{p}_j\right|^3$ is expanded in a binomial series and multiplied by the numerator, retaining terms up to first order in δ. Making the substitutions described above, the denominator is

Eqn. 5-15

$$\left|\vec{p}_i - \vec{p}_j\right|^{-3} = \left[\left[(\bar{x}_i + \delta x_i) - (\bar{x}_j + \delta x_j)\right]^2 + \left[(\bar{y}_i + \delta y_i) - (\bar{y}_j + \delta y_j)\right]^2 + \left[(\bar{z}_i + \delta z_i) - (\bar{z}_j + \delta z_j)\right]^2\right]^{3/2}$$

$$= \left[(\bar{x}_i - \bar{x}_j)^2 + (\bar{y}_i - \bar{y}_j)^2 + (\bar{z}_i - \bar{z}_j)^2\right]^{-3/2} \cdot$$
$$\left\{1 + 2\left[\frac{(\bar{x}_i - \bar{x}_j)(\delta x_i - \delta x_j) + (\bar{y}_i - \bar{y}_j)(\delta y_i - \delta y_j) + (\bar{z}_i - \bar{z}_j)(\delta z_i - \delta z_j)}{(\bar{x}_i - \bar{x}_j)^2 + (\bar{y}_i - \bar{y}_j)^2 + (\bar{z}_i - \bar{z}_j)^2}\right] + \right.$$
$$\left.\frac{(\delta x_i - \delta x_j)^2 + (\delta y_i - \delta y_j)^2 + (\delta z_i - \delta z_j)^2}{(\bar{x}_i - \bar{x}_j)^2 + (\bar{y}_i - \bar{y}_j)^2 + (\bar{z}_i - \bar{z}_j)^2}\right\}^{-3/2}$$

Eqn. 5-16

$$(\bar{x}_i - \bar{x}_j)^2 + (\bar{y}_i - \bar{y}_j)^2 + (\bar{z}_i - \bar{z}_j)^2 >> (\delta x_i - \delta x_j)^2$$
$$(\bar{x}_i - \bar{x}_j)^2 + (\bar{y}_i - \bar{y}_j)^2 + (\bar{z}_i - \bar{z}_j)^2 >> (\delta y_i - \delta y_j)^2$$
$$(\bar{x}_i - \bar{x}_j)^2 + (\bar{y}_i - \bar{y}_j)^2 + (\bar{z}_i - \bar{z}_j)^2 >> (\delta z_i - \delta z_j)^2$$

Thus, $\left|\vec{p}_i - \vec{p}_j\right|^{-3}$ can be simplified as

Eqn. 5-17

$$\left|\vec{p}_i - \vec{p}_j\right|^{-3} \approx \left[(\bar{x}_i - \bar{x}_j)^2 + (\bar{y}_i - \bar{y}_j)^2 + (\bar{z}_i - \bar{z}_j)^2\right]^{-3/2} \cdot$$
$$\left\{1 - 3\left[\frac{(\bar{x}_i - \bar{x}_j)(\delta x_i - \delta x_j) + (\bar{y}_i - \bar{y}_j)(\delta y_i - \delta y_j) + (\bar{z}_i - \bar{z}_j)(\delta z_i - \delta z_j)}{(\bar{x}_i - \bar{x}_j)^2 + (\bar{y}_i - \bar{y}_j)^2 + (\bar{z}_i - \bar{z}_j)^2}\right]\right\}$$

Substitute both Eqn. 5-14 and Eqn. 5-17 into Eqn. 5-13, the Coulomb forcing terms of Hill's equations are

$$\sum_{j=0}^{n} \frac{(x_i - x_j)}{\left|\vec{p}_i - \vec{p}_j\right|^3} \hat{q}_i \hat{q}_j = \sum_{j=0}^{n} \frac{1}{P^3} \left\{ Q\left(1 - \frac{3X^2}{P^2}\right)\delta X - \frac{3XQ}{P^2}\left[Y\,\delta Y + Z\,\delta Z\right] + X\,\delta Q \right\}$$

Eqn. 5-18

$$\sum_{j=0}^{n} \frac{(y_i - y_j)}{\left|\vec{p}_i - \vec{p}_j\right|^3} \hat{q}_i \hat{q}_j = \sum_{j=0}^{n} \frac{1}{P^3} \left\{ Q\left(1 - \frac{3Y^2}{P^2}\right)\delta Y - \frac{3YQ}{P^2}\left[X\,\delta X + Z\,\delta Z\right] + Y\,\delta Q \right\}$$

$$\sum_{j=0}^{n} \frac{(z_i - z_j)}{\left|\vec{p}_i - \vec{p}_j\right|^3} \hat{q}_i \hat{q}_{j\,j} = \sum_{j=0}^{n} \frac{1}{P^3} \left\{ Q\left(1 - \frac{3Z^2}{P^2}\right)\delta Z - \frac{3ZQ}{P^2}\left[X\,\delta X + Y\,\delta Y\right] + Z\,\delta Q \right\}$$

where

Eqn. 5-19

$$\begin{aligned}
&P \equiv \left|\underline{\vec{p}}_i - \underline{\vec{p}}_j\right| \\
&X \equiv \bar{x}_i - \bar{x}_j \qquad Y \equiv \bar{y}_i - \bar{y}_j \qquad Z \equiv \bar{z}_i - \bar{z}_j \\
&\delta X \equiv \delta\bar{x}_i - \delta\bar{x}_j \qquad \delta Y \equiv \delta\bar{y}_i - \delta\bar{y}_j \qquad \delta Z \equiv \delta\bar{z}_i - \delta\bar{z}_j \\
&Q \equiv \bar{\hat{q}}_i \bar{\hat{q}}_j \qquad \delta Q \equiv \bar{\hat{q}}_j \delta\hat{q}_i + \bar{\hat{q}}_i \delta\hat{q}_j
\end{aligned}$$

and the equilibrium terms have been removed since they are cancelled with the equilibrium terms in the left hand side of Hill's equations.

The final linearized dynamic equations for the ith satellites are given by substituting Eqn. 5-19 into Eqn. 5-18.

$$\delta x_i'' - 2\delta y_i' - 3(\bar{x}_i + \delta x_i) = \sum_{j=0}^{n} \frac{1}{\left|\underline{\bar{p}}_i - \underline{\bar{p}}_j\right|^3} \cdot \left\{ \left(1 - \frac{3(\bar{x}_i - \bar{x}_j)^2}{\left|\bar{p}_i - \bar{p}_j\right|^2} \right) \bar{\hat{q}}_i \bar{\hat{q}}_j (\delta x_i - \delta x_j) + \right.$$

$$(\bar{x}_i - \bar{x}_j)(\bar{\hat{q}}_j \delta\hat{q}_i + \bar{\hat{q}}_i \delta\hat{q}_j) -$$

$$\left. \frac{3(\bar{x}_i - \bar{x}_j)}{\left|\bar{p}_i - \bar{p}_j\right|^2} \bar{\hat{q}}_i \bar{\hat{q}}_j \left[(\bar{y}_i - \bar{y}_j)(\delta y_i - \delta y_j) + (\bar{z}_i - \bar{z}_j)(\delta z_i - \delta z_j) \right] \right\}$$

$$\delta y_i'' + 2\delta x_i' - \delta y = \sum_{j=0}^{n} \frac{1}{\left|\underline{\bar{p}}_i - \underline{\bar{p}}_j\right|^3} \cdot \left\{ \left(1 - \frac{3(\bar{y}_i - \bar{y}_j)^2}{\left|\bar{p}_i - \bar{p}_j\right|^2} \right) \bar{\hat{q}}_i \bar{\hat{q}}_j (\delta y_i - \delta y_j) + \right.$$

$$(\bar{y}_i - \bar{y}_j)(\bar{\hat{q}}_j \delta\hat{q}_i + \bar{\hat{q}}_i \delta\hat{q}_j) -$$

$$\left. \frac{3(\bar{y}_i - \bar{y}_j)}{\left|\bar{p}_i - \bar{p}_j\right|^2} \bar{\hat{q}}_i \bar{\hat{q}}_j \left[(\bar{x}_i - \bar{x}_j)(\delta x_i - \delta x_j) + (\bar{z}_i - \bar{z}_j)(\delta z_i - \delta z_j) \right] \right\}$$

$$\delta z_i'' + \delta z_i = \sum_{j=0}^{n} \frac{1}{\left|\underline{\bar{p}}_i - \underline{\bar{p}}_j\right|^3} \cdot \left\{ \left(1 - \frac{3(\bar{z}_i - \bar{z}_j)^2}{\left|\bar{p}_i - \bar{p}_j\right|^2} \right) \bar{\hat{q}}_i \bar{\hat{q}}_j (\delta z_i - \delta z_j) + \right.$$

$$(\bar{z}_i - \bar{z}_j)(\bar{\hat{q}}_j \delta\hat{q}_i + \bar{\hat{q}}_i \delta\hat{q}_j) -$$

$$\left. \frac{3(\bar{z}_i - \bar{z}_j)}{\left|\bar{p}_i - \bar{p}_j\right|^2} \bar{\hat{q}}_i \bar{\hat{q}}_j \left[(\bar{x}_i - \bar{x}_j)(\delta x_i - \delta x_j) + (\bar{y}_i - \bar{y}_j)(\delta y_i - \delta y_j) \right] \right\}$$

Eqn. 5-20

$i = 1, \ldots, n$ *and* $i \neq j$

Eqn. 5-20 will be used to form the $\underline{\underline{A}}$ and $\underline{\underline{B}}$ matrices needed to evaluate stability and controllability in the remainder of this Chapter.

5.5. *Earth Orbiting Three-satellite Formation*

The three-satellite formation aligned on the x-axis shown in Figure 3-3(a) and described in Section 3.1.1 and the equilibrium equations and solutions is examined in Section 4.1.1.

5.5.1. Linearized Dynamic System

Six dynamic equations are formed by substituting the relative displacement constraint, Eqn. 4-5, into Eqn. 5-20.

$$
\begin{aligned}
&\delta x_1'' - 2\delta y_1' + a_1\delta x_1 + a_2\delta x_2 + b_1\delta\hat{q}_0 + b_2\delta\hat{q}_1 + b_3\delta\hat{q}_2 = 0\\
&\delta y_1'' + 2\delta x_1' + a_3\delta y_1 + a_4\delta y_2 = 0\\
&\delta z_1'' + a_5\delta z_1 + a_4\delta z_2 = 0\\
&\delta x_2'' - 2\delta y_2' + a_1\delta x_2 + a_2\delta x_1 + b_4\delta\hat{q}_0 + b_5\delta\hat{q}_2 + b_6\delta\hat{q}_1 = 0\\
&\delta y_2'' + 2\delta x_2' + a_3\delta y_2 + a_4\delta y_1 = 0\\
&\delta z_2'' + a_5\delta z_2 + a_4\delta z_1 = 0
\end{aligned}
$$

Eqn. 5-21

where

$$
\begin{aligned}
&a_1 = \left(-3 + \frac{2\bar{\hat{q}}_0\bar{\hat{q}}_1}{L^3} + \frac{\bar{\hat{q}}_2\bar{\hat{q}}_1}{4L^3}\right) \qquad a_2 = -\frac{\bar{\hat{q}}_2\bar{\hat{q}}_1}{4L^3} \qquad a_3 = -\left(\frac{\bar{\hat{q}}_0\bar{\hat{q}}_1}{L^3} + \frac{\bar{\hat{q}}_2\bar{\hat{q}}_1}{8L^3}\right)\\
&a_4 = \frac{\bar{\hat{q}}_2\bar{\hat{q}}_1}{8L^3} \qquad a_5 = \left(1 - \frac{\bar{\hat{q}}_0\bar{\hat{q}}_1}{L^3} - \frac{\bar{\hat{q}}_2\bar{\hat{q}}_1}{8L^3}\right)\\
&b_1 = -\frac{\bar{\hat{q}}_1}{L^2} \qquad b_2 = -\left(\frac{\bar{\hat{q}}_0}{L^2} + \frac{\bar{\hat{q}}_2}{4L^2}\right) \qquad b_3 = -\frac{\bar{\hat{q}}_1}{4L^2}\\
&b_4 = \frac{\bar{\hat{q}}_2}{L^2} \qquad b_5 = \left(\frac{\bar{\hat{q}}_0}{L^2} + \frac{\bar{\hat{q}}_1}{4L^2}\right) \qquad b_6 = \frac{\bar{\hat{q}}_2}{4L^2}
\end{aligned}
$$

Eqn. 5-22

After finding the dynamic equations, the equilibrium equations were obtained from Section 4.1.1 assuming the relative speeds and acceleration are equal to zero, and the perturbation terms $\left(\delta x_i, \delta y_i, \delta z_i, \text{and } \delta\bar{\hat{q}}_i\right)$ must equal zero as well. The linearized dynamic system is formed as

Eqn. 5-23

$$\underline{\dot{x}} = \underline{\underline{A}}\,\underline{x} + \underline{\underline{B}}\,\underline{u}$$

$$\begin{bmatrix} \delta x_1' \\ \delta y_1' \\ \delta z_1 \\ \delta x_2' \\ \delta y_2' \\ \delta z_2' \\ \delta x_1'' \\ \delta y_1'' \\ \delta z_1'' \\ \delta x_2'' \\ \delta y_2'' \\ \delta z_2'' \end{bmatrix} = \underline{\underline{A}} \begin{bmatrix} \delta x_1 \\ \delta y_1 \\ \delta z_1 \\ \delta x_2 \\ \delta y_2 \\ \delta z_2 \\ \delta x_1' \\ \delta y_1' \\ \delta z_1' \\ \delta x_2' \\ \delta y_2' \\ \delta z_2' \end{bmatrix} + \underline{\underline{B}} \begin{bmatrix} \delta\hat{q}_0 \\ \delta\hat{q}_1 \\ \delta\hat{q}_2 \end{bmatrix}$$

where $\underline{\underline{A}}$ is a 12×12 matrix, $\underline{x}$ is a 12×1 matrix, $\underline{\underline{B}}$ is a 12×3 matrix, and $\underline{u}$ is a 3×1 matrix. Using the variables of in Eqn. 5-22, matrices $\underline{\underline{A}}$ and $\underline{\underline{B}}$ are

Eqn. 5-24

$$A = \begin{bmatrix} 0 & 0 & 0 & 0 & 0 & 0 & 1 & 0 & 0 & 0 & 0 & 0 \\ 0 & 0 & 0 & 0 & 0 & 0 & 0 & 1 & 0 & 0 & 0 & 0 \\ 0 & 0 & 0 & 0 & 0 & 0 & 0 & 0 & 1 & 0 & 0 & 0 \\ 0 & 0 & 0 & 0 & 0 & 0 & 0 & 0 & 0 & 1 & 0 & 0 \\ 0 & 0 & 0 & 0 & 0 & 0 & 0 & 0 & 0 & 0 & 1 & 0 \\ 0 & 0 & 0 & 0 & 0 & 0 & 0 & 0 & 0 & 0 & 0 & 1 \\ a_1 & 0 & 0 & a_2 & 0 & 0 & 0 & -2 & 0 & 0 & 0 & 0 \\ 0 & a_3 & 0 & 0 & a_4 & 0 & 2 & 0 & 0 & 0 & 0 & 0 \\ 0 & 0 & a_5 & 0 & 0 & a_4 & 0 & 0 & 0 & 0 & 0 & 0 \\ a_2 & 0 & 0 & a_1 & 0 & 0 & 0 & 0 & 0 & 0 & -2 & 0 \\ 0 & a_4 & 0 & 0 & a_3 & 0 & 0 & 0 & 0 & 2 & 0 & 0 \\ 0 & 0 & a_4 & 0 & 0 & a_5 & 0 & 0 & 0 & 0 & 0 & 0 \end{bmatrix}$$

$$B = \begin{bmatrix} 0 & 0 & 0 \\ 0 & 0 & 0 \\ 0 & 0 & 0 \\ 0 & 0 & 0 \\ 0 & 0 & 0 \\ 0 & 0 & 0 \\ b_0 & b_1 & b_2 \\ 0 & 0 & 0 \\ 0 & 0 & 0 \\ b_3 & b_4 & b_5 \\ 0 & 0 & 0 \\ 0 & 0 & 0 \end{bmatrix}$$

5.5.2. *Stability and Controllability of Earth Orbiting Three-satellite Formation*

After finding the $\underline{\underline{A}}$ and $\underline{\underline{B}}$ matrices from linearized dynamic equations, Matlab is used to find the eigenvalues of $\underline{\underline{A}}$ and the rank of the controllability matrix. There exist eigenvalues of $\underline{\underline{A}}$ having positive real parts, so the equilibrium point is unstable. In addition, the rank of the controllability matrix is 8 instead of 12 so it is also uncontrollable.

Earth orbiting three-satellite formation aligned at the *x*-axis is obviously unstable and uncontrollable because there are no forces acting in the *y* and *z*-direction, which

means there is nothing to balance the small tiny forces that exist in the y and z-direction. However, if the linear system is constrained to motion in the x-direction, which means $\underline{\underline{B}}$ is a 4×4 matrix, then the linear system is controllable.

Eqn. 5-25

$$B = \begin{bmatrix} 0 & 0 & 0 \\ 0 & 0 & 0 \\ b_0 & b_1 & b_2 \\ b_3 & b_4 & b_5 \end{bmatrix}$$

5.6. Earth Orbiting Triangular Formation

This formation was motivated by the controllability results of the previous section. Specifically, the actuation capability is required along more axes. The formation diagram is shown in Figure 3-4 and described in Section 3.1.2. The equilibrium equations and solutions are determined in Section 4.2.

5.6.1. Linearized Dynamic System

Six linearized dynamic equations are first derived from Eqn. 5-20, along with the relative displacement constraints in Eqn. 4-32. Since the charges of the collectors are the same, $\bar{\hat{q}}_1 = \bar{\hat{q}}_2$, the linearized dynamic equations can be simplified as

Eqn. 5-26

$$
\begin{aligned}
&\delta x_1'' - 2\delta y_1' + a_1\delta x_1 + a_2\delta x_2 + a_3\delta y_1 + b_0\delta\hat{q}_1 + b_1\delta\hat{q}_0 = 0 \\
&\delta y_1'' + 2\delta x_1' + a_3\delta x_1 + a_4\delta y_1 + a_5\delta y_2 + b_1\delta\hat{q}_0 + b_3\delta\hat{q}_1 + b_2\delta\hat{q}_2 = 0 \\
&\delta z_1'' + a_6\delta z_1 + a_2\delta z_2 = 0 \\
&\delta x_2'' - 2\delta y_2' + a_1\delta x_2 + a_2\delta x_1 - a_3\delta y_2 + b_0\delta\hat{q}_2 + b_1\delta\hat{q}_0 = 0 \\
&\delta y_2'' + 2\delta x_2' - a_3\delta x_2 + a_4\delta y_2 + a_5\delta y_1 - b_1\delta\hat{q}_0 - b_3\delta\hat{q}_2 - b_2\delta\hat{q}_1 = 0 \\
&\delta z_2'' + a_6\delta z_2 + a_2\delta z_1 = 0
\end{aligned}
$$

where

Eqn. 5-27

$$
\begin{aligned}
&a_1 = -3 + \frac{1}{2L^3}\bar{\hat{q}}_0\bar{\hat{q}}_1 - \frac{\sqrt{2}}{4L^3}\bar{\hat{q}}_1^2 \qquad a_2 = \frac{\sqrt{2}}{4L^3}\bar{\hat{q}}_1^2 \qquad a_3 = \frac{3}{2L^3}\bar{\hat{q}}_0\bar{\hat{q}}_1 \\
&a_4 = \frac{1}{2L^3}\bar{\hat{q}}_0\bar{\hat{q}}_1 + \frac{\sqrt{2}}{2L^3}\bar{\hat{q}}_1^2 \qquad a_5 = -\frac{\sqrt{2}}{2L^3}\bar{\hat{q}}_1^2 \qquad a_6 = 1 - \frac{1}{L^3}\bar{\hat{q}}_0\bar{\hat{q}}_1 - \frac{\sqrt{2}}{4L^3}\bar{\hat{q}}_1^2 \\
&b_0 = -\frac{\sqrt{2}}{2L^2}\bar{\hat{q}}_0 \qquad b_1 = -\frac{\sqrt{2}}{2L^2}\bar{\hat{q}}_1 \qquad b_2 = -\frac{1}{2L^2}\bar{\hat{q}}_1 \\
&b_3 = -\left(\frac{\sqrt{2}}{2L^2}\bar{\hat{q}}_0 + \frac{1}{2L^2}\bar{\hat{q}}_1\right)
\end{aligned}
$$

After obtaining the dynamic equations, the linearized dynamic system is formed, and the $\underline{\underline{A}}$ and $\underline{\underline{B}}$ matrices are

Eqn. 5-28

$$A = \begin{bmatrix} 0 & 0 & 0 & 0 & 0 & 0 & 1 & 0 & 0 & 0 & 0 & 0 \\ 0 & 0 & 0 & 0 & 0 & 0 & 0 & 1 & 0 & 0 & 0 & 0 \\ 0 & 0 & 0 & 0 & 0 & 0 & 0 & 0 & 1 & 0 & 0 & 0 \\ 0 & 0 & 0 & 0 & 0 & 0 & 0 & 0 & 0 & 1 & 0 & 0 \\ 0 & 0 & 0 & 0 & 0 & 0 & 0 & 0 & 0 & 0 & 1 & 0 \\ 0 & 0 & 0 & 0 & 0 & 0 & 0 & 0 & 0 & 0 & 0 & 1 \\ a_1 & a_3 & 0 & a_2 & 0 & 0 & 0 & -2 & 0 & 0 & 0 & 0 \\ a_3 & a_4 & 0 & 0 & -a_5 & 0 & 2 & 0 & 0 & 0 & 0 & 0 \\ 0 & 0 & a_6 & 0 & 0 & a_2 & 0 & 0 & 0 & 0 & 0 & 0 \\ a_2 & 0 & 0 & a_1 & -a_3 & 0 & 0 & 0 & 0 & 0 & -2 & 0 \\ 0 & -a_5 & 0 & -a_3 & a_4 & 0 & 0 & 0 & 0 & 2 & 0 & 0 \\ 0 & 0 & a_2 & 0 & 0 & a_6 & 0 & 0 & 0 & 0 & 0 & 0 \end{bmatrix}$$

$$B = \begin{bmatrix} 0 & 0 & 0 \\ 0 & 0 & 0 \\ 0 & 0 & 0 \\ 0 & 0 & 0 \\ 0 & 0 & 0 \\ 0 & 0 & 0 \\ b_1 & b_0 & 0 \\ b_1 & b_3 & b_2 \\ 0 & 0 & 0 \\ b_1 & 0 & b_0 \\ -b_1 & -b_2 & -b_3 \\ 0 & 0 & 0 \end{bmatrix}$$

5.6.2. *Stability and Controllability of Earth Orbiting Triangular Formation*

The stability and controllability can be determined again using Matlab by finding the eigenvalues of $\underline{\underline{A}}$ and the rank of the controllability matrix. There exist eigenvalues of $\underline{\underline{A}}$ having positive real parts so the equilibrium point is unstable. In addition, the rank of the controllability matrix obtained from Matlab is 8 instead of 12 so it is uncontrollable as well. In physically, this makes sense because: Earth orbiting triangular formation is aligned on the x_c-y_c plane. There is no way to apply z_c forces to move the spacecraft so this formation is unstable and uncontrollable. If the linear system is

constrained to maintain in x_c-y_c direction instead of the x_c-y_c-z_c direction, given that $\underline{\underline{B}}$ is an 8×8 matrix which is shown in Eqn. 5-29 and is 8 linearly independent (i.e. rank = 8), the linear system is controllable.

Eqn. 5-29

$$B = \begin{bmatrix} 0 & 0 & 0 \\ 0 & 0 & 0 \\ 0 & 0 & 0 \\ 0 & 0 & 0 \\ b_1 & b_0 & 0 \\ b_1 & b_3 & b_2 \\ b_1 & 0 & b_0 \\ -b_1 & -b_2 & -b_3 \end{bmatrix}$$

5.7. Earth Orbiting Seven-satellite Formation

The Earth Orbiting seven-satellite formation is shown in Figure 3-7 and is described in Section 3.1.5. The equilibrium equations and solutions are presented in Section 4.5.

5.7.1. Linearized Dynamic System

Eighteen dynamic equations are derived by substituting the relative displacement constraint, Eqn. 4-60, into Eqn. 5-20 and the Maple program that was used to create the dynamic equations is located in Appendix A.2. The linear dynamic system is formed. $\underline{\underline{A}}$ is a 36×36 matrix, $\underline{x}$ is a 36×1 matrix, $\underline{\underline{B}}$ is a 36×7 matrix and $\underline{u}$ is a 7×1 matrix. Both the $\underline{\underline{A}}$ and $\underline{\underline{B}}$ matrices are derived from Maple program in Appendix A.4.

5.7.2. *Stability and Controllability of Earth Orbiting Seven-satellite Formation*

After obtaining the $\underline{\underline{A}}$ and $\underline{\underline{B}}$ matrices from linearized dynamic equations, Matlab is used to find the eigenvalues of $\underline{\underline{A}}$ and the rank of controllability matrix. There exist eigenvalues of $\underline{\underline{A}}$ having positive real parts so the equilibrium point is not stable. When finding the rank of controllability matrix using Matlab, a problem occurs. Rank code in Matlab could not find the correct rank because Matlab automatically ignores the row or column when it multiples by a tiny number. However, the rank of the controllability matrix is 36 by calculating the controllability matrix. This implies that the linear dynamic system can be controlled. This is what is expected because all the forces are balanced when the satellites are located in the x_c-y_c-z_c plane.

5.8. Summary

The concept of stability and controllability are discussed in this section. The equilibrium solutions were obtained to determine if the system is stable or unstable, controllable or uncontrollable. The linearized dynamic system is formed as $\dot{\underline{x}} = \underline{\underline{A}}\underline{x} + \underline{\underline{B}}\underline{u}$. If $\underline{\underline{A}}$ matrix has all negative real parts of eigenvalues, then the equilibrium point is defined as stable. If $\underline{\underline{A}}$ matrix has positive real parts of eigenvalues, then the equilibrium point is defined as unstable. If the $\underline{\underline{A}}$ matrix has pure imaginary parts of eigenvalues then the equilibrium point is undefined. If the rank of controllability matrix is n where the vector is an $n \times mn$ matrix, then it is controllable.

Three different formations are discussed in this section: the Earth orbiting three-satellite formation, the Earth orbiting triangular formation, and the Earth orbiting seven-satellite formation. The linearized dynamic system is derived. All cases are unstable. Considering controllability, the Earth orbiting three-satellite formation is controlled in the x_c-axis. The Earth orbiting triangular formation can be controlled only in the x_c-y_c plane whereas the Earth orbiting seven-satellite formation is controllable in all 3 axes. Future work should focus on constructing a control law that can stabilize the formation. The full nonlinear equations should be used if not for the design, then at least for the closed-loop stability and performance evaluation.

6. Conclusions and Recommendations

6.1. Conclusions

This research investigated the Coulomb control concept for swarm satellites formations. Aside from the detailed analytic and numeric solutions found for specific cases, the research produced four main conclusions:

1. *Equilibrium (or at least near-equilibrium) rigid static formations were found for all cases considered.*

Purely analytic solutions were obtained for the Earth orbiting three, triangular, five, and seven spacecraft formations. Although analytic methods were not successful in analyzing the Earth orbiting six-spacecraft planar and libration five-spacecraft rotating formations, close numeric solutions were obtained. Based on this success, it might be summarized that most, if not all, formations may demonstrate equilibrium solutions using Coulomb control. No attempts to prove nor dis-prove this statement are made in the present work.

2. *Formations with spacing on the orders of ten meters can be maintained with spacecraft charged to tens of kilovolts (1 kVm – 26 kVm) in geostationary orbit.* Assuming the spacecraft radius are r = 1 m, the highest voltage required for maintaining the vehicle to stay at equilibrium state is less than 26 kV in the Earth orbiting six-spacecraft formation (pentagon shape). Spacecraft located along the x-axis normally required more voltage than the y and z-axis.

3. *All of the formations studied were unstable but one was found to be controllable.*

   A linear dynamic system was formed to determine the stability and controllability. If all the eigenvalues of $\underline{\underline{A}}$ matrix have negative real parts, then the formation is stable. Also, if the controllability matrix is of rank n, then it is controllable. All of the formations considered in this research were unstable. All but one were uncontrollable in 3D. The controllability was proven for all cases.

4. *To ensure 3-D controllability, a 3-D formation must be created.*

   A linear formation (the Earth orbiting three-satellite formation) can be controlled when constrained such that all three spacecraft are in a line. A planer formation (the Earth orbiting triangular formation) can be controlled only when constrained to be a plane. A 3D formation (the Earth orbiting seven-satellite formation) can be controlled in 3D.

6.2. Recommendations for Future Work

Many questions remain unanswered regarding Coulomb control. Logical follow-on work may be:

- Construct a control law for Coulomb Formations

  Although all formations were proven to be controllable, no attempt was made to construct a control law. The full nonlinear equations are suggested to use for close-loop stability and performance evaluation.

- *Evaluate position uncertainty in a formation using Coulomb control*

  It seems reasonable that a Coulomb controlled formation should enable precise position-keeping, however an analysis was not attempted. It would be interesting

to explore the position errors expected in a Coulomb system and compare them with those from a thruster-controlled system.

- *Determine an intelligent way to configure a Coulomb formation based on some performance metric rather than trial and error.*

  Formations chosen for the present work were loosely based on relevant interferometric geometries. For the most part, however, the formations were chosen simply to explore the feasibility and orbital mechanics. There are perhaps better formations which may require less charging and/or be more valuable for a specific mission. It would be helpful to develop some method to determine such formations a priori.

- *Investigate the proper integration of a Coulomb control system with thruster controls.*

  The Coulomb control concept has its greatest benefits in formation situations where thruster control has its greatest drawbacks and vice-versa. It would be helpful to develop a combined control scheme where both systems can exploit their strengths to provide the greatest mission enhancement.

References

[1] Pollard, J.E., Chao, C.C., and Janson, S.W., "Populating and maintaining cluster constellations in low-earth orbit," AIAA-99-2878, AIAA Meeting Papers on Disk Vol. 4, No. 3, Proc. Of 35th AIAA/ASME/SAE/ASEE Joint Propulsion Conference, June 20-24, 1999, Los Angeles, CA.

[2] Walker, J.G., "The geometry of cluster orbits," J. Brit. Interplan. Soc., Vol. 35, 1982, p. 345.

[3] Murdoch, J. and Pocha, J.J., "The orbit dynamics of satellite clusters," Paper IAF-82-54, 33rd International Astronautical Congress, Sept. 27-Oct. 2, 1982, Paris, France.

[4] Micci, M.M. and Ketsdever, A.D., Micropropulsion for Small Spacecraft, Progress in Astronautics and Aeronautics Vol. 187, AIAA Press, Reston VA, 2000, pp. 3-22.

[5] Hoskins, W.A., Wilson, M.J., Willey, M.J., Meckel, N.J., Campell, M., and Chung, S., "PPT development efforts at Primex Aerospace Company," Paper AIAA-99-2291, AIAA Meeting Papers on Disk Vol. 4, No. 3, Proc. Of 35th AIAA/ASME/SAE/ASEE Joint Propulsion Conference, June 20-24, 1999, Los Angeles, CA.

[6] Chao, C.C., Pollard, J.E., and Janson, S.W., "Dynamics and control of cluster orbits for distributed space missions," Paper AAS-99-126, Space Flight Mechanics Meeting, Feb. 7-10 1999, Breckenridge, CO.

[7] Kong, E.M.C., Miller, D.W., and Sedwick, R.J., "Exploiting orbital dynamics for aperture synthesis using distributed satellite systems: Applications to a visible Earth imager system," Paper AAS-99-122, Space Flight Mechanics Meeting, Feb. 7-10 1999, Breckenridge, CO.

[8] Sedwick, R., Miller, D., and Kong, E., "Mitigation of differential perturbations in clusters of formation flying satellites," Paper AAS-99-124, Space Flight Mechanics Meeting, Feb. 7-10 1999, Breckenridge, CO.

[9] Miller, D.W. and Spores, R.A., "Proceedings of the Formation Flying and Micropropulsion Workshop," unpublished, Oct. 20-21 1998, available from Dr. Ronald Spores, Air Force Research Laboratory, Edwards AFB, CA.

[10] Micci, M.M. and Ketsdever, A.D., Micropropulsion for Small Spacecraft, Progress in Astronautics and Aeronautics, Vol. 187, AIAA Press, Reston, VA, 2000.

[11] Corazzini, T., Robertson, A., Adams, J.C., Hassibi, A., and How, J.P., "GPS sensing for spacecraft formation flying," Proceedings of the 10th International Technical Meeting, ION/GPS, Sept. 16-19 1997, Kansas City, MO.

[12] Vassar, R.H. and Sherwood, R.B., "Formationkeeping for a pair of satellites in a circular orbit," Journal of Guidance, Control, and Dynamics, Vol. 8, No. 2, 1985.

[13] Leonard, C.L., "Fuel penalty of using ballistic coefficient control for satellite formationkeeping," AAS 13th Annual Guidance and Control Conference, Keystone, CO, Feb. 1990.

[14] Jilla, Cyrus D., Separated Spacecraft Interferometry – System Architecture Design and Optimization, Master's Thesis, Dept. of Aeronautics and Astronautics, Massachusetts Institute of Technology, Feb. 1999.

[15] Kong, Edmund M., Optimal Trajectories and Orbit Design for Separated Spacecraft Interferometry, Master's Thesis, Dept. of Aeronautics and Astronautics, Massachusetts Institute of Technology, Nov. 1998.

[16] Yashko, Gregory, Ion Micro-Propulsion and Cost Modelling for Satellite Clusters, Master's Thesis, Dept. of Aeronautics and Astronautics, Massachusetts Institute of Technology, June 1998.

[17] Hacker, Troy L., Performance of a Space-based GMTI Radar System using Separated Spacecraft Interferometry, Master's Thesis, Dept. of Aeronautics and Astronautics, Massachusetts Institute of Technology, May 2000.

[18] Janson, S.W., Helvajian, H., Hansen, W.W., and Lodmell, J., "Microthrusters for nanosatellites," 2nd International Conference on Integraed Micro Nanotechnology for Space Applications (MNT99), Apr. 11-14 1999, Pasadena, CA.

[19] Janson, S.W., Helvajian, H., Hansen, W.W., and Lodmell, J., "Batch-fabricated CW microthrusters for kilogram-class spacecraft," Paper AIAA-99-2722, AIAA Meeting Papers on Disk Vol. 4, No. 3, Proc. Of 35th AIAA/ASME/SAE/ASEE Joint Propulsion Conference, June 20-24, 1999, Los Angeles, CA.

[20] Tajmar, M., Mitterauer, J., and Wang, J., "Field-emission-electric-propulsion (FEEP) plasma modeling: 3D full particle simulations," Paper AIAA-99-2298, AIAA Meeting Papers on Disk Vol. 4, No. 3, Proc. Of 35th AIAA/ASME/SAE/ASEE Joint Propulsion Conference, June 20-24, 1999, Los Angeles, CA.

[21] Martinez-Sanchez, M. and Pollard, J.E., "Spacecraft electric propulsion – An overview," Journal of Propulsion and Power, Vol. 14, No. 5, Sept-Oct 1998, pp. 688-699.

[22] Martinez-Sanchez, M., and Pollard, J.E., "Spacecraft Electric Propulsion – An Overview," Journal of Propulsion and Power, Vol. 14, No. 5, Sept.-Oct. 1998, pp. 688-699.

[23] Osgood, R.N., "Operational status of the space test program P78-2 spacecraft and payloads," reported in Proceedings of 3rd Spacecraft Charging Technology Conference, Nov. 12-14, 1980, NASA Conference Publication 2182, pp. 365-369.

[24] Gussenhoven, M.S., Cohen, H.A., Hardy, D.A., Burke, W.J., and Chesley, A., "Analysis of ambient and beam particle characteristics during the ejection of an electron beam from a satellite in near-geosynchronous orbit on March 30, 1979," reported in Proc. of 3rd Spacecraft Charging Technology Conference, No. 12-14, 1980, NASA Conference Publication 2182, pp. 642-664.

[25] Cohen, H.A., Adamo, R.C., Aggson, T., Chesley, A.L., Clark, D.M., Damron, S.A., Delorey, D.E., Fennell, J.F., Gussenhoven, M.S., Hanser, F.A., Hall, D., Hardy, D.A., Huber, W.B., Katz, I., Koons, H.C., Lau, S.T., Ledley, B., Mizera, P.F., Mullen, E.G., Nanevicz, J.E., Olsen, R.C., Rubin, A.G., Schnuelle, G.W., Saflekos, N.A., Tautz, M.F., and Whipple, E.C., "P78-2 Satellite and payload responses to electron beam operations on March 30, 1979," reported in Proc. of 3rd Spacecraft Charging Technology Conference, Nov. 12-14, 1980, NASA Conference Publication 2182, pp. 509-559.

[26] Osgood, R.N., "Operational status of the space test program P78-2 spacecraft and payloads," reported in Proc. of 3rd Spacecraft Charging Technology Conference, Nov. 12-14, 1980, NASA conference Publication 2182, pp. 412-432.

[27] Whipple, E.C., and Olsen, R.C., "Importance of differential charging for controlling both natural and induced vehicle potentials on ATS-5 and ATS-6," reported in Proc. of 3rd Spacecraft Charging Technology Conference, Nov. 12-14, 1980, NASA Conference Publication 2182, p. 887.

[28] Deininger, W.D., Aston, G., and Pless, L.C., "Hollow-cathode plasma source for active spacecraft charge control," Review of Scientific Instruments, Vol. 58, No. 6, June 1987, pp. 1053-1062.

[29] Ridgeway, S.T., "The scientific support for a space interferometry mission," SPIE Vol. 1947 Spaceborne Interferometry, 1993, pp. 2-11.

[30] See, for instance, Hecht, E., Optics, Addison-Wesley, 1998.

[31] Golay, M., "Point arrays having compact non-redundant autocorrelations, Journal of Optical Society of America, Vol. 61, pg. 272, 1971.

[32] Cornwell, T.J., "A Novel Principle for Optimization of the Instantaneous Fourier Plane Coverage of Correlation Arrays," IEEE Trans. On Antennas and Propagation, Vol. 36, No. 8, pp. 1165-1167.

[33] Sabol, Chris, Burns, Richard, and McLaughlin, Craig A., "Satellite Formation Flying Design and Evolution," AAS 99-121, pp.265-283

[34] Lo, Martin W., "Satellite-constellation Design," California Institute of Technology, IEEE 1521-9615/99, January-February 1999.

[35] See, for instance, Proceedings of 1st and 2nd Spacebone Interferometry Conference, SPIE Vol. 1947, 2477, 1993, and 1995.

[36] Kong, Edmund M. C., Miller, David W., and Sedwick , Raymond J., "Exploiting Orbital Dynamics for Aperture Synthesis Using Distributed Satellite Systems: Applications to A Visible Earth Imager System," American Astronautical Society, Paper AAS 99-122, 1999, pp. 285-301

[37] Sabol, Chris, Burns, Richard, and McLaughlin Craig A., "Satellite Formation Flying Design and Evolution," American Astronautical Society, Paper AAS 99-121, 1999, pp.265-283

[38] Sparks A., "Linear Control of Satellite Formation Flying," American Institute of Aeronautics and Astronautics, Paper AIAA-2000-4438.

[39] Schweighart, Samuel A., Development and Analysis of a High Fidelity Linearized J_2 model for Satellite Formation Flying, Master's Thesis, Dept. of Aeronautical and Astronautical, Massachusetts Institute of Technology, June 2001.

[40] Sedwick, Raymond J., Miller, David W., and Kong, Edmund M.C., "Mitigation of Differential Perturbations in Clusters of Formation Flying Satellites," American Astronautical Society, Paper AAS 99-124, pp. 323-342.

[41] Pollard, James E., Chao, C.C. (George), Janson, Siegfried W., "Populating and Maintaining Cluster Constellations in Low-Earth Orbit," The Aerospace Corporation, American Institute of Aeronautics and Astronautics, Paper AIAA-99-2871.

[42] Leonard, C.L., "Orbital Formation-keeping with Differential Drag," Vol.12, No.1, Jan-Feb. 1989.

[43] Schaub, Hanspeter and Alfriend, Kyle T., "Hybrid Cartesian and Orbit Element Feedback Law for Formation Flying Spacecraft," American Institute of Aeronautics and Astronautics, Paper AIAA 2000-4131, August 14-17, 2000.

[44] Wang, P.K.C. and Hadaegh, F.Y., "Coordination and Control of Multiple Microspacecraft Moving in Formation," The Journal of the Astronautical Sciences, Vol. 44, No. 3, July-September 1996, pp.315-355.

[45] Queiroz, Marcio S. de, Kapila, Vikram, and Yan, Qigua, "Adaptive Nonlinear Control of Multiple Spacecraft Formation Flying," Polytechnic University, Journal of Guidance, Vol. 23, No. 3, May-June 2000.

[46] Kapila, Vikram, Sparks, Andrew G., Buffington, James M., and Yan, Qiguo, "Spacecraft formation flying: Dynamics and Control," Journal of Guidance, Vol. 23, No. 3. pp. 561-564.

[47] Lau, Kenneth, Lichten, Stephen, Young, Lawrence, Haines, Bruce, "An Innovative Deep Space Application of GPS Technology for Formation Flying Spacecraft," California Institute of Technology, American Institute of Aeronautics and Astronautics, Paper AIAA 96-3819, July 1996.

[48] Inalhan, Gokhan, Busse, Franz D., How, Jonathan P., "Precise Formation Flying Control of Multiple Spacecraft Using Carrier-phase Differential GPS," American Astronautical Society, Paper AAS 00-109.

[49] Tan, Zhaozhi, Bainum, Peter M., and Strong, Avine, "A Strategy for Maintaining Distance Between Satellites in an Orbiting Constellation," American Astronautical Society, Paper AAS 99-125, 1999, pp. 343-353

[50] Cornwell, T.J., "A Novel Principle for Optimization of the Instantaneous Fourier Plane Coverage of Correlation Arrays," IEEE Trans. On Antennas and Propagation, Vol. 36, No. 8, pp.1165-1167.

[51] Slotine, Jean-Jaques E., and Li, Weiping, "Applied Nonlinear Control," Prentice Hall, pp.55-58.

[52] Dr. Gordon Parker, 'MEEM 6702:Nonlinear System Analysis and Control' Handout, Spring 2002.

Appendix A

Maple Program of Dynamic Equations of Satellite Formations

A.1. Creating Lagrange Equation Program

```
with(linalg):

ft2sym := proc(fn,sym_ar,ft_ar)
  local ncols, temp, i;

  temp := fn:
  ncols := rowdim(sym_ar):
  for i from 1 to ncols do
    temp := subs(ft_ar[i,1]=sym_ar[i,1],temp):
  od;

  temp;
end;

sym2ft := proc(fn,sym_ar,ft_ar)
  local ncols, temp, i;

  temp := fn:
  ncols := rowdim(sym_ar):
  for i from 1 to ncols do
    temp := subs(sym_ar[i,1]=ft_ar[i,1],temp):
  od;
  temp;
end;

time_deriv := proc(interm,vars,varsd,varsdd)

 local varsd_t, varsdd_t, temp, d_dt, d_dt_sym;

 varsd_t := map(diff,vars(t),t):
 varsdd_t := map(diff,varsd_t,t):

 temp := sym2ft(interm,vars,vars(t)):
 temp := sym2ft(temp,varsd,varsd_t):
 d_dt := diff(temp,t):
 d_dt_sym := ft2sym(d_dt,varsdd,varsdd_t):
 d_dt_sym := ft2sym(d_dt_sym,varsd,varsd_t):
 d_dt_sym := ft2sym(d_dt_sym,vars,vars(t)):
```

```
  eval(d_dt_sym):
end;

time_deriv_vector := proc(invec,vars,varsd,varsdd)
  local temp, k, i;

  k := nops(convert(invec,list)):
  temp := array(1..k):

  for i from 1 to k do
    temp[i] := time_deriv(invec[i],vars,varsd,varsdd):
  od;
  evalm(temp):
end;


MakeEQMO := proc(L,vars,deriv_sym,deriv2_sym)

   local ncols, EQ, d_dt, i, temp, vars_dt, vars2_dt;

   ncols := rowdim(deriv_sym);
print(ncols);
   EQ:= array(1..ncols):
   d_dt:= array(1..ncols):

   vars_dt := map(diff,vars(t),t):
   vars2_dt := map(diff,vars_dt,t):

   for i from 1 to ncols do
      temp := diff(L,deriv_sym[i,1]):
      temp := sym2ft(temp,vars,vars(t)):
      temp := sym2ft(temp,deriv_sym,vars_dt):
      d_dt[i] := diff(temp,t):
   od;

   for i from 1 to ncols do
      EQ[i]:= d_dt[i] - diff(L,vars[i,1]):
   od;

   for i from 1 to ncols do
      EQ[i]:= ft2sym(EQ[i],deriv2_sym,vars2_dt):
      EQ[i]:= ft2sym(EQ[i],deriv_sym,vars_dt):
      EQ[i]:= ft2sym(EQ[i],vars,vars(t)):
   od;
```

```
  EQ;
end;

MakeEQ := proc(L,vars,deriv_sym,deriv2_sym)

  local ncols, EQ, d_dt, i, temp, vars_dt, vars2_dt;

  ncols := rowdim(deriv_sym);
print(ncols);
  EQ:= array(1..ncols):
  d_dt:= array(1..ncols):

  vars_dt := map(diff,vars(t),t):
  vars2_dt := map(diff,vars_dt,t):

  for i from 1 to ncols do
    EQ[i]:=  diff(L,vars[i,1]):
  od;

  for i from 1 to ncols do
    EQ[i]:= ft2sym(EQ[i],deriv2_sym,vars2_dt):
    EQ[i]:= ft2sym(EQ[i],deriv_sym,vars_dt):
    EQ[i]:= ft2sym(EQ[i],vars,vars(t)):
  od;

  EQ;
end;
```

A.2. Maple Program of Creating Dynamic Equations of Satellite Formations

This is a programming to create the dynamic equations of Earth orbiting three-satellite, five-satellite, six-satellite, and seven-satellite formation. The program below is the program generate dynamic equations of Earth orbiting seven-satellite formation:

```
# Maple script for calculating the dynamic equations for 6 collector,
# and one combiner.


# Maple Libraries
with(linalg):
#(C);
#readlib(mtaylor);
```

```
# Custom library for implementing Lagrange's equations
read '/home/megrad/jchong/files/res-maple/eqmo_util.mpl';

# ************** ARRAY and MATRIX INITIALIZATION

# The array "vars" contains a list of the names given to independent
# variables used to describe the kinematics, and ultimately, the
# dynamics. Each member of this list is assume to be independent, and
# a function of time. Any quantity used to describe the position of
# the payload and is an independent function of time must be in this
# list.
vars   := array([ [rr]    , [tht] ,
                  [x1]    , [y1]  , [z1] ,
                  [x2]    , [y2]  , [z2] ,
                  [x3]    , [y3]  , [z3] ,
                  [x4]    , [y4]  , [z4] ,
                  [x5]    , [y5]  , [z5] ,
                  [x6]    , [y6]  , [z6]  ]):

# The array "varsd" contains the names given to the time derivatives
# of the quantities in "vars". Although Maple can display time derivatives
# using a d/dt notation, the ability to let the user assign the
# names results in more compact dynamic equations, and facilitates
# their use in automatically generated C code.
varsd  := array([ [rrd]   , [thtd]  ,
                  [x1d]    , [y1d]  , [z1d]  ,
                  [x2d]    , [y2d]  , [z2d]  ,
                  [x3d]    , [y3d]  , [z3d]  ,
                  [x4d]    , [y4d]  , [z4d]  ,
                  [x5d]    , [y5d]  , [z5d]  ,
                  [x6d]    , [y6d]  , [z6d]  ]):

# The array "varsdd" is similar to "varsd", but for the second
# derivatives of the variables in "vars". You guessed it, the "d"
# suffix designates a time derivative.
varsdd := array([ [rrdd]  , [thtdd]  ,
                  [x1dd]    , [y1dd]  , [z1dd]  ,
                  [x2dd]    , [y2dd]  , [z2dd]  ,
                  [x3dd]    , [y3dd]  , [z3dd]  ,
                  [x4dd]    , [y4dd]  , [z4dd]  ,
                  [x5dd]    , [y5dd]  , [z5dd]  ,
                  [x6dd]    , [y6dd]  , [z6dd]  ]):

# ******************** ENERGY CALCULATION
# Deriving the differential equations of motion using Lagrange's equations
# requires the computation of the kinetic and potential energy of the
```

```
# payload. This is accomplished by first forming the absolute position vector
# from the origin of the inertial frame {I} to the payload, represented in
# inertial coordinates. Although the expression would be more compact using
# a rotating coordinate system, we are using inertial coordinates and
# letting Maple perform all the simplifications.
#
# After getting position, the absolute velocity is easily computed leading
# directly to the kinetic energy. Potential energy is computed by taking the
# the z-component of the position vector.

# *** POSITION VECTORS
# Form position vectors
p0 := array([rr, 0, 0]):
p1 := array([rr+x1, y1, z1]):
p2 := array([rr+x2, y2, z2]):
p3 := array([rr+x3, y3, z3]):
p4 := array([rr+x4, y4, z4]):
p5 := array([rr+x5, y5, z5]):
p6 := array([rr+x6, y6, z6]):
angvel := array([0, 0, thtd]):

p0d := evalm(time_deriv_vector(p0,vars,varsd,varsdd) +
   crossprod(angvel,p0)):
p1d := evalm(time_deriv_vector(p1,vars,varsd,varsdd) +
   crossprod(angvel,p1)):
p2d := evalm(time_deriv_vector(p2,vars,varsd,varsdd) +
   crossprod(angvel,p2)):
p3d := evalm(time_deriv_vector(p3,vars,varsd,varsdd) +
  crossprod(angvel,p3)):
p4d := evalm(time_deriv_vector(p4,vars,varsd,varsdd) +
   crossprod(angvel,p4)):
p5d := evalm(time_deriv_vector(p5,vars,varsd,varsdd) +
   crossprod(angvel,p5)):
p6d := evalm(time_deriv_vector(p6,vars,varsd,varsdd) +
   crossprod(angvel,p6)):

KE := (Mc*evalm(transpose(p0d)&*p0d) +
     Ms*evalm(transpose(p1d)&*p1d) +
     Ms*evalm(transpose(p2d)&*p2d) +
     Ms*evalm(transpose(p3d)&*p3d) +
     Ms*evalm(transpose(p4d)&*p4d) +
     Ms*evalm(transpose(p5d)&*p5d) +
     Ms*evalm(transpose(p6d)&*p6d) )/2:

KE := simplify(expand(KE)):
```

```
Peg := -mu*Mc/rr - mu*Ms/sqrt( (rr+x1)^2+y1^2+z1^2 ) -
            mu*Ms/sqrt( (rr+x2)^2+y2^2+z2^2 ) -
            mu*Ms/sqrt( (rr+x3)^2+y3^2+z3^2 ) -
            mu*Ms/sqrt( (rr+x4)^2+y4^2+z4^2 ) -
            mu*Ms/sqrt( (rr+x5)^2+y5^2+z5^2 ) -
            mu*Ms/sqrt( (rr+x6)^2+y6^2+z6^2 ):

Peg := simplify(expand(Peg)):

Pec := kk*q0*q1/sqrt(x1^2+y1^2+z1^2) +
     kk*q0*q2/sqrt(x2^2+y2^2+z2^2) +
     kk*q0*q3/sqrt(x3^2+y3^2+z3^2) +
     kk*q0*q4/sqrt(x4^2+y4^2+z4^2) +
     kk*q0*q5/sqrt(x5^2+y5^2+z5^2) +
     kk*q0*q6/sqrt(x6^2+y6^2+z6^2) +
     kk*q1*q2/sqrt( (x2-x1)^2 + (y2-y1)^2 + (z2-z1)^2  ) +
     kk*q1*q3/sqrt( (x3-x1)^2 + (y3-y1)^2 + (z3-z1)^2  ) +
     kk*q1*q4/sqrt( (x4-x1)^2 + (y4-y1)^2 + (z4-z1)^2  ) +
     kk*q1*q5/sqrt( (x5-x1)^2 + (y5-y1)^2 + (z5-z1)^2  ) +
     kk*q1*q6/sqrt( (x6-x1)^2 + (y6-y1)^2 + (z6-z1)^2  ) +
     kk*q2*q3/sqrt( (x3-x2)^2 + (y3-y2)^2 + (z3-z2)^2  ) +
     kk*q2*q4/sqrt( (x4-x2)^2 + (y4-y2)^2 + (z4-z2)^2  ) +
     kk*q2*q5/sqrt( (x5-x2)^2 + (y5-y2)^2 + (z5-z2)^2  ) +
     kk*q2*q6/sqrt( (x6-x2)^2 + (y6-y2)^2 + (z6-z2)^2  ) +
     kk*q3*q4/sqrt( (x4-x3)^2 + (y4-y3)^2 + (z4-z3)^2  ) +
     kk*q3*q5/sqrt( (x5-x3)^2 + (y5-y3)^2 + (z5-z3)^2  ) +
     kk*q3*q6/sqrt( (x6-x3)^2 + (y6-y3)^2 + (z6-z3)^2  ) +
     kk*q4*q5/sqrt( (x5-x4)^2 + (y5-y4)^2 + (z5-z4)^2  ) +
     kk*q4*q6/sqrt( (x6-x4)^2 + (y6-y4)^2 + (z6-z4)^2  ) +
     kk*q5*q6/sqrt( (x6-x5)^2 + (y6-y5)^2 + (z6-z5)^2  ) :

Pec := simplify(expand(Pec)):

Lag := KE -  Pec:

# ************ IMPLEMENTATION OF LAGRANGE'S EQUATIONS
eq := MakeEQMO(Lag,vars,varsd,varsdd):

GenF := MakeEQMO(-Peg,vars,varsd,varsdd):

for i from 1 to 20 do
  eq[i] := expand(eq[i]):
  GenF[i] := expand(GenF[i]):
od:

NewGenF := array(1..20):
```

```
mu:=rr*rr*rr*thtd*thtd:

for i from 1 to 20 do

  temp1:= mtaylor(GenF[i],
    [x1,y1,z1,x2,y2,z2,x3,y3,z3,x4,y4,z4,x5,y5,z5,x6,y6,z6],2):
  temp2 := simplify(expand(temp1)):
  NewGenF[i] := expand(temp2/csgn(rr)):
od;

for i from 1 to 20 do
  eq[i] := eq[i] + NewGenF[i]:
od;

x1:=0:
x2:=0:
x3:=0:
x4:=0:
x5:=-L:
x6:=L:

y1:=L*sin(phi):
y2:=-L*cos(phi):
y3:=-L*sin(phi):
y4:=L*cos(phi):
y5:=0:
y6:=0:

z1:=-L*cos(phi):
z2:=-L*sin(phi):
z3:=L*cos(phi):
z4:=L*sin(phi):
z5:=0:
z6:=0:

x1d:=0:
x2d:=0:
x3d:=0:
x4d:=0:
x5d:=0:
x6d:=0:

y1d:=L*phid*cos(phi):
y2d:=L*phid*sin(phi):
y3d:=-L*phid*cos(phi):
y4d:=-L*phid*sin(phi):
```

```
y5d:=0:
y6d:=0:

z1d:=L*phid*sin(phi):
z2d:=-L*phid*cos(phi):
z3d:=-L*phid*sin(phi):
z4d:=L*phid*cos(phi):
z5d:=0:
z6d:=0:

x1dd:=0:
x2dd:=0:
x3dd:=0:
x4dd:=0:
x5dd:=0:
x6dd:=0:

y1dd:=L*phidd*cos(phi) - L*phid*phid*sin(phi):
y2dd:=L*phidd*sin(phi) + L*phid*phid*cos(phi):
y3dd:=-L*phidd*cos(phi) + L*phid*phid*sin(phi):
y4dd:=-L*phidd*sin(phi) - L*phid*phid*cos(phi):
y5dd:=0:
y6dd:=0:

z1dd:=L*phidd*sin(phi) + L*phid*phid*cos(phi):
z2dd:=-L*phidd*cos(phi) + L*phid*phid*sin(phi):
z3dd:=-L*phidd*sin(phi) - L*phid*phid*cos(phi):
z4dd:=L*phidd*cos(phi) - L*phid*phid*sin(phi):
z5dd:=0:
z6dd:=0:

rrd :=0:
rrdd := 0:
thtdd := 0:

# Constant equilibrium setting:
u1:=kk/L^2:
u2:=sqrt(2)*kk/(2*L^2):
u3:=sqrt(4)*kk/(8*L^2):
c1:=Ms*thtd^2*L:

# Equilibrium Solutions:
q3:=q1:
q4:=q2:
q6:=q5:
q2:=sqrt(12*c1*(u3-u2)/(u2-u3)^2):
```

```
q1:=(-(u2-u3)*q2+sqrt((u2-u3)^2*q2^2+4*(u3-u2)*c1))/(2*(u3-u2)):
q5:=(-(u2-u3)*q2+sqrt((u2-u3)^2*q2^2-12*c1*(u3-u2)))/(2*(u3-u2)):
q0:=(-u2*q5-u3*q2-u2*q1)/u1:

phi:=0:
phid:=0:
phidd:=0:
```

A.3. Maple Program of Libration Point Five-satellite Formation

```
# ************************* LIBRARIES
# Maple Libraries
with(linalg):
#(C);
#readlib(mtaylor);

# Custom library for implementing Lagrange's equations
read '/home/megrad/jchong/files/res-maple/eqmo_util.mpl';

# ************** ARRAY and MATRIX INITIALIZATION

# The array "vars" contains a list of the names given to independent
# variables used to describe the kinematics, and ultimately, the
# dynamics. Each member of this list is assume to be independent, and
# a function of time. Any quantity used to describe the position of
# the payload and is an independent function of time must be in this
# list.
vars   := array([ [x0]    , [y0]  , [z0] ,
                  [x1]    , [y1]  , [z1] ,
                  [x2]    , [y2]  , [z2] ,
                  [x3]    , [y3]  , [z3] ,
                  [x4]    , [y4]  , [z4]  ]):

# The array "varsd" contains the names given to the time derivatives
# of the quantities in "vars". Although Maple can display time derivatives
# using a d/dt notation, the ability to let the user assign the
# names results in more compact dynamic equations, and facilitates
# their use in automatically generated C code.
varsd  := array([ [x0d]    , [y0d]  , [z0d]  ,
                  [x1d]    , [y1d]  , [z1d]  ,
                  [x2d]    , [y2d]  , [z2d]  ,
                  [x3d]    , [y3d]  , [z3d]  ,
                  [x4d]    , [y4d]  , [z4d]  ]):
```

```
# The array "varsdd" is similar to "varsd", but for the second
# derivatives of the variables in "vars". You guessed it, the "d"
# suffix designates a time derivative.
varsdd := array([ [x0dd]    , [y0dd]  , [z0dd]  ,
                  [x1dd]    , [y1dd]  , [z1dd]  ,
                  [x2dd]    , [y2dd]  , [z2dd]  ,
                  [x3dd]    , [y3dd]  , [z3dd]  ,
                  [x4dd]    , [y4dd]  , [z4dd]  ]):

# ******************* ENERGY CALCULATION
# Deriving the differential equations of motion using Lagrange's equations
# requires the computation of the kinetic and potential energy of the
# payload. This is accomplished by first forming the absolute position vector
# from the origin of the inertial frame {I} to the payload, represented in
# inertial coordinates. Although the expression would be more compact using
# a rotating coordinate system, we are using inertial coordinates and
# letting Maple perform all the simplifications.
#
# After getting position, the absolute velocity is easily computed leading
# directly to the kinetic energy. Potential energy is computed by taking the
# the z-component of the position vector.

# *** POSITION VECTORS
# Form position vectors
p0 := array([x0, y0, z0]):
p1 := array([x1, y1, z1]):
p2 := array([x2, y2, z2]):
p3 := array([x3, y3, z3]):
p4 := array([x4, y4, z4]):

angvel := array([0, 0, thtd]):

p0d := evalm(time_deriv_vector(p0,vars,varsd,varsdd) +
   crossprod(angvel,p0)):
p1d := evalm(time_deriv_vector(p1,vars,varsd,varsdd) +
   crossprod(angvel,p1)):
p2d := evalm(time_deriv_vector(p2,vars,varsd,varsdd) +
   crossprod(angvel,p2)):
p3d := evalm(time_deriv_vector(p3,vars,varsd,varsdd) +
  crossprod(angvel,p3)):
p4d := evalm(time_deriv_vector(p4,vars,varsd,varsdd) +
   crossprod(angvel,p4)):

KE := (M0*evalm(transpose(p0d)&*p0d) +
     M1*evalm(transpose(p1d)&*p1d) +
     M2*evalm(transpose(p2d)&*p2d) +
```

```
    M3*evalm(transpose(p3d)&*p3d) +
    M4*evalm(transpose(p4d)&*p4d) )/2:

KE := simplify(expand(KE)):

Pec := kk*q0*q1/sqrt( (x1-x0)^2+(y1-y0)^2+(z1-z0)^2) +
     kk*q0*q2/sqrt( (x2-x0)^2+(y2-y0)^2+(z2-z0)^2) +
     kk*q0*q3/sqrt( (x3-x0)^2+(y3-y0)^2+(z3-z0)^2) +
     kk*q0*q4/sqrt( (x4-x0)^2+(y4-y0)^2+(z4-z0)^2) +
     kk*q1*q2/sqrt( (x2-x1)^2 + (y2-y1)^2 + (z2-z1)^2  ) +
     kk*q1*q3/sqrt( (x3-x1)^2 + (y3-y1)^2 + (z3-z1)^2  ) +
     kk*q1*q4/sqrt( (x4-x1)^2 + (y4-y1)^2 + (z4-z1)^2  ) +
     kk*q2*q3/sqrt( (x3-x2)^2 + (y3-y2)^2 + (z3-z2)^2  ) +
     kk*q2*q4/sqrt( (x4-x2)^2 + (y4-y2)^2 + (z4-z2)^2  ) +
     kk*q3*q4/sqrt( (x4-x3)^2 + (y4-y3)^2 + (z4-z3)^2  ):

Pec := simplify(expand(Pec)):

Lag:= KE - Pec:
# ************ IMPLEMENTATION OF LAGRANGE'S EQUATIONS
eq := MakeEQMO(Lag,vars,varsd,varsdd):



for i from 1 to 15 do
  eq[i] := expand(eq[i]):
od:

x0:=0:
y0:=0:
z0:=0:

x0d:=0:
x1d:=0:
x2d:=0:
x3d:=0:
x4d:=0:

y0d:=0:
y1d:=L*phid*cos(phi):
y2d:=L*phid*sin(phi):
y3d:=-L*phid*cos(phi):
y4d:=-L*phid*sin(phi):

z0d:=0:
z1d:=L*phid*sin(phi):
```

```
z2d:=-L*phid*cos(phi):
z3d:=-L*phid*sin(phi):
z4d:=L*phid*cos(phi):

x0dd:=0:
x1dd:=0:
x2dd:=0:
x3dd:=0:
x4dd:=0:

y0dd:=0:
y1dd:=L*phidd*cos(phi) - L*phid*phid*sin(phi):
y2dd:=L*phidd*sin(phi) + L*phid*phid*cos(phi):
y3dd:=-L*phidd*cos(phi) + L*phid*phid*sin(phi):
y4dd:=-L*phidd*sin(phi) - L*phid*phid*cos(phi):

z0dd:=0:
z1dd:=L*phidd*sin(phi) + L*phid*phid*cos(phi):
z2dd:=-L*phidd*cos(phi) + L*phid*phid*sin(phi):
z3dd:=-L*phidd*sin(phi) - L*phid*phid*cos(phi):
z4dd:=L*phidd*cos(phi) - L*phid*phid*sin(phi):

rrd :=0:
rrdd := 0:
thtdd := 0:

phi:=0:
phid:=0:
phidd:=0:

x1:=L1:
x2:=L1+L2:
x3:=-L1:
x4:=-L1-L2:

y0:=0:
y1:=0:
y2:=0:
y3:=0:
y4:=0:


z0:=0:
z1:=0:
z2:=0:
z3:=0:
```

```
z4:=0:

q3:=q1:
q4:=q2:
kk := 8.99e9:
thtd:=0.01*Pi/3600:
M0:=150:
M1:=150:
M2:=130:
M3:=150:
M4:=130:

L1:=12.5:
L2:=25:
q0:=-6.03227402380943e-08:
q1:= -1e-07:
q2:= 1.99e-07:
q3:=-4.11441709029563e-08:
q4:=1.672751600554e-08:
```

A.4. Program for Creating Stability Linearize Equation of Satellite Formations

This is an example of stability program of Earth orbiting seven-satellite formation:

```
# ************************* LIBRARIES
# Maple Libraries
with(linalg):
#(C);
#readlib(mtaylor);

# Custom library for implementing Lagrange's equations
read '/home/megrad/jchong/files/res-maple/eqmo_util.mpl';

# ************** ARRAY and MATRIX INITIALIZATION

# The array "vars" contains a list of the names given to independent
# variables used to describe the kinematics, and ultimately, the
# dynamics. Each member of this list is assume to be independent, and
# a function of time. Any quantity used to describe the position of
# the payload and is an independent function of time must be in this
# list.
vars   := array([ [rr]    , [tht] ,
                  [x1]    , [y1]  , [z1] ,
```

```
                [x2]    , [y2]  , [z2] ,
                [x3]    , [y3]  , [z3] ,
                [x4]    , [y4]  , [z4] ,
                [x5]    , [y5]  , [z5] ,
                [x6]    , [y6]  , [z6]  ]):

# The array "varsd" contains the names given to the time derivatives
# of the quantities in "vars". Although Maple can display time derivatives
# using a d/dt notation, the ability to let the user assign the
# names results in more compact dynamic equations, and facilitates
# their use in automatically generated C code.
varsd  := array([ [rrd]   , [thtd]  ,
                [x1d]    , [y1d]  , [z1d]  ,
                [x2d]    , [y2d]  , [z2d]  ,
                [x3d]    , [y3d]  , [z3d]  ,
                [x4d]    , [y4d]  , [z4d]  ,
                [x5d]    , [y5d]  , [z5d]  ,
                [x6d]    , [y6d]  , [z6d]  ]):

# The array "varsdd" is similar to "varsd", but for the second
# derivatives of the variables in "vars". You guessed it, the "d"
# suffix designates a time derivative.
varsdd := array([ [rrdd]  , [thtdd]  ,
                [x1dd]    , [y1dd]  , [z1dd]  ,
                [x2dd]    , [y2dd]  , [z2dd]  ,
                [x3dd]    , [y3dd]  , [z3dd]  ,
                [x4dd]    , [y4dd]  , [z4dd]  ,
                [x5dd]    , [y5dd]  , [z5dd]  ,
                [x6dd]    , [y6dd]  , [z6dd]  ]):

# ******************** ENERGY CALCULATION
# Deriving the differential equations of motion using Lagrange's equations
# requires the computation of the kinetic and potential energy of the
# payload. This is accomplished by first forming the absolute position vector
# from the origin of the inertial frame {I} to the payload, represented in
# inertial coordinates. Although the expression would be more compact using
# a rotating coordinate system, we are using inertial coordinates and
# letting Maple perform all the simplifications.
# After getting position, the absolute velocity is easily computed leading
# directly to the kinetic energy. Potential energy is computed by taking the
# the z-component of the position vector.

# *** POSITION VECTORS
# Form position vectors
p0 := array([rr, 0, 0]):
p1 := array([rr+x1, y1, z1]):
```

```
p2 := array([rr+x2, y2, z2]):
p3 := array([rr+x3, y3, z3]):
p4 := array([rr+x4, y4, z4]):
p5 := array([rr+x5, y5, z5]):
p6 := array([rr+x6, y6, z6]):
angvel := array([0, 0, thtd]):

p0d := evalm(time_deriv_vector(p0,vars,varsd,varsdd) +
   crossprod(angvel,p0)):
p1d := evalm(time_deriv_vector(p1,vars,varsd,varsdd) +
   crossprod(angvel,p1)):
p2d := evalm(time_deriv_vector(p2,vars,varsd,varsdd) +
   crossprod(angvel,p2)):
p3d := evalm(time_deriv_vector(p3,vars,varsd,varsdd) +
  crossprod(angvel,p3)):
p4d := evalm(time_deriv_vector(p4,vars,varsd,varsdd) +
   crossprod(angvel,p4)):
p5d := evalm(time_deriv_vector(p5,vars,varsd,varsdd) +
   crossprod(angvel,p5)):
p6d := evalm(time_deriv_vector(p6,vars,varsd,varsdd) +
   crossprod(angvel,p6)):

KE := (Mc*evalm(transpose(p0d)&*p0d) +
     Ms*evalm(transpose(p1d)&*p1d) +
     Ms*evalm(transpose(p2d)&*p2d) +
     Ms*evalm(transpose(p3d)&*p3d) +
     Ms*evalm(transpose(p4d)&*p4d) +
     Ms*evalm(transpose(p5d)&*p5d) +
     Ms*evalm(transpose(p6d)&*p6d) )/2:

KE := simplify(expand(KE)):

Peg := -mu*Mc/rr - mu*Ms/sqrt( (rr+x1)^2+y1^2+z1^2 ) -
              mu*Ms/sqrt( (rr+x2)^2+y2^2+z2^2 ) -
              mu*Ms/sqrt( (rr+x3)^2+y3^2+z3^2 ) -
              mu*Ms/sqrt( (rr+x4)^2+y4^2+z4^2 ) -
              mu*Ms/sqrt( (rr+x5)^2+y5^2+z5^2 ) -
              mu*Ms/sqrt( (rr+x6)^2+y6^2+z6^2 ):

Peg := simplify(expand(Peg)):

Pec := kk*q0*q1/sqrt(x1^2+y1^2+z1^2) +
      kk*q0*q2/sqrt(x2^2+y2^2+z2^2) +
      kk*q0*q3/sqrt(x3^2+y3^2+z3^2) +
      kk*q0*q4/sqrt(x4^2+y4^2+z4^2) +
      kk*q0*q5/sqrt(x5^2+y5^2+z5^2) +
```

```
    kk*q0*q6/sqrt(x6^2+y6^2+z6^2) +
    kk*q1*q2/sqrt( (x2-x1)^2 + (y2-y1)^2 + (z2-z1)^2  ) +
    kk*q1*q3/sqrt( (x3-x1)^2 + (y3-y1)^2 + (z3-z1)^2  ) +
    kk*q1*q4/sqrt( (x4-x1)^2 + (y4-y1)^2 + (z4-z1)^2  ) +
    kk*q1*q5/sqrt( (x5-x1)^2 + (y5-y1)^2 + (z5-z1)^2  ) +
    kk*q1*q6/sqrt( (x6-x1)^2 + (y6-y1)^2 + (z6-z1)^2  ) +
    kk*q2*q3/sqrt( (x3-x2)^2 + (y3-y2)^2 + (z3-z2)^2  ) +
    kk*q2*q4/sqrt( (x4-x2)^2 + (y4-y2)^2 + (z4-z2)^2  ) +
    kk*q2*q5/sqrt( (x5-x2)^2 + (y5-y2)^2 + (z5-z2)^2  ) +
    kk*q2*q6/sqrt( (x6-x2)^2 + (y6-y2)^2 + (z6-z2)^2  ) +
    kk*q3*q4/sqrt( (x4-x3)^2 + (y4-y3)^2 + (z4-z3)^2  ) +
    kk*q3*q5/sqrt( (x5-x3)^2 + (y5-y3)^2 + (z5-z3)^2  ) +
    kk*q3*q6/sqrt( (x6-x3)^2 + (y6-y3)^2 + (z6-z3)^2  ) +
    kk*q4*q5/sqrt( (x5-x4)^2 + (y5-y4)^2 + (z5-z4)^2  ) +
    kk*q4*q6/sqrt( (x6-x4)^2 + (y6-y4)^2 + (z6-z4)^2  ) +
    kk*q5*q6/sqrt( (x6-x5)^2 + (y6-y5)^2 + (z6-z5)^2  ) :

Pec := simplify(expand(Pec)):

# ************ IMPLEMENTATION OF LAGRANGE'S EQUATIONS
eq := MakeEQMO(KE,vars,varsd,varsdd):

GenF := MakeEQMO(-Peg,vars,varsd,varsdd):
GenF1 := MakeEQMO(-Pec,vars,varsd,varsdd):

for i from 1 to 20 do
  eq[i] := expand(eq[i]):
  GenF[i] := expand(GenF[i]):
  GenF1[i] := expand(GenF1[i]):

  eq[i] := subs({x1=dx1,   y1=dy1,   z1=-L+dz1,
              x2=dx2,   y2=-L+dy2,z2=dz2,
              x3=dx3,   y3=dy3,   z3=L+dz3,
              x4=dx4,   y4=L+dy4, z4=dz4,
              x5=-L+dx5,y5=dy5,   z5=dz5,
              x6=L+dx6, y6=dy6,   z6=dz6},eq[i]):

  GenF1[i] := subs({x1=dx1,   y1=dy1,   z1=-L+dz1,
                x2=dx2,   y2=-L+dy2,z2=dz2,
                x3=dx3,   y3=dy3,   z3=L+dz3,
                x4=dx4,   y4=L+dy4, z4=dz4,
                x5=-L+dx5,y5=dy5,   z5=dz5,
                x6=L+dx6, y6=dy6,   z6=dz6,
                q0=q0b+dq0,q1=q1b+dq1,q2=q2b+dq2,
                q3=q3b+dq3,q4=q4b+dq4,q5=q5b+dq5,
                q6=q6b+dq6},GenF1[i]):
```

```
od:

NewGenF := array(1..20):
NewGenF1 := array(1..20):
mu:=rr*rr*rr*thtd*thtd:

for i from 1 to 20 do

  temp1:= mtaylor(GenF[i],
    [x1,y1,z1,x2,y2,z2,x3,y3,z3,x4,y4,z4,x5,y5,z5,x6,y6,z6],2):
  temp2 := simplify(expand(temp1)):
  NewGenF[i] := expand(temp2/csgn(rr)):

  NewGenF[i] := subs({x1=dx1,   y1=dy1,   z1=-L+dz1,
                  x2=dx2,   y2=-L+dy2,z2=dz2,
                  x3=dx3,   y3=dy3,   z3=L+dz3,
                  x4=dx4,   y4=L+dy4, z4=dz4,
                  x5=-L+dx5,y5=dy5,   z5=dz5,
                  x6=L+dx6, y6=dy6,   z6=dz6},NewGenF[i]):

  temp3:= mtaylor(GenF1[i],
    [dx1,dy1,dz1,dx2,dy2,dz2,dx3,dy3,dz3,dx4,dy4,dz4,dx5,dy5,dz5,dx6,dy6,dz6,
     dq0,dq1,dq2,dq3,dq4,dq5,dq6],2):
  temp4 := simplify(expand(temp3)):
  NewGenF1[i] := expand(temp4/csgn(rr)):
od;

for i from 1 to 20 do
  eq[i] := eq[i] + NewGenF[i] + NewGenF1[i]:
od;
rrd :=0:
rrdd := 0:
thtdd := 0:
phi:=0:
phid:=0:
phidd:=0:
```

Table of Contents

List of Figures

List of Tables

[1] Pollard, J.E., Chao, C.C., and Janson, S.W., "Populating and maintaining cluster constellations in low-earth orbit," AIAA-99-2878, AIAA Meeting Papers on Disk Vol. 4, No. 3, Proc. Of 35th AIAA/ASME/SAE/ASEE Joint Propulsion Conference, June 20-24, 1999, Los Angeles, CA.

[2] Walker, J.G., "The geometry of cluster orbits," J. Brit. Interplan. Soc., Vol. 35, 1982, p. 345.

[3] Murdoch, J. and Pocha, J.J., "The orbit dynamics of satellite clusters," Paper IAF-82-54, 33rd International Astronautical Congress, Sept. 27-Oct. 2, 1982, Paris, France.

[4] Micci, M.M. and Ketsdever, A.D., Micropropulsion for Small Spacecraft, Progress in Astronautics and Aeronautics Vol. 187, AIAA Press, Reston VA, 2000, pp. 3-22.

[5] Hoskins, W.A., Wilson, M.J., Willey, M.J., Meckel, N.J., Campell, M., and Chung, S., "PPT development efforts at Primex Aerospace Company," Paper AIAA-99-2291, AIAA Meeting Papers on Disk Vol. 4, No. 3, Proc. Of 35th AIAA/ASME/SAE/ASEE Joint Propulsion Conference, June 20-24, 1999, Los Angeles, CA.

[6] Chao, C.C., Pollard, J.E., and Janson, S.W., "Dynamics and control of cluster orbits for distributed space missions," Paper AAS-99-126, Space Flight Mechanics Meeting, Feb. 7-10 1999, Breckenridge, CO.

[7] Kong, E.M.C., Miller, D.W., and Sedwick, R.J., "Exploiting orbital dynamics for aperture synthesis using distributed satellite systems: Applications to a visible Earth imager system," Paper AAS-99-122, Space Flight Mechanics Meeting, Feb. 7-10 1999, Breckenridge, CO.

[8] Sedwick, R., Miller, D., and Kong, E., "Mitigation of differential perturbations in clusters of formation flying satellites," Paper AAS-99-124, Space Flight Mechanics Meeting, Feb. 7-10 1999, Breckenridge, CO.

[9] Miller, D.W. and Spores, R.A., "Proceedings of the Formation Flying and Micropropulsion Workshop," unpublished, Oct. 20-21 1998, available from Dr. Ronald Spores, Air Force Research Laboratory, Edwards AFB, CA.

[10] Micci, M.M. and Ketsdever, A.D., Micropropulsion for Small Spacecraft, Progress in Astronautics and Aeronautics, Vol. 187, AIAA Press, Reston, VA, 2000.

[11] Corazzini, T., Robertson, A., Adams, J.C., Hassibi, A., and How, J.P., "GPS sensing for spacecraft formation flying," Proceedings of the 10th International Technical Meeting, ION/GPS, Sept. 16-19 1997, Kansas City, MO.

[12] Vassar, R.H. and Sherwood, R.B., "Formationkeeping for a pair of satellites in a circular orbit," Journal of Guidance, Control, and Dynamics, Vol. 8, No. 2, 1985.

[13] Leonard, C.L., "Fuel penalty of using ballistic coefficient control for satellite formationkeeping," AAS 13th Annual Guidance and Control Conference, Keystone, CO, Feb. 1990.

[14] Jilla, Cyrus D., Separated Spacecraft Interferometry – System Architecture Design and Optimization, Master's Thesis, Dept. of Aeronautics and Astronautics, Massachusetts Institute of Technology, Feb. 1999.

[15] Kong, Edmund M., Optimal Trajectories and Orbit Design for Separated Spacecraft Interferometry, Master's Thesis, Dept. of Aeronautics and Astronautics, Massachusetts Institute of Technology, Nov. 1998.

[16] Yashko, Gregory, Ion Micro-Propulsion and Cost Modelling for Satellite Clusters, Master's Thesis, Dept. of Aeronautics and Astronautics, Massachusetts Institute of Technology, June 1998.

[17] Hacker, Troy L., Performance of a Space-based GMTI Radar System using Separated Spacecraft Interferometry, Master's Thesis, Dept. of Aeronautics and Astronautics, Massachusetts Institute of Technology, May 2000.

[18] Janson, S.W., Helvajian, H., Hansen, W.W., and Lodmell, J., "Microthrusters for nanosatellites," 2nd International Conference on Integraed Micro Nanotechnology for Space Applications (MNT99), Apr. 11-14 1999, Pasadena, CA.

[19] Janson, S.W., Helvajian, H., Hansen, W.W., and Lodmell, J., "Batch-fabricated CW microthrusters for kilogram-class spacecraft," Paper AIAA-99-2722, AIAA Meeting Papers on Disk Vol. 4, No. 3, Proc. Of 35th AIAA/ASME/SAE/ASEE Joint Propulsion Conference, June 20-24, 1999, Los Angeles, CA.

[20] Tajmar, M., Mitterauer, J., and Wang, J., "Field-emission-electric-propulsion (FEEP) plasma modeling: 3D full particle simulations," Paper AIAA-99-2298, AIAA Meeting Papers on Disk Vol. 4, No. 3, Proc. Of 35th AIAA/ASME/SAE/ASEE Joint Propulsion Conference, June 20-24, 1999, Los Angeles, CA.

[21] Martinez-Sanchez, M. and Pollard, J.E., "Spacecraft electric propulsion – An overview," Journal of Propulsion and Power, Vol. 14, No. 5, Sept-Oct 1998, pp. 688-699.

[22] Martinez-Sanchez, M., and Pollard, J.E., "Spacecraft Electric Propulsion – An Overview," Journal of Propulsion and Power, Vol. 14, No. 5, Sept.-Oct. 1998, pp. 688-699.

[23] Osgood, R.N., "Operational status of the space test program P78-2 spacecraft and payloads," reported in Proceedings of 3rd Spacecraft Charging Technology Conference, Nov. 12-14, 1980, NASA Conference Publication 2182, pp. 365-369.

[24] Gussenhoven, M.S., Cohen, H.A., Hardy, D.A., Burke, W.J., and Chesley, A., "Analysis of ambient and beam particle characteristics during the ejection of an electron beam from a satellite in near-geosynchronous orbit on March 30, 1979," reported in Proc. of 3rd Spacecraft Charging Technology Conference, No. 12-14, 1980, NASA Conference Publication 2182, pp. 642-664.

[25] Cohen, H.A., Adamo, R.C., Aggson, T., Chesley, A.L., Clark, D.M., Damron, S.A., Delorey, D.E., Fennell, J.F., Gussenhoven, M.S., Hanser, F.A., Hall, D., Hardy, D.A., Huber, W.B., Katz, I., Koons, H.C., Lau, S.T., Ledley, B., Mizera, P.F., Mullen, E.G., Nanevicz, J.E., Olsen, R.C., Rubin, A.G., Schnuelle, G.W., Saflekos, N.A., Tautz, M.F., and Whipple, E.C., "P78-2 Satellite and payload responses to electron beam operations on March 30, 1979," reported in Proc. of 3rd Spacecraft Charging Technology Conference, Nov. 12-14, 1980, NASA Conference Publication 2182, pp. 509-559.

[26] Osgood, R.N., "Operational status of the space test program P78-2 spacecraft and payloads," reported in Proc. of 3rd Spacecraft Charging Technology Conference, Nov. 12-14, 1980, NASA conference Publication 2182, pp. 412-432.

[27] Whipple, E.C., and Olsen, R.C., "Importance of differential charging for controlling both natural and induced vehicle potentials on ATS-5 and ATS-6," reported in Proc. of 3rd Spacecraft Charging Technology Conference, Nov. 12-14, 1980, NASA Conference Publication 2182, p. 887.

[28] Deininger, W.D., Aston, G., and Pless, L.C., "Hollow-cathode plasma source for active spacecraft charge control," Review of Scientific Instruments, Vol. 58, No. 6, June 1987, pp. 1053-1062.

[29] Ridgeway, S.T., "The scientific support for a space interferometry mission," SPIE Vol. 1947 Spaceborne Interferometry, 1993, pp. 2-11.

[30] See, for instance, Hecht, E., Optics, Addison-Wesley, 1998.

[31] Golay, M., "Point arrays having compact non-redundant autocorrelations, Journal of Optical Society of America, Vol. 61, pg. 272, 1971.

[32] Cornwell, T.J., "A Novel Principle for Optimization of the Instantaneous Fourier Plane Coverage of Correlation Arrays," IEEE Trans. On Antennas and Propagation, Vol. 36, No. 8, pp. 1165-1167.

[33] Sabol, Chris, Burns, Richard, and McLaughlin, Craig A., "Satellite Formation Flying Design and Evolution," AAS 99-121, pp.265-283

[34] Lo, Martin W., "Satellite-constellation Design," California Institute of Technology, IEEE 1521-9615/99, January-February 1999.

[35] See, for instance, Proceedings of 1st and 2nd Spacebone Interferometry Conference, SPIE Vol. 1947, 2477, 1993, and 1995.

[36] Kong, Edmund M. C., Miller, David W., and Sedwick , Raymond J., "Exploiting Orbital Dynamics for Aperture Synthesis Using Distributed Satellite Systems: Applications to A Visible Earth Imager System," American Astronautical Society, Paper AAS 99-122, 1999, pp. 285-301

[37] Sabol, Chris, Burns, Richard, and McLaughlin Craig A., "Satellite Formation Flying Design and Evolution," American Astronautical Society, Paper AAS 99-121, 1999, pp.265-283

[38] Sparks A., "Linear Control of Satellite Formation Flying," American Institute of Aeronautics and Astronautics, Paper AIAA-2000-4438.

[39] Schweighart, Samuel A., Development and Analysis of a High Fidelity Linearized J_2 model for Satellite Formation Flying, Master's Thesis, Dept. of Aeronautical and Astronautical, Massachusetts Institute of Technology, June 2001.

[40] Sedwick, Raymond J., Miller, David W., and Kong, Edmund M.C., "Mitigation of Differential Perturbations in Clusters of Formation Flying Satellites," American Astronautical Society, Paper AAS 99-124, pp. 323-342.

[41] Pollard, James E., Chao, C.C. (George), Janson, Siegfried W., "Populating and Maintaining Cluster Constellations in Low-Earth Orbit," The Aerospace Corporation, American Institute of Aeronautics and Astronautics, Paper AIAA-99-2871.

[42] Leonard, C.L., "Orbital Formation-keeping with Differential Drag," Vol.12, No.1, Jan-Feb. 1989.

[43] Schaub, Hanspeter and Alfriend, Kyle T., "Hybrid Cartesian and Orbit Element Feedback Law for Formation Flying Spacecraft," American Institute of Aeronautics and Astronautics, Paper AIAA 2000-4131, August 14-17, 2000.

[44] Wang, P.K.C. and Hadaegh, F.Y., "Coordination and Control of Multiple Microspacecraft Moving in Formation," The Journal of the Astronautical Sciences, Vol. 44, No. 3, July-September 1996, pp.315-355.

[45] Queiroz, Marcio S. de, Kapila, Vikram, and Yan, Qigua, "Adaptive Nonlinear Control of Multiple Spacecraft Formation Flying," Polytechnic University, Journal of Guidance, Vol. 23, No. 3, May-June 2000.

[46] Kapila, Vikram, Sparks, Andrew G., Buffington, James M., and Yan, Qiguo, "Spacecraft formation flying: Dynamics and Control," Journal of Guidance, Vol. 23, No. 3. pp. 561-564.

[47] Lau, Kenneth, Lichten, Stephen, Young, Lawrence, Haines, Bruce, "An Innovative Deep Space Application of GPS Technology for Formation Flying Spacecraft," California Institute of Technology, American Institute of Aeronautics and Astronautics, Paper AIAA 96-3819, July 1996.

[48] Inalhan, Gokhan, Busse, Franz D., How, Jonathan P., "Precise Formation Flying Control of Multiple Spacecraft Using Carrier-phase Differential GPS," American Astronautical Society, Paper AAS 00-109.

[49] Tan, Zhaozhi, Bainum, Peter M., and Strong, Avine, "A Strategy for Maintaining Distance Between Satellites in an Orbiting Constellation," American Astronautical Society, Paper AAS 99-125, 1999, pp. 343-353

[50] Cornwell, T.J., "A Novel Principle for Optimization of the Instantaneous Fourier Plane Coverage of Correlation Arrays," IEEE Trans. On Antennas and Propagation, Vol. 36, No. 8, pp.1165-1167.

[51] Slotine, Jean-Jaques E., and Li, Weiping, "Applied Nonlinear Control," Prentice Hall, pp.55-58.

[52] Dr. Gordon Parker, 'MEEM 6702:Nonlinear System Analysis and Control' Handout, Spring 2002.